POLITÉCNICO DE LEIRIA | ESCOLA SUPERIOR DE TURISMO E TECNOLOGIA DO MAR

Seaweed exploration by sustainable technologies - Evaluation of their antifouling and bioremediation potential

Juliana Antunes Gaspar

Dissertation to obtain the Master's degree in Marine Resources Biotechnology

2024

POLITÉCNICO DE LEIRIA | ESCOLA SUPERIOR DE TURISMO E TECNOLOGIA DO MAR

Seaweed exploration by sustainable technologies - Evaluation of their antifouling and bioremediation potential

Juliana Antunes Gaspar

Dissertation to obtain the Master's degree in Marine Resources Biotechnology

Master's project carried out under the supervision of PhD Alice Martins, PhD Susete Pintéus and PhD Ana Sofia Mestre

2024

ACKNOWLEDGMENTS

This dissertation would not have been possible without the invaluable guidance, support, and kindness of many remarkable people.

I want to start by thanking the excellent facilities of MARE – Marine and Environmental Sciences Centre, IPLeiria, that provide the support necessary to carry out high-quality scientific research, as well as to the Chemistry and Biochemistry Department-Faculty of Sciences, University of Lisbon, where I completed the second part of this work. This experience, though outside my usual field, expanded my knowledge immensely, and I am thankful for the excellent conditions and scientific community there.

I would like to express my deepest gratitude to my supervisor, Doctor Alice Isabel Mendes Martins, whose patience, kindness, and expertise provided the foundation for my journey. Her encouragement and willingness to support me at every step made this process much easier and filled it with learning experiences.

My sincere thanks go to my supervisor, Doctor Susete Filipa Gonçalves Pinteus, whose warmth, friendship, and wisdom inspired and motivated me. Her good advice, open conversations, and generosity left a lasting impact on me, both professionally and personally. I am truly fortunate to have had the opportunity to learn from someone like her.

I am also immensely grateful to Doctor Ana Sofia Dias Mestre Homem, who brought unmatched enthusiasm and generosity to this work. Her intelligence and openness were uplifting, and her dedication to sharing knowledge with others set an inspiring example. Her support was crucial, and I am thankful for her guidance that made every step of this project feel attainable.

To the entire research group at MARE – IPLeiria, I extend my heartfelt thanks for welcoming me. Their kindness, willingness to help, and passion for discovery created a rich environment that made my time at MARE unforgettable. I also thank Prof. Marco Lemos from ESTM- IPLeiria for providing the biomass for this study—a very generous contribution that made this work possible.

Special thanks to my wonderful colleagues in the master's program: Miguel Oliveira, Henrique Ferreira, Diogo Moreira, Victoria Pérez, Andreia Sousa, João Costa, Joana Fernandes, and Raissa Nunes. Their friendship, good humor, and constant support made these two years truly memorable, filled with laughter and countless memories that I will cherish.

Finally, I owe my deepest thanks to my family and friends. To my mother, for her unwavering strength and support; and to my closest friends—Luana Frade, Mário Matias Santos, Beatriz Costa, Cibele Taveira, Delmar Santos, and Mariana Domingos—for being my anchor throughout this journey. Their presence in my life has been the most important and cherished part of this experience.

Looking back, this journey has had its challenges and rewards, with highs and lows that have taught me so much. I am grateful for everyone who has been a part of this chapter, and I look forward to continuing my path with the same strength and dedication.

Thank you, all.

Part of the results obtained in this study were presented as a poster communication (Appendix A1) in the CQE Days Meeting, University of Lisbon, June 2024: “A sustainable valorization of seaweed: extraction of antifouling compounds and synthesis of new carbon materials from *Undaria pinnatifida*”
Authors: Juliana Gaspar, Susete Pinteus, Alice Martins, Ana P. Carvalho, Ana S. Mestre

Abstract

Biofouling is the accumulation and growth of micro- and macroorganisms on submerged artificial structures or living surfaces. This process leads to increased fuel consumption and maintenance costs, reduced efficiency of equipment, and contributes to the spread of invasive species, while increasing greenhouse gas emissions.

This study explores the antifouling potential of the invasive seaweed *Undaria pinnatifida* crude extracts obtained with water, ethanol, *n*-hexane and ethyl acetate, through evaluation of inhibition of bacteria growth, biofilm formation, *quorum sensing*, and acetylcholinesterase and tyrosinase activities, two enzymes involved in macroinvertebrates settlement process. The results were compared with the ones obtained with methanol and dichloromethane extracts. A field assay was also carried out. Aiming a circular economy approach, the study also investigates biochar produced from the intact and post-extracted seaweed biomass, by pyrolysis process (800 °C and 400 °C), hydrothermal carbonization (170 °C) and activation by a steam process (700 °C), assessing its properties and potential for water bioremediation through adsorption of ibuprofen, diclofenac and paracetamol.

While the ethanol: water (50:50) afforded the highest extraction yield (10.3%), the extracts obtained with *n*-hexane and ethyl acetate, showed the broadest antimicrobial spectrum, exhibiting the highest potency against *Citricoccus* sp., (IC_{50} of 203.1 µg/mL and 435.2 µg/mL, respectively). The *n*-hexane extract also showed the highest capacity to inhibit the diatoms *Chaetoceros calcitrans* and *Amphora* sp. growth (10 mm and 8 mm inhibition halo, respectively). Concerning the anti-enzymatic activity, the ethyl acetate extract exhibited significant tyrosinase inhibition with an IC_{50} of 643 µg/mL. In the field test, in the assayed conditions, *U. pinnatifida* extracts did not reduce the biofouling process.

Pyrolysis at lower temperatures (400 °C) yielded a higher biochar amount of 30-40%, whereas hydrochar synthesis yielded 27-31%. Biochars showed a range of ash content, with values between 53-80% at high pyrolysis temperatures. Surface areas increased with temperature and post-synthesis washing, yielding a maximum of 138 m^2/g in pyrochar of post-extracted biomass. *Undaria*-derived biochar may be suited as a fertilizer, for adsorption of heavy metals or oxidation processes. This study aligns with the principles of a circular economy by exploring the valorization of *U. pinnatifida*, an invasive species, to create high-value, sustainable antifouling agents and biochars.

Keywords

Antimicrobial potential, biochar, biofouling, marine biotechnology, marine invasive species, *Undaria pinnatifida* biorefinary

Resumo

A bioincrustação é a acumulação e crescimento de micro e macrorganismos em estruturas artificiais submersas ou superfícies vivas. Este processo leva ao aumento do consumo de combustível e dos custos de manutenção, à redução da eficiência dos equipamentos e contribui para a propagação de espécies invasoras, ao mesmo tempo que aumenta as emissões de gases com efeito de estufa.

Este estudo explora o potencial anti-incrustante dos extratos brutos da alga invasora *Undaria pinnatifida* obtidos com água, etanol, *n*-hexano e acetato de etilo, avaliando a inibição do crescimento de bactérias, formação de biofilme, *quorum sensing* e atividades da acetilcolinesterase e tirosinase, duas enzimas envolvidas. no processo de adesão de macroinvertebrados. Os resultados foram comparados com os extratos em metanol e diclorometano. Foi igualmente realizado um ensaio de campo. Visando uma abordagem de economia circular, o presente estudo também estudou os biocarbonizados produzidos a partir da biomassa algal intacta e pós-extraída, por processos de pirólise (800 °C e 400 °C), carbonização hidrotérmica (170 °C) e ativação por vapor (700 °C), avaliando as suas propriedades e potencial de biorremediação da água através da adsorção de ibuprofeno, diclofenac e paracetamol.

Enquanto o sistema etanol: água (50:50) proporcionou o maior rendimento de extração (10.3%), os extratos obtidos com *n*-hexano e acetato de etilo apresentaram o maior espectro antimicrobiano, exibindo a maior potência contra *Citricoccus* sp., (IC_{50} de 203.1 µg/mL e 435.2 µg/mL, respetivamente). O extrato de *n*-hexano também apresentou maior capacidade de inibir o crescimento das diatomáceas *Chaetoceros calcitrans* e *Amphora* sp. (halo de inibição de 10 mm e 8 mm, respetivamente). Quanto à atividade anti-enzimática, o extrato de acetato de etilo inibiu significativamente a tirosinase (IC_{50} de 643 µg/mL). No ensaio de campo, nas condições testadas, os extratos de *U. pinnatifida* não reduziram o processo de bioincrustação.

A pirólise a temperaturas mais baixas (400 ° C) resultou num maior rendimento (30-40%), enquanto a síntese de hidrocarbonizado produziu 27-31%. Os biocarbonizados apresentaram teores de cinzas entre 53-80% a altas temperaturas de pirólise. As áreas superficiais aumentaram com a temperatura e lavagem pós-síntese, tendo atingido um máximo de 138 m^2/g no pirocarbonizado de biomassa pós-extraída (800 ^{O}C). Os biocarbonizados derivados de *U. pinnatifida* podem ter potencial como fertilizante, para adsorção de metais pesados ou processos de oxidação. Este estudo está alinhado com os princípios da economia circular, valorizando *U. pinnatifida*, de modo a criar agentes *antifouling* e biocarbonizados sustentáveis de alto valor acrescentado.

Palavras-chave

Anti-incrustante, biocarbonizado, biotecnologia marinha, espécies invasoras marinhas, potencial antimicrobiano, *Undaria pinnatifida* biorrefinaria

Index

ACKNOWLEDGMENTS IV

ABSTRACT VI

RESUMO VII

INDEX VIII

LIST OF FIGURES XI

LIST OF TABLES XIV

ABBREVIATIONS AND ACRONYMS XV

1. INTRODUCTION 1

1.1. Marine biofouling 1
1.1.1. *Definition and causes* 1
1.1.2. *Biofouling – a multistep process* 3
1.1.3. *Factors that influence biofouling formation* 4
1.1.4. *Quorum Sensing (QS)* 4
1.1.5. *Methods used to combat biofouling* 4

1.2. Biotechnological potential of seaweed 6
1.2.1. *Invasive seaweed species* 7
1.2.1.1. Undaria pinnatifida 8
1.2.1.1.1. *Distribution* 8
1.2.1.1.2. *Ecology* 9
1.2.1.1.3. *Biotechnological potential* 11

1.3. Circular Economy 12

1.4. Biochar 12
1.4.1. *Biochar from seaweed* 13

1.5. Aim and outline of the thesis 14

2. MATERIALS AND METHODS 15

2.1. Seaweed biomass 15

2.2. Solvents 15

2.2.1. *Extractions* 15
2.2.2. *Chemical profile of extracts* 16

2.3. Biological evaluation 16
2.3.1. *Ecotoxicity studies* 16
2.3.2. *Antifouling activity* 17
2.3.2.1. Antimicrobial activity against marine bacteria 17
2.3.2.2. Biofilm inhibition activity 17
2.3.2.3. Quorum sensing inhibition activity 17
2.3.2.4. Inhibition of microalgae growth 18
2.3.2.5. In vitro enzymatic assays 18
2.3.2.5.1. *Acetylcholinesterase inhibitory activity* 18
2.3.2.5.2. *Anti-tyrosinase activity* 19
2.3.2.6. Antifouling field assay 19

2.4. Valorization of the post-extracted seaweed biomass 19
2.4.1. *Carbonization of seaweed biomass* 20
2.4.1.1. Slow pyrolysis 20
2.4.1.2. Hydrothermal carbonization 20
2.4.1.3. Steam activation 21
2.4.1.4. Nomenclature of the materials 22
2.4.2. *Characterization of biochars from Undaria pinnatifida* 22
2.4.2.1. Moisture and ash 22
2.4.2.2.Surface chemistry (pH at the point of zero charge, pHpzc) 22
2.4.2.3. Apparent density 23
2.4.2.4. N_2 Adsorption isotherm at -196 ºC 23
2.4.2.5. Scanning electron microscopy with Energy-Dispersive X-ray Spectroscopy (SEM-EDS) 23
2.4.2.6. X-ray diffraction (XRD) 24
2.4.3. *Preliminary assays in liquid phase* 24

2.5. Process water 25
2.5.1. *Antimicrobial assays with process water* 25
2.5.2. *Biofilm inhibition assays with process water* 25

2.6. Data assessment and statistical analysis 25

3. RESULTS 26

3.1. Extractions 26
3.1.1. *Extraction yields* 26
3.1.2. *Chemical profile of extracts* 27

3.2. Biological assays 27
3.2.1. *Ecotoxicity studies* 27
3.2.2. *Antifouling activity* 28
3.2.2.1. Antimicrobial activity against marine bacteria 28
3.2.2.2. Biofilm inhibition activity 30
3.2.2.3. Quorum sensing inhibition activity 32
3.2.2.5. Anti-enzymatic activity of extracts 34
3.2.2.6. Antifouling field assay 36

3.3. Valorization of residual biomass 38

2.3.1. Characterization of biomass and biochars 38
3.3.2. *Morphological and mineral characterization* 43
3.3.2.1. SEM analysis 43
3.3.2.2. XRD analysis 45
3.3.3. *Preliminary assays in liquid phase* 47
3.3.3.1. Adsorption of ibuprofen 47
3.3.3.2. Adsorption of diclofenac 48
3.3.3.3. Adsorption of paracetamol 49

3.4. Process water assay 50
3.4.1. *Antimicrobial activity assay* 50
3.4.2. *Biofilm inhibition activity* 51

4. DISCUSSION 53

6. CONCLUSIONS AND FUTURE PERSPECTIVES 61

7. REFERENCES 63

8. APPENDIX 69

List of Figures

Figure 1.1. Green sea turtle (*Chelonia mydas*, Linnaeus, 1758) (Pendergrast. A., 2020) on the left and Loggerhead sea turtle (*Caretta caretta*, Linnaeus, 1758) (Blue World Institute, 2021) on the right, covered by epibionts such as seaweed and barnacles. 1
Figure 1.2. Examples of biofouling on marine infrastructures, including pipelines, submerged systems, ship hulls, and aquaculture equipment. 2
Figure 1.3. Schematic illustration of the marine biofouling stages over time (figure created with BioRender.com). 3
Figure 1.4. History of antifouling coatings (Jin et al., 2022). 5
Figure 1.5. Bioactivity of metabolites or extract fractions from a total of 24 species of red seaweed (Rhodophyta), 13 species of green seaweed (Chlorophyta), and 18 species of brown seaweed (Phaeophyceae), active against marine relevant species during the period of 2010-2016. Antibacterial activity (AB), antifungal (AF), anti-microalgal including diatoms and cyanobacteria (AA), anti-macrofouling including mollusks and crustacean (AMF), *quorum-sensing* disruptor (QSD), toxins (TX), and anti-biofilm (ABF) (Saha et al., 2018). 7
Figure 1.6. Main producer countries of *Undaria pinnatifida* (FAO Fishery Statistics, 2013, https://www.fao.org/fishery/en/culturedspecies/undaria_pinnatifida/en). 8
Figure 1.7. Global distribution of *Undaria pinnatifida* (Smithsonian, Environmental Research Center, https://invasions.si.edu/nemesis/species_summary/-21). In red the non-native species and in blue native species. 9
Figure 1.8. Distribution, showing dates of first records for each invaded country in Europe. Purple: cultivation of *Undaria pinnatifida*, Red: other populations. Red star: first Mediterranean record. Purple star: first Atlantic record. The first Irish record arrowed. Lines indicate the probable future range of *Undaria pinnatifida* (Minchin & Nunn, 2014). 9
Figure 1.9. Life history of *Undaria pinnatifida* illustrating the microscopic spores, gametophytes and sporelings, and the macroscopic sporophytes (Cunningham et al., 2020). 10
Figure 1.10. Temperature tolerances for *Undaria pinnatifida* (Minchin & Nunn, 2014). 10
Figure 1.11. Illustration of *Undaria pinnatifida* (Yin et al., 2019). 11
Figure 2.1. Preparation of the extracts to be tested: (1) extractions, (2) stock solutions of each extract and (3) remaining biomass obtained from the process. 16
Figure 2.2. Acrylic plates painted with non-active paint incorporated with samples, fixed to the crate and lowered in the Marina of Peniche (Leiria, Portugal) in May of 2024. 19
Figure 2.3. Chemical structures of (1) Diclofenac, (2) Ibuprofen, and (3) Paracetamol (Acetaminophen) (https://go.drugbank.com/drugs). 20
Figure 2.4. Process of Pyrolysis (1) and process of Hydrothermal carbonization (2). 21
Figure 2.5. Vertical furnace (Thermolyne, model 21100). 21
Figure 2.6. Preliminary assay to assess the adsorption capacity of the biochars to remove pharmaceutical compounds in liquid phase. 25
Figure 3.1. Overview of the experimental workflow for the extraction and evaluation of antifouling activity from *Undaria pinnatifida* (figure made in Biorender.com). Biomass of *Undaria pinnatifida* was collected from Portugal and Spain and subjected to extraction using various solvents. The extracts were tested for antifouling activity. Residual post-extracted (pe) biomass and intact (in) biomass were processed using conventional pyrolysis and advanced hydrothermal carbonization (HTC) at varying conditions. Preliminary assays in liquid phase were conducted with the biochars that presented the higher BET area values. 26
Figure 3.2. *Artemia salina* survival after 24 h of exposure to *Undaria pinnatifida* extracts from (water; DCM:MEOH – dichloromethane-methanol; E:W – ethanol-water; *n*-hexane; AceE – ethyl acetate; ethanol). The negative controls were SW (salt water only) and another with

DMSO added. The positive control was commercial antifouling paint (AFp). Each bar represents the mean of 6 replicas in the experiment and vertical lines represent SEM. The symbol * represent significant differences with DMSO - dimethyl sulfoxide (One-Way ANOVA, Dunnett's test; $p < 0.05$). 28
Figure 3.3. Capacity of *Undaria pinnatifida* extracts (1000 µg/mL to 62.5 µg/mL) to inhibit the growth of (A) *Serratia* sp., (B) *Vibrio* sp., (C) *Citricoccus* sp., (D) *Pseudomonas* sp., and (E) *Bacillus subtilis*. The values in each column represent the mean ± standard error of the mean (SEM) from three independent experiments carried out in triplicate. The symbol * represent significant differences with DMSO - dimethyl sulfoxide (One-Way ANOVA, Dunnett's test; $p < 0.05$); DCM:MeOH – dichloromethane-methanol; E:W – ethanol-water; AceE – ethyl acetate. 29
Figure 3.4. Dose-response analysis and IC_{50} determination of the most potent extracts. A- *Serratia* sp. growth exposed to DCM:MeOH, and *n*-Hexane extracts; B- *Vibrio* sp. growth exposed to AceE extract; C- *Citricoccus* sp. growth exposed to *n*-Hexane and AceE extracts. Data are shown as means ± SEM, n = 3. IC_{50} values were determined for a 95% confidence interval. 30
Figure 3.5. *Undaria pinnatifida* extracts (1000 µg/mL - 62.5 µg/mL) capacity to inhibit the biofilm production of (A) *Serratia* sp., (B) *Vibrio* sp., (C) *Citricoccus* sp., (D) *Pseudomonas* sp., and (E) *Bacillus subtilis*. The values in each column represent the mean ± standard error of the mean (SEM) from three independent experiments carried out in triplicate. The symbol * represent significant differences with DMSO - dimethyl sulfoxide) (One-Way ANOVA, Dunnett's test; $p < 0.05$). DMSO – dimethyl sulfoxide; DCM:MeOH – dichloromethane-methanol; E:W – ethanol-water; AceE – ethyl acetate. 31
Figure 3.6. Effects of *Undaria pinnatifida* extracts on *Chromobacterium violaceum* growth and QS mechanism. Violet represents areas with functioning QS mechanism.White halos represent an inhibition of the QS mechanism and transparent halos represent growth inhibition. 32
Figure 3.7. Disk diffusion assays for growth inhibition of diatoms by the extracts from *Undaria pinnatifida*. *Chaetoceros calcitrans* – A and B; *Phaeodactylum tricornutum* – C and D; *Nitzschia* sp. – E and F; *Amphora* sp. – G and H. Inhibition halos are characterized by their transparency in the plates. DMSO and CuSO4 were used negative and positive controls, respectively. 34
Figure 3.8. Enzymatic inhibitory activity of *Undaria pinnatifida* extracts: Water, DM:MeOH (dichloromethane-methanol extract), E:W (ethanol-water), n-Hexane, AceE (ethyl acetate) and ethanol on A) Acetylcholinesterase and B-C) Tyrosinase. The DMSO and Donepezil were used as negative and positive controls, respectively, for the acetylcholinesterase activity and Kojic acid as positive for the tyrosinase enzyme. The extracts were tested in three different concentrations 1000, 500 and 250 µg/mL. Bars correspond to the mean ± standard error of the mean (SEM) from three independent experiments carried out in triplicate. The symbol * represent significant differences with DMSO (One-Way ANOVA, Dunnett's test; $p < 0.05$). IC_{50} values were determined for a 95% confidence interval. 35
Figure 3.9. Acrylic plates containing paint incorporated with extracts of *Undaria pinnatifida* collected after two months underwater, in triplicate. Negative control (C-) with DMSO; Ethanol-water extract (50:50) (1); *n*-Hexane (2); Ethyl acetate (3); Ethanol (4); Antifouling paint (5); Water (6); Dichloromethane-methanol (50:50) (7); Ethanol-water (80:20) (8). The replicas are labeled alphabetically (a,b,c). 36
Figure 3.10. Weight, in percentage of control, for each acrylic plate containing paint incorporated with *Undaria pinnatifida* extracts. C- refers to the negative control (DMSO). The AFp is commercial antifouling paint and represents the positive control. Bars correspond to

the mean ± standard error of the mean (SEM) of three independent replicas. The symbol * represent significant differences with DMSO (One-Way ANOVA, Dunnett's test; $p < 0.05$)... 37
Figure 3.11. Observations of some biofouling organisms in the acrylic plates under a Zoom Stereoscopic Microscope. 38
Figure 3.12. N_2 adsorption isotherms at -196 ºC for the hydrochars (Hydro) and pyrochars (Pyro) at different temperatures - 400 ºC (A) or 800 ºC (B) - obtained from *Undaria pinnatifida* intact (in-) and post-extracted (pe-) biomass. The W means that the biochar was washed with distilled water after being produced. Type I refers to a hydrochar prepared with ultrapure water (C) and the PW to a hydrochar prepared with 1st or 2nd processed water (D). The graph E shows the best BET areas of all the materials. Insets in A, C and D allow discriminating adsorption isotherm profiles for the less adsorbing materials . Empty symbols correspond to adsorption data and full symbols represent desorption data. The textural parameters reported were obtained from the report generated by the equipment (NOVA 2200e from Quantachrome) software. 41
Figure 3.13. SEM images for the intact (in-) and post-extracted (pe-) biomass of *Undaria pinnatifida* and some of the derived materials (amplification – x750) on the left column and the corresponding ash (amplification x155) on the right column Hydro – Hydrothermal carbonization; Pyro – Pyrolysis, followed by the temperature used (400ºC or 800ºC); 1st and 2nd PW – process water; Type I – ultrapure water; W- post-washed. 44
Figure 3.14. XRD pattern of the ashes obtained from intact (in-) and post-extracted (pe-) biomass from *Undaria pinnatifida.* 45
Figure 3.15. XRD pattern of the ashes from pyrochars (pyro) processed at 400 °C or 800 °C derived from intact (in-) or post-extracted (pe-) biomass from *Undaria pinnatifida*. W- washed with distilled water. 46
Figure 3.16. XRD pattern of the ashes obtained from hydrochars (Hydro) derived from intact (in-) and post-extracted (pe-) biomass from *Undaria pinnatifida*. AP – Process water. Type I – Ultrapure water. The S700 refers to the steam treatment sample at 700 ºC. 46
Figure 3.17. Calibration plot of ibuprofen solution obtained using a quartz cuvette with 5 mm of optical path 47
Figure 3.18. UV absorption spectra of ibuprofen solution (60 mg/L) before and after adsorption by the selected pyrochars (Pyro) at 800 ºC and hydrochar (Hydro) with steam treatment (700 ºC) from intact (in-) and post-extracted (pe-) biomass of *Undaria pinnatifida* (PW – Process water, W – washed). 48
Figure 3.19. Calibration plot of diclofenac solution obtained using a quartz cuvette with 5 mm of optical path 48
Figure 3.20. UV absorption spectra of diclofenac solution (60 mg/L) before and after adsorption by the selected pyrochars (Pyro) at 800 ºC and hydrochar (Hydro) with steam treatment (700 ºC) from intact (in-) and post-extracted (pe-) biomass of *Undaria pinnatifida* (PW – Process water, W – washed). 49
Figure 3.21. UV absorption spectra of paracetamol solution (60 mg/L) before and after adsorption by the selected pyrochars (Pyro) at 800 ºC and hydrochar (Hydro) with steam treatment (700 ºC) from intact (in-) and post-extracted (pe-) biomass of *Undaria pinnatifida* (PW – Process water, W – washed). 49
Figure 3.22. Process water (residual from HTC at 170 °C) capacity to inhibit the growth of (A) *Serratia* sp., (B) *Vibrio* sp., (C) *Citricoccus* sp., (D) *Pseudomonas* sp., and (E) *Bacillus subtilis*. The values in each column represent the mean ± standard error of the mean (SEM) from three independent experiments carried out in triplicate. Negative control (C-) was conducted with the addiction of ultrapure water. The symbol * represent significant differences with negative control (One-Way ANOVA, Dunnett's test; $p < 0.05$). 51

Figure 3.23. Process water (residual from HTC at 170 °C) capacity to inhibit the biofilm of (A) *Serratia* sp., (B) *Vibrio* sp., (C) *Citricoccus* sp., (D) *Pseudomonas* sp., and (E) *Bacillus subtilis*. The values in each column represent the mean ± standard error of the mean (SEM) from three independent experiments carried out in triplicate. Negative control was conducted with the addiction of ultrapure water. The symbol * represent significant differences with negative control (One-Way ANOVA, Dunnett's test; $p < 0.05$) 52

Figure A 1. Poster presented at CQE Days 2024. 69

List of Tables

Table 2.1. Slurries of 2%, 4%, 6%, 8%, and 10%, measured over 5 days for each biochar. . 23
Table 3.1. Yield of extraction (w/w, %) of *Undaria pinnatifida* biomass with different solvents. DCM-MeOH – dichloromethane-methanol. 27
Table 3.2. Effect of *Undaria pinnatifida* extracts on the growth (mm) of diatoms *Chaetoceros calcitrans*, *Phaeodactylum tricornutum*, *Nitzschia* sp. and *Amphora* sp. 32
Table 3.3. Ash content, moisture and apparent density of the initial biomass (inUP) and post-extracted biomass (peUP) from *Undaria pinnatifida*. 39
Table 3.4. Yield of the hydrothermal carbonization process, ash content, moisture, apparent density and textural and surface characterization of hydrochar materials obtained from original biomass and post-extracted biomass of *Undaria pinnatifida*. 39
Table 3.5. Yield, ash content, moisture and textural and surface characterization of the steam treatment material after the process of hydrothermal carbonization with post-extracted biomass of *Undaria pinnatifida* (peUP/Hydro/1stPW/S700). The same material was also analyzed after being washed with distilled water (peUP/ Hydro/1stPW/S700/W). n.a – not analyzed. 39
Table 3.6. Yield of the pyrolysis process at different temperatures (400 °C and 800 °C), ash content and moisture, textural and surface characterization of pyrochars derived from non-extracted biomass (in-) and post-extraction biomass (pe-) of *Undaria pinnatifida*. The same material was also analyzed after being washed with distilled water (W). n.a – not analysed. 40
Table 3.7. Total pore volume, micropore volume, micropore area and external surface area of the biochar samples from *Undaria pinnatifida*. 42
Table 3.8. Atomic percentage of the elements identified in *Undaria pinnatifida* biomass (intact and post-extracted) and respective ash. 45
Table 3.9. Ibuprofen adsorption capacity for the presented biochars. 48
Table 3.10. Diclofenac adsorption capacity for the presented biochars. 49

Abbreviations and acronyms

AA - Anti-microalgal
AB - Antibacterial
ABF - Anti-biofilm
AChE - Acetylcholinesterase
AceE - Ethyl acetate
AF - Antifungal
AFp - Antifouling paint
AMF - Anti-macrofouling
AP - Process water
ATCI - Acetylthiocholine iodine
Ads - Adsorption
BET - Brunauer–Emmett–Teller
$CaCO_3$ - Calcium carbonate
CaO - Calcium oxide
$CuSO_4$ - Copper (II) sulfate
DCM - Dichloromethane
DCM:MeOH- Dichloromethane:methanol
DMSO - Dimethyl sulfoxide
DNA - Deoxyribonucleic acid
DOPA - 3,4-dihydroxy-L-phenylalanine
DTNB - Dithionitrobenzoic acid
E: W - Ethanol:water
Fe_3O_4 - Iron (II, III) oxide
HTC - Hydrothermal carbonization
IUPAC - International Union of Pure and Applied Chemistry
$MgCO_3$ - Magnesium carbonate
MgO - Magnesium oxide
NaCl - Sodium chloride
N_2 - Nitrogen
PhCs - Pharmaceutical compounds
PSU - Practical salinity unit
Pyro - Pyrolysis
PZC - Point of zero charge
QS - *Quorum sensing*
QSD - *Quorum sensing* disruptor
SEM - Scanning electron microscopy
SiO_2 - Silicon dioxide
SW - Saltwater
TBT - Tributyltin
TLC - Thin layer chromatography
TSB - Trypticase soy broth
TX - Toxins
Type I - Ultrapure water
UP - *Undaria pinnatifida*
W - Washed
XRD - X-ray diffraction
in - Intact biomass
n.a. - Not analyzed
n.i. - Not identified
pe - Post-extracted biomass

1. Introduction

1.1. Marine biofouling

1.1.1. *Definition and causes*

Biofouling is the accumulation and growth of both microscopic organisms (e.g., bacteria, diatoms, fungi, and microalgae) and macroorganisms (e.g., macroalgae, corals, anemones, tunicates, sponges, barnacles, tubeworms, bivalves, and polychaetes) on artificial structures or living surfaces (Gizer et al., 2023).

The benthic marine environment boasts remarkable diversity, making it a highly competitive setting for resources like food, space and light (Saha et al., 2018). Due to the scarcity of space, benthic organisms frequently become hosts for both microorganisms and macroorganisms (Saha et al., 2018). When the substrate is a living organism, this process is referred to as epibiosis (Figure 1.1), which typically negatively impacts the host (Saha et al., 2018). To cope with this, hosts have evolved physical or chemical defense strategies, either independently or through symbiotic relationships with bacteria (Saha et al., 2018).

Globally, over four thousand species are known to contribute to marine biofouling (Gizer et al., 2023). This colonization process creates an environment that enhances the survival and reproduction of these organisms (Gizer et al., 2023). Most aquatic fouling species prefer to settle on hard surfaces, attaching themselves to various man-made structures such as ship hulls, navigation equipment, oceanographic sensors, aquaculture installations, stationary infrastructures, industrial pipelines, basically all submerged systems can be a home for these organisms (Figure 1.2) (Gizer et al., 2023).

Figure 1.1. Green sea turtle (*Chelonia mydas*, Linnaeus, 1758) (Pendergrast. A., 2020) on the left and Loggerhead sea turtle (*Caretta caretta*, Linnaeus, 1758) (Blue World Institute, 2021) on the right, covered by epibionts such as seaweed and barnacles.

The unchecked growth of biofouling organisms on artificial structures can lead to significant malfunctions and high repair costs, estimated at around 120 billion euros annually for ship hull maintenance (Saha et al., 2018). On vessels, biofouling results in increased fuel consumption, reduced speed, hull damage, and a shortened lifespan of the vessel—all highly undesirable outcomes (Saha et al., 2018). For instance, a biofouling layer only 1 mm thick can decrease a ship's speed by 15% (Gizer et al., 2023).

Moreover, biofouling exacerbates environmental pollution by raising emissions of gases such as carbon dioxide, carbon monoxide, and sulfur dioxide (Gizer et al., 2023). Even a 5% coverage on a ship's hull can lead to a 14% increase in greenhouse gas emissions (Gizer et al., 2023). The adverse effects of biofouling extend to fishing equipment and nets, resulting in higher mark prices for economically important species like oysters and salmon (Gizer et al., 2023). Additionally, biofouling facilitates the spread of invasive species, with ports and harbors becoming hotspots for their introduction (Gizer et al., 2023). Evidence indicates that these exotic species can outcompete native ones, posing significant risks to marine ecosystems (Gizer et al., 2023).

Figure 1.2. Examples of biofouling on marine infrastructures, including pipelines, submerged systems, ship hulls, and aquaculture equipment.

1.1.2. *Biofouling – a multistep process*

The colonization process of submerged surfaces in marine environments begins almost instantaneously, driven by the high likelihood of surface settlement by microscopic organisms present in seawater (Saha et al., 2018). Typically, in one milliliter of seawater, there are around 100 bacterial cells, microalgae propagules, and benthic invertebrate larvae that contribute to this rapid colonization (Saha et al., 2018). Marine bacteria are usually the first to adhere to these surfaces, clustering to form microbial biofilms (Gomez-Banderas, 2022).

These microbial biofilms, primarily composed of bacteria and diatoms, are embedded in a matrix of extracellular polymeric substances (Gomez-Banderas, 2022). This matrix includes polysaccharides, proteins, glycolipids, and extracellular DNA, which allow the biofilms to adhere strongly to surfaces through cumulative physicochemical interactions like Van der Waals forces, hydrogen bonds, and electrostatic forces (Gomez-Banderas, 2022). While individually weak, these forces collectively provide significant mechanical stability to the biofilm (Gomez-Banderas, 2022).

As the biofilm forms, it attracts the spores of seaweed and larvae of marine invertebrates, such as barnacles, mussels, and stony corals, eventually giving rise to a more complex community that includes larger aquatic species, including plants and animals (Gomez-Banderas, 2022) (Figure 1.3). Each biofilm contains over 4 000 different bacteria, which quickly alter the physicochemical properties of the surface once they settle, further facilitating the development of a diverse and stable marine ecosystem (Gizer et al., 2023).

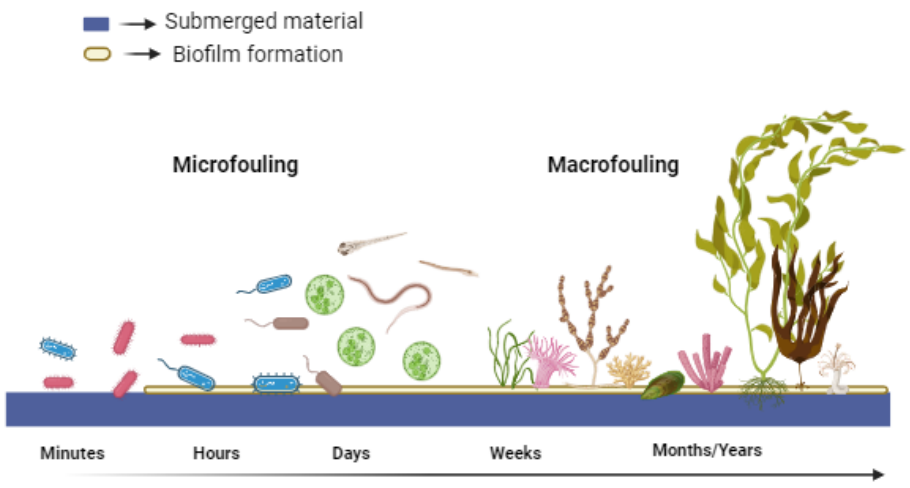

Figure 1.3. Schematic illustration of the marine biofouling stages over time (figure created with BioRender.com).

1.1.3. *Factors that influence biofouling formation*

A variety of factors influence biofouling formation, including nutrient availability, water velocity and turbulence, temperature, pH, surface characteristics, and particle sizes (Gizer et al., 2023). Key surface factors include wettability, color, and microtexture. Wettability can vary, showing behaviors like hydrophilicity and hydrophobicity, which significantly impact how fouling organisms colonize surfaces (Gizer et al., 2023). Hydrophobic surfaces have low wettability and energy, while hydrophilic surfaces have high wettability and energy (Gizer et al., 2023). Surface color also plays a crucial role in biofilm development. Experiments with different colored media—such as white, red, blue, and black—showed notable differences in cyanobacterial performance (Gizer et al., 2023). Specifically, darker colors were found to promote greater biofouling formation than lighter colors over short periods (Gizer et al., 2023).

1.1.4. *Quorum Sensing (QS)*

In the 1970s, Nealson et al. identified and described *quorum sensing* (QS) in two bioluminescent marine bacteria, *Vibrio fischeri* (Beijerinck, 1889) and *Vibrio harveyi* (Johnson & Shunk, 1936), as described in Dimitrova et al., 2023. Since then, this bacterial feature has been found in many Gram-negative and Gram-positive species. QS involves complex communication systems among bacteria that rely on gene expression in response to changes in population density (Dimitrova et al., 2023). Bacteria produce and release chemical signaling molecules known as autoinducers, with their concentration rising as the bacterial population increases (Dimitrova et al., 2023). Initially low in fresh cultures, the concentration of autoinducers reaches a threshold that allows them to bind to receptors, triggering a signaling cascade that results in coordinated changes in gene expression within the population (Dimitrova et al., 2023).

QS also enhances the mechanical stability of biofilms (Gomez-Banderas, 2022). Through cell-to-cell interactions, bacteria can recruit other organisms and organize themselves effectively on surfaces (Gizer et al., 2023). Most macrofoulants, with some exceptions like bryozoans and barnacles, depend on the prior formation of a slimy biofilm to settle on a substrate (Gizer et al., 2023).

1.1.5. *Methods used to combat biofouling*

To address the economic impacts of biofouling, several strategies have been developed to reduce its accumulation on surfaces, prevent or delay biofilm formation and the attachment of macrofoulers (Figure 1.4). When selecting the most suitable strategy, several factors should be considered, including effectiveness, safety, biosecurity, material compatibility, and feasibility (Romeu & Mergulhão, 2023). Effectiveness involves assessing the intensity and duration of antifouling activity, while safety ensures no harm to the environment or operators (Romeu & Mergulhão, 2023). The strategy should also prevent the spread of non-indigenous species and be compatible with equipment to avoid damage (Romeu & Mergulhão, 2023). Additionally, it should be cost-effective and meet infrastructure needs (Romeu & Mergulhão, 2023).

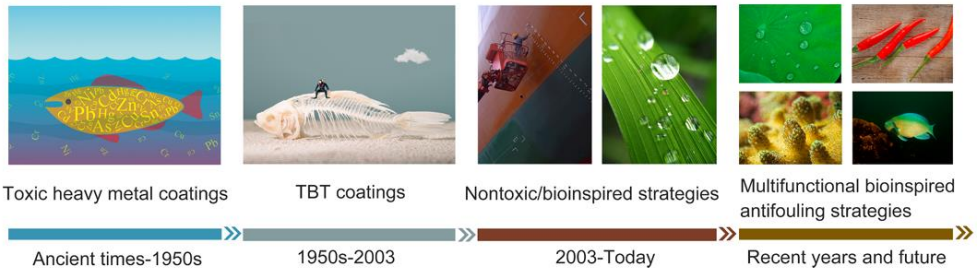

Figure 1.4. History of antifouling coatings (Jin et al., 2022).

Physical antifouling methods, such as water washing, ultrasonic cleaning, high-frequency vibration, and mechanical cleaning, are environmentally friendly options. However, these methods do not apply to all surfaces and tend to exhibit poorer antifouling performance compared to chemical coatings, which limits their effectiveness (Gizer et al., 2023).

Chemical methods are commonly employed across different industries, often involving protective coatings that contain copper-based biocides. These biocides are toxic to microorganisms, leading to cell death and preventing biofouling, however, they can harm the environment and contribute to the development of resistance (Gizer et al., 2023). Historically, the remediation of biofouling was costly and relied on highly toxic compounds like tributyltin (TBT) (Figure 1.4) and copper oxide. In these coatings, seawater gradually penetrates soluble pigment particles, resulting in controlled hydrolysis that removes TBT, layer by layer, until the coating is completely dissolved (Gizer et al., 2023).

Despite TBT's effectiveness, its harmful effects on non-target marine organisms—including toxicity, bioaccumulation, and food chain contamination—have led to a total ban on TBT-based coatings in many countries since 2008, enforced by the International Maritime Organization (Saha et al., 2018). Additionally, some non-toxic silicone-based coatings, known as foul-release coatings, have been developed. These coatings do not prevent the settlement of fouling organisms but reduce their attachment strength, allowing any accumulated biofouling to slough off as drag increases when the vessel is in motion (Dafforn et al., 2011). However, foul-release coatings have limited application since they only self-clean effectively on high-speed or high-activity vessels (Dafforn et al., 2011).

Bioinspired strategies, including nanostructured surfaces, slippery liquid-infused coatings, and natural antifouling compounds from marine organisms, are being explored for their eco-friendly and cost-effective potential. The challenge remains translating these innovations from the lab to real-world marine environments, balancing both biofouling and corrosion prevention (Romeu & Mergulhão, 2023). Natural alternatives derived from marine organisms, including primary and secondary metabolites, have been shown to inhibit the settlement of various biofouling species (Gaudêncio & Pereira, 2022). Research began with bromo-derived metabolites from red seaweed and from sponges, leading to the synthesis of over 50 analogues (Gaudêncio & Pereira, 2022). Several marine natural products with antifouling activity have been identified, including 2,5-diketopiperazine compounds from marine sponges and actinomycetes (Gaudêncio & Pereira, 2022). Notably, napyradiomycin derivatives from bacterium *Streptomyces aculeolatus* have shown potential as antifouling inhibitors, effective against both microfouling and macrofouling (Gaudêncio & Pereira, 2022).

In the quest to create environmentally friendly antifouling paints, researchers are increasingly focused on utilizing naturally occurring antifouling compounds. For these compounds to be practical for industrial applications, they need to be not only effective but

also cost-efficient to produce, durable enough to withstand harsh environmental conditions, easy to apply, and non-toxic to other marine organisms before being released into the field (Saha et al., 2018). A major hurdle in this development process is the stability of natural compounds; many do not maintain their effectiveness over time when exposed to varying environmental factors. Consequently, ensuring that these compounds can endure conditions such as temperature fluctuations, UV exposure, and salinity changes is crucial (Saha et al., 2018).

In this study, we took a different approach by testing whole crude extracts rather than isolated compounds. This method allowed us to assess the full spectrum of bioactive substances present in the natural extracts, which could work synergistically to enhance antifouling properties. By evaluating the crude extracts directly, we aimed to capture the complexity and potential of natural antifouling mechanisms more effectively. This strategy also aligns with the increasing recognition that the interactions among various compounds within an extract might lead to greater efficacy compared to single, isolated compounds.

1.2. Biotechnological potential of seaweed

Oceans cover 70% of the earth and are rich in biodiversity, which contributes to a wealth of chemical diversity, making them a renewable source of bioactive compounds (Stabili et al., 2023). Modern technologies have facilitated the exploration of marine organisms, particularly seaweed, for therapeutic agents. Seaweeds are especially notable for their bioactive compounds used in pharmaceuticals, cosmetics, nutraceuticals, biotechnology, and food (Stabili et al., 2023). Research shows that seaweed extracts exhibit various biological activities, including antiviral, anticoagulant, anticancer, antioxidant, and anti-inflammatory properties, with secondary metabolites produced as defenses against biotic and abiotic stresses (Stabili et al., 2023).

Seaweeds are efficient at photosynthesis and carbon sequestration, requiring minimal nutrients, allowing them to achieve higher yields despite their short life cycles (Tan et al., 2023). They also display diverse biochemical compositions (Tan et al., 2023). As key primary producers in marine ecosystems, they create ideal conditions for epibiont organisms. Being sessile, they are exposed to light, and their three-dimensional structure offer ample surface area for these organisms to settle (Tan et al., 2023). Consequently, seaweed evolved effective defense mechanisms, producing numerous antifouling compounds (Figure 1.5). Research has identified antifouling activity in 89 macroalgal species and 13 microalgal species, leading to the isolation of various bioactive metabolites (Saha et al., 2018).

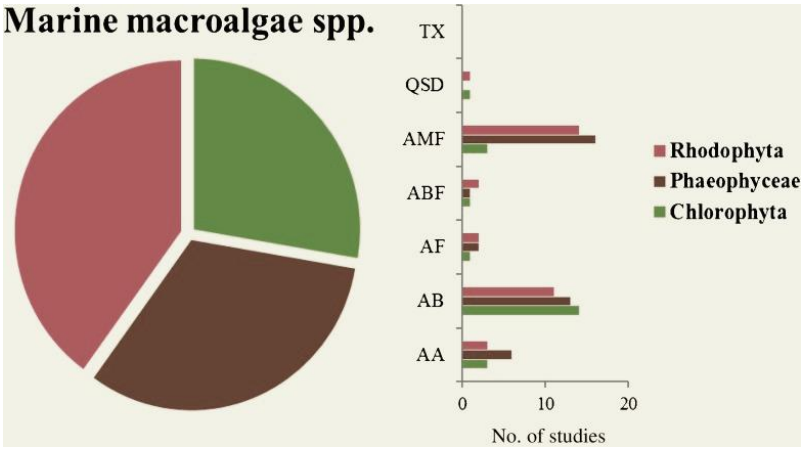

Figure 1.5. Bioactivity of metabolites or extract fractions from a total of 24 species of red seaweed (Rhodophyta), 13 species of green seaweed (Chlorophyta), and 18 species of brown seaweed (Phaeophyceae), active against marine relevant species during the period of 2010-2016. Antibacterial activity (AB), antifungal (AF), anti-microalgal including diatoms and cyanobacteria (AA), anti-macrofouling including mollusks and crustacean (AMF), *quorum-sensing* disruptor (QSD), toxins (TX), and anti-biofilm (ABF) (Saha et al., 2018).

Seaweed employs secondary metabolites as a chemical defense against microorganisms and predators. Some marine halogenated compounds help to prevent the formation of bacterial biofilms, inhibit the attachment of other seaweed, and deter barnacles from settling (Herget et al., 2017). For instance, the red alga *Delisea pulchra* (Greville) Montagne (1844), produces halogenated substances that effectively inhibit bacterial fouling without being toxic or hindering growth, they instead interfere with the bacteria's *quorum sensing* mechanisms (Herget et al., 2017).

1.2.1. *Invasive seaweed species*

The marine environment is made up of complex ecosystems with a great diversity of species. Ecosystems normally have an order and structure. However, factors such as overexploitation, pollution, and climate change severely impact these ecosystems, facilitating the introduction and spread of invasive species (Pinteus et al., 2018).

Biotic invasions occur when organisms are transported to new, often distant areas where their descendants proliferate and spread, as described by Elton (1958) cited in Mack et al., (2000). Although invasions are neither entirely new nor exclusively caused by human activities, their scale, frequency, and the number of species involved have grown dramatically due to the expansion of transportation and commerce (Mack et al., 2000). Invaders can change key ecological aspects, such as altering dominant species, ecosystem features, nutrient cycling, and plant productivity (Mack et al., 2000). The cumulative impact of human-driven invasions threatens biodiversity conservation, agricultural productivity, natural ecosystems and human health (Mack et al., 2000). More recently, invasive species are defined as those that humans intentionally or accidentally introduce into ecosystems where they do not naturally occur, leading to their establishment and growth (Pinteus et al., 2018). These species compete with native organisms, disrupt habitat structures, and contribute to biodiversity loss (Pinteus et al., 2018).

Examples of invasive seaweed include *Sargassum muticum* (Yendo) Fensholt (1955), *Asparagopsis armata* (Harvey, 1855), and *Undaria pinnatifida* (Harvey) Suringar, (1873)

(Pinteus et al., 2018). Utilizing invasive seaweed with biotechnological potential can help to preserve habitats, protect native species,and maintain local biodiversity, particularly since much of this biomass is often discarded.

1.2.1.1. *Undaria pinnatifida*

1.2.1.1.1. *Distribution*

The brown seaweed *U. pinnatifida* commonly known as wakame, is a large, brown seaweed belonging to the family Alariaceae within the order Laminariales. Native to the temperate waters of the Northwest Pacific, particularly along the coastlines of Japan, China, and Korea (Zeng et al., 2022,Yin et al., 2019) (Figure 1.6).

Figure 1.6. Main producer countries of *Undaria pinnatifida* (FAO Fishery Statistics, 2013, https://www.fao.org/fishery/en/culturedspecies/undaria_pinnatifida/en).

However, it has also become a global invasive species (Figure 1.7) and is listed among the top ten invasive species in Europe (González-Ballesteros et al., 2023). It was initially discovered in Europe in 1971 at the Etang du Thau in France (Figure 1.8). It is believed to have been introduced alongside Pacific oysters *Crassostrea gigas* (Thunberg, 1793), likely during the small, stress-resistant gametophyte stage (Minchin & Nunn, 2014).The first record in the Iberian Peninsula was in the Ría de Arousa (north-west Spain) in 1988 (Veiga et al., 2014).

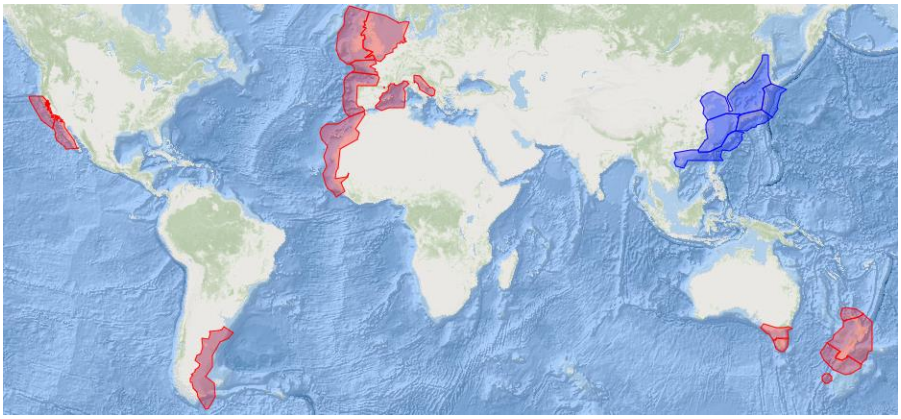

Figure 1.7. Global distribution of *Undaria pinnatifida* (Smithsonian, Environmental Research Center, https://invasions.si.edu/nemesis/species_summary/-21). In red the non-native species and in blue native species.

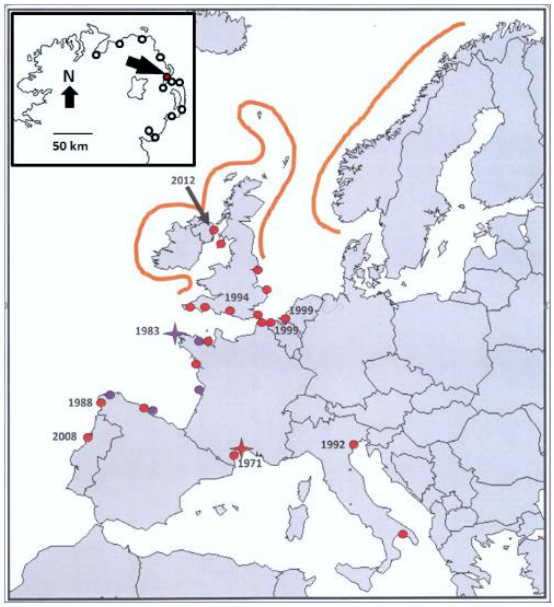

Figure 1.8. Distribution, showing dates of first records for each invaded country in Europe. Purple: cultivation of *Undaria pinnatifida*, Red: other populations. Red star: first Mediterranean record. Purple star: first Atlantic record. The first Irish record arrowed. Lines indicate the probable future range of *Undaria pinnatifida* (Minchin & Nunn, 2014).

1.2.1.1.2. *Ecology*

The brown seaweed *U. pinnatifida* is a winter annual species that inhabits temperate rocky substrates from the low intertidal to 18 m (González-Ballesteros et al., 2023). *U. pinnatifida* has an annual two-phase lifecycle, with macroscopic sporophytes and microscopic gametophytes and sporelings (Figure 1.9), their reproductive output is up to 700 million zoospores per individual (Cunningham et al., 2020). They have fast growth of 10-15 mm blade length per day (Cunningham et al., 2020). The development of reproductive maturity is rapid, occurring within 40 days of macroscopic growth (Cunningham et al., 2020). The gametophytes and plantlets have a capacity to remain dormant for extended periods of time until conditions favor their development (Cunningham et al., 2020).

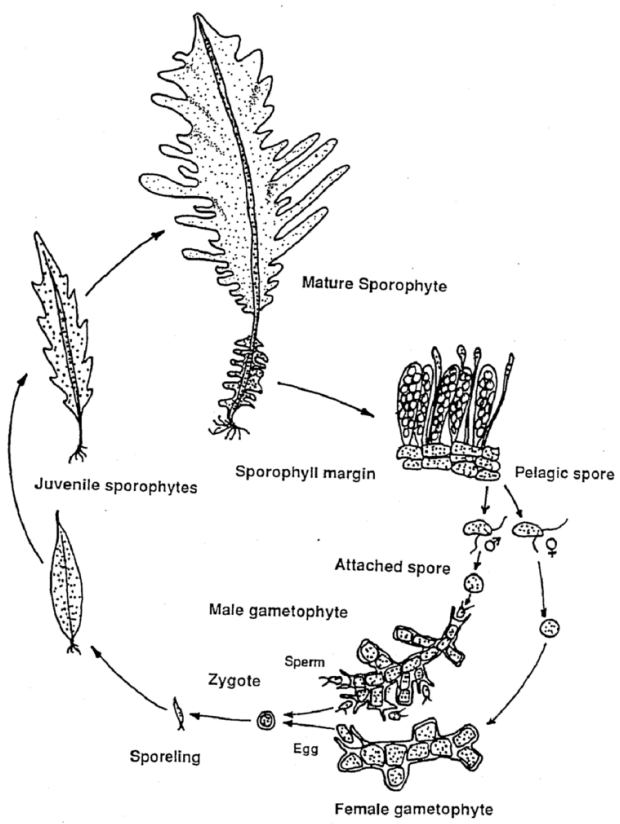

Figure 1.9. Life history of *Undaria pinnatifida* illustrating the microscopic spores, gametophytes and sporelings, and the macroscopic sporophytes (Cunningham et al., 2020).

U. pinnatifida also has tolerance to wide variations in water temperature (Figure 1.10), substrate types, wave action, nutrients, and light (Cunningham et al., 2020). Thrives primarily in fully saline conditions, with optimal salinity levels above 27 psu (practical salinity unit). It can attach at lower salinities of 19 psu, while both gametophytes and sporophytes can survive in salinities down to 6 psu, although damage may occur below 16 psu (Epstein & Smale, 2017).

According to the NASA Jet Propulsion Laboratory (n.d.), a salinity of 1 psu is equivalent to 1 gram of salt in 1000 grams of water. It is a standard measure in oceanography, typically ranging between 32 to 37 psu in the open ocean.

	Sporophyte	**Gametophyte**
Survival ranges	< 0 - > 25 ºC	< -1 - 29 ºC
Growth ranges	3.5 - 20 ºC	10 - 24 ºC
Reproductive ranges	7 - > 23 ºC	< 10 - > 24 ºC

Figure 1.10. Temperature tolerances for *Undaria pinnatifida* (Minchin & Nunn, 2014).

1.2.1.1.3. *Biotechnological potential*

U. pinnatifida is considered the most consumed brown seaweed as it has many proteins, polysaccharides and fucoxanthin (González-Ballesteros et al., 2023). Thus, its biotechnological exploration could have a positive impact in terms of biosustainability and biodiversity. Furthermore, it contains valuable pharmacological compounds with diverse biological activities, such as the prevention of hyperglycemia, the suppression of chemically induced breast tumors or the inhibition of anti-hypertension (González-Ballesteros et al., 2023). Recently, it was also revealed that polysaccharides extracted from *U. pinnatifida*, such as fucoidan, have antibacterial activity (González-Ballesteros et al., 2023).

Asian seaweed consist of several distinct parts: the blade, midrib, stipe (stem), sporophyll, and a root-like support structure (Figure 1.11). In Korea and Japan, the blade and sporophyll are popular for consumption, while in China, both the sporophyll and midrib are used as food and in traditional medicine to treat dropsy, stomach issues, and fistulas (Lee et al., 2022). Environmental factors influence characteristics like midrib and stipe length, lamina division, and sporophyll placement (Lee et al., 2022). Additionally, regional differences impact the seaweed's lipid composition (Lee et al., 2022). Currently, the blade and midrib are the most utilized parts, with the other sections often discarded, indicating a need for further research on how to make better use of the entire seaweed (Lee et al., 2022).

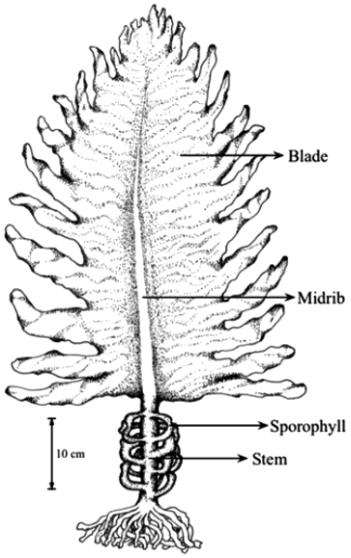

Figure 1.11. Illustration of *Undaria pinnatifida* (Yin et al., 2019).

Asian seaweeds are abundant in bioactive compounds, including phenolic compounds like phlorotannins, polysaccharides such as fucoidan and alginic acid, along with essential vitamins and minerals (Lee et al., 2022). They are also high in viscous polysaccharides and soluble fiber, making them a low-calorie food that supports dieting and may help to prevent diabetes (Lee et al., 2022). Phlorotannin from the seaweed's sporophyll has shown antioxidant, anti-inflammatory, and antimicrobial properties (Ferreira et al., 2021), while fucoidan offers antioxidant, anticancer, and antibacterial benefits (Lee et al., 2022).

The amount of *U. pinnatifida* waste is greater than 200,000 tons/year in Japan, leading to environmental difficulties (Yin et al., 2019). Furthermore, *U.* pinn*atifida* has been regarded as a dangerous invasive seaweed species worldwide, posing an important threat to marine ecosystems because it can grow rapidly and multiply in various environments (Yin et al., 2019). Given this background, making full use of this seaweed is an urgent issue.

The concentrations of polyphenols, flavonoids, fucoxanthin, epicatechin, and gallic acid contents in seaweed reportedly depend on many variables such as habitat, season of harvesting, and environmental conditions including light, temperature, and salinity. Because *U. pinnatifida* has a higher amount of fucoxanthin than other seaweeds, it has recently attracted much attention from researchers (Yin et al., 2019).

1.3. Circular Economy

Circular and resource-efficient economic models consider the entire material cycle to promote reuse as well as waste reduction and efficient resource utilization and are increasingly replacing linear economic models based on production-consumption-disposal systems (Athanasiadou et al., 2023). This new model seeks to maintain balance between economic and environmental issues (Athanasiadou et al., 2023).

The concept is to maximize the use and exploitation of secondary materials and byproducts, close the cycle of linear production, and promote the sustainable development of business, society, and the environment (Athanasiadou et al., 2023).

One of the objectives of this work is the development of a circle economy by optimizing the use of all the biomass of this seaweed. *U. pinnatifida* has several applications in the industry, being widely used as food and having interesting compounds to explore in biotechnology, however, there are discarded parts that are normally not suitable for consumption due to their rigidity or simple waste after the use of other parts of the seaweed. To combat this waste, the remaining biomass can be further valorized through the production of biochars which can have a panoply of applications.

1.4. Biochar

Biochar is the product of thermal degradation of organic materials in the absence of air (pyrolysis) and is distinguished from charcoal by its use as a soil amendment, definition attributed to Lehmann and Joseph (2009) and cited in Lehmann et al. (2011). Biochar has been described as a possible means to improve soil fertility as well as other ecosystem services and sequester carbon (C) to mitigate climate change (Lehmann et al., 2011). The word biochar comes from biomass (bio) and coal (char). The raw material source of biochar consists of a wide range of biomass, such as fruit waste, sawdust, wood, rice straw and other waste (Tan et al., 2023). Although the term 'biochar' is commonly associated with soil amendment applications, the term is used in this work to describe the materials prepared and tested for the adsorption of pharmaceutical compounds from water, rather than for agricultural purposes. In recent studies, the term 'biochar' has also been applied to describe its use in a variety of environmental applications, including water treatment and pollutant removal, beyond its traditional association with soil improvement.

Biomass is converted into biochar mainly through thermochemical processes like pyrolysis and hydrothermal carbonization (HTC). Pyrolysis is the conventional process and involves heating the biomass in the absence of oxygen at temperatures between 300 and 700 °C, with factors such as temperature, heating rate, residence time, and feedstock characteristics significantly affecting the pyrochar yield; lower temperatures, longer residence times, and slower heating rates enhance production (Yu et al., 2017). In contrast, HTC is a

newer technique that converts carbohydrate components of biomass into carbon-rich solids in water at lower temperatures (180–260 °C) and elevated pressures (up to 10 bar), eliminating the need for drying wet biomass (Yu et al., 2017). HTC is inspired in the natural processes of coal formation that take millions years and request temperature and pressure in a nonoxidizing atmosphere to transform biomass into a carbon-rich material (Mestre & Carvalho, 2018). This method is not only environmentally friendly and cost-effective but may also yield hydrochar with lower energy requirements compared to traditional carbonization processes like pyrolysis, making it particularly advantageous for the valorization of wet precursors and wastes (Yu et al., 2017).

In recent years, biochar and biochar-derived activated carbon materials have attracted increasing attention for the adsorption of heavy metals, pesticides, antibiotics, microplastics and organic pollutants in water through different mechanisms such as electrostatic adsorption, physical adsorption, and hydrophobic force (Tan et al., 2023). The adsorption performance of biochar and derived materials is closely related to their surface parameters such as specific surface area, surface charge, pore size and type of functional group, these physicochemical properties vary with preparatory conditions, biomass sources and synthesis protocols (Tan et al., 2023). It is recognized that higher hydrophilicity of the surface of biochar and derived materials is favorable to the adsorption of heavy metals, while higher hydrophobicity is favorable to the adsorption of organic pollutants like dyes and antibiotics (Tan et al., 2023).

1.4.1. *Biochar from seaweed*

Biochar possesses diverse properties — such as pore structure, aromaticity, polarity, hydrophilicity/hydrophobicity, surface charge, and pH — that influence its effectiveness in adsorption and catalysis, which vary according to the biomass source and preparation methods (Tan et al., 2023). Seaweed waste can be converted into biochar with significant potential for bioremediation, either in its natural form or through modifications to enhance its efficacy (Pinteus et al., 2022). One notable advantage of seaweed biochar is its recyclability; it can release its adsorbed chemical components and be reused for further adsorption applications. Seaweed biochars are frequently obtained by pyrolysis process of the seaweed biomass and can achieve a highly adsorbent, porous, carbon-rich material (Pinteus et al., 2022).

Additionally, the physical and chemical properties of seaweed biochar can be tailored to improve specificity and efficiency for targeted compounds, enhancing its recycling potential (Pinteus et al., 2022). Seaweed biomass is rich in minerals such as magnesium, calcium, sodium, and potassium, while typically having low carbon content, which contributes to its high cation exchange capacity, and tends to have a wider range of microporosity, making it particularly effective at absorbing various pollutants, especially metal ions (Pinteus et al., 2022). Studies indicate that marine biomass yield more biochar than terrestrial plants from the same biomass due to their lower lignin content, and they demonstrate greater efficacy in removing contaminants from aqueous environments (Pinteus et al., 2022).

1.5. Aim and outline of the thesis

The aim of this thesis is to:

1. Select green solvents for the extraction of bioactive compounds from the invasive brown seaweed *Undaria pinnatifida*.
2. Evaluate the antifouling potential of the extracts against bacterial growth, biofilm formation, *quorum sensing* mechanism, diatoms growth and enzymes activity.
3. Investigate the production of biochar from non-extracted (intact) and post-extracted *Undaria pinnatifida* biomass through slow pyrolysis and hydrothermal carbonization.
4. Assess the adsorption capacity of the resulting biochars for pharmaceutical contaminants in water.
5. Assess the antimicrobial and biofilm inhibition potential of the process water from the hydrothermal carbonization.

2. Materials and Methods

2.1. Seaweed biomass

The brown seaweed *Undaria pinnatifida* was collected from Estai Cape (42°11'13.2" N, 8°48'53.4" W) in Spain. After collection, the fresh algal biomass was sorted and sediments and epibionts removed, rinsed with fresh water, and dried in a wind tunnel at 25 ºC, and after, ground to a fine powder (50 µm). This powder was then stored under vacuum, in the dark, at room temperature until usage, as described by Ferreira et al. (2021). Additionally, pre-prepared extracts from the same seaweed species collected in Figueira da Foz, Portugal, were also evaluated. Biochemical and biological assays for antifouling evaluation — encompassing both microscopic and macroscopic analyses — were conducted at MARE-IPLeiria lab facilities. Additionally, biochar production, the chemical composition of biochars obtained from the intact (meaning it was not extracted) and post-extracted seaweed biomass, as well as assessments of their bioremediation potential, were carried out at the Department of Chemistry and Biochemistry, Faculty of Sciences, University of Lisbon.

2.2. Solvents

Solvents for extraction purposes were sourced from different suppliers: ethanol – 99,5% (AGA-Álcool e Géneros Alimentares, Lisbon, Portugal); *n*-hexane (CARLO ERBA reagents - Emmendingen, Germany); ethyl acetate (Labchem, Zelienople, PA, USA), while the ultrapure water (also known as type I water) was obtained in lab from a Mili-Q Water System (Merck KGaA, Darmstadt, Germany).

2.2.1. *Extractions*

Two extraction methodologies were performed: one with ethanol-water (80:20) and a sequential extraction with solvents of increasing polarity: *n*-hexane, ethyl acetate, ethanol, and water (Figure 2.1). The biomass-to-solvent ratio used for these extractions was 1:20, as previously optimized in our laboratory.

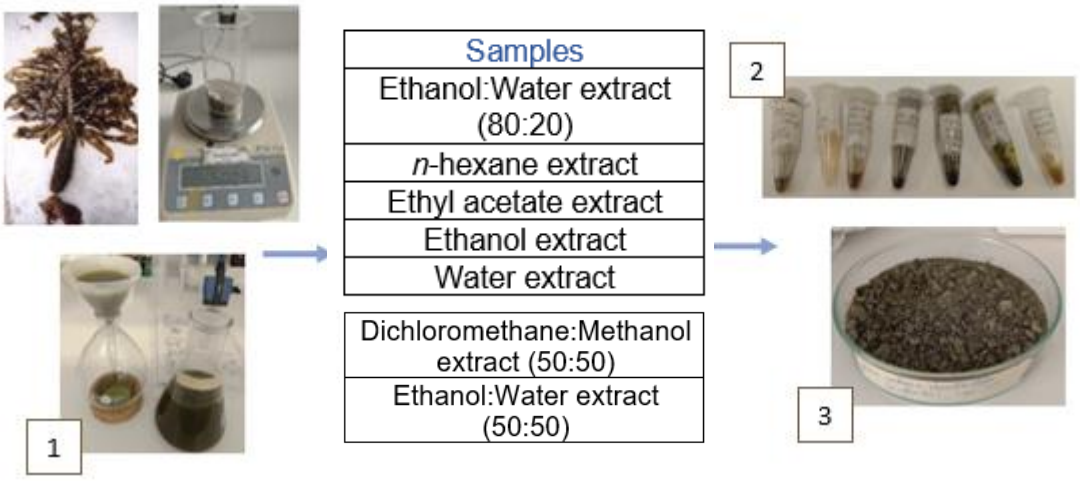

Figure 2.1. Preparation of the extracts to be tested: (1) extractions, (2) stock solutions of each extract and (3) remaining biomass obtained from the process.

To begin the extraction process, powdered seaweed was weighed (50 g) and mixed with the hydroethanolic solvent (1000 mL). The mixture was stirred (600 rpm) for 3h, at room temperature, and protected from light. The resulting organic solution was then filtered (Fisherbrand® qualitative filter paper, nº 4) and concentrated to dryness at low temperature (40 °C) under vacuum in a rotary evaporator (Laborota 4000, Heidolph, Germany).

For the sequential extraction process, the dried seaweed (50 g) was extracted with *n*-hexane (1000 mL), stirred (3 h), at room temperature and protected from light. The resulting solution was filtered (VWR® qualitative filter paper, nº4) and the solvent was removed in the rotary evaporator. Next, ethyl acetate was added to the remaining seaweed biomass and the process was repeated with ethanol, followed by ultrapure water. The final extract obtained with ultrapure water was more viscous due to the presence of polysaccharides, necessitating centrifugation (Eppendorf® Centrifuge 5810/5810R) before solvent evaporation in the rotary evaporator. Five extracts were ultimately obtained, and the leftover seaweed biomass was reserved for biochar synthesis. Two pre-prepared extracts of the same seaweed species, obtained with dichloromethane: methanol (50:50) and ethanol: water (50:50) were also tested.

2.2.2. *Chemical profile of extracts*

A preliminary chemical profile of the obtained extracts was performed by thin layer chromatography (TLC) using aluminium TLC plates (Kieselgel 60 F_{254}, Merck, Darmstadt, Germany). Elution systems were composed of mixtures of *n*-hexane:ethyl acetate; dichloromethane:methanol or ethanol:water. Small aliquots of each sample were applied in the baseline of the silica-gel plate, which was then dried at 50 °C. After elution, plates were dried again and visualized under UV light (254 nm; 365 nm). Afterwards, plates were sprayed with a revealing solution (10 % concentrated sulfuric acid in ethanol) and heated to 200 ºC to visualize compounds not detected under the UV light.

2.3. Biological evaluation

For *in vitro* bioassays, stock solutions of each extract were prepared in dimethylsulfoxide (DMSO) (Sigma, Steinheim, Germany) at a concentration of 100 mg/mL.

2.3.1. *Ecotoxicity studies*

Despite the extracts being from natural sources in this study, their ecotoxicity is a relevant characteristic for their applicability as a biofouling sustainable solution.

Considering the main goal is to replace current biocides, it is important to assess how they might affect nontarget aquatic organisms. The brine shrimp *Artemia salina* (Linnaeus, 1758) were used in this assay for ecotoxicity assessment, due to their wide geographical distribution, adaptability to wide ranges of salinity (5–250 g L^{-1}) and temperature (6–35 °C), short life cycle, high fecundity, small body size, and adaptability to varied nutrient resources as it is a non-selective filter feeder (Nunes et al., 2006).

Artemia cysts (Ocean Nutrition (ref 3367)) were decapsulated before being stored in a refrigerator chamber at 4 °C. Then, cysts were incubated in seawater with high aeration for approximately 24 h.

One *Artemia salina* was placed in each well of a 96-well plate with seawater. The

negative controls were prepared with sea water only and DMSO, while an antifouling paint was used as a positive control. The concentration used in this study was 1 mg/mL and there were 6 replicas of each tested component. Ecotoxicity was determined as the percentage of survival relative to control. Three independent assays were carried out.

2.3.2. *Antifouling activity*

2.3.2.1. *Antimicrobial activity against marine bacteria*

The antibacterial potential of *Undaria pinnatifida* extracts was tested against 4 biofilm-forming bacteria, previously isolated from the surface of macroalgae (Horta et al., 2014): *Citricoccus* sp., *Vibrio* sp., *Serratia* sp., *Pseudomonas* sp.; and *Bacillus subtilis* (DSM 6633; obtained from the DSMZ-German collection of Microorganisms and cell cultures GmbH).

Following the method described by Pinteus et al., (2021) the bacteria were cultured in Trypticase Soy Broth (TSB), with 1.5% NaCl at 30 °C. *B. subtilis* was cultured in TSB without NaCl at 37 °C. An overnight culture of each microorganism was used to inoculate a 96-well plate, adjusting the OD600 to 0.15 ± 0.01. The extracts were tested in a gradient of concentration between 62.5 and 1000 µg/mL, obtained through serial dilution in the 96-well plate.

DMSO served as the negative control (< 2%), while oxytetracycline functioned as the positive control. Bacterial growth was measured by measuring the optical density at 600 nm using a microplate reader (Synergy H1 Multi-Mode Microplate Reader, Biotek Instruments). The growth percentage relative to the control was calculated from data obtained in the exponential growth phase of each microorganism. Each experiment was performed in triplicate across three independent trials for reliability.

2.3.2.2. *Biofilm inhibition activity*

To assess the ability of each extract to inhibit biofilm formation, the same biofilm-producing bacteria from the antibacterial assay were used. The initial steps of the antibiofilm assay mirrored those of the antibacterial assay. The negative control was conducted with DMSO. After 30 h incubation, bacteria were removed from the wells, and washed with distilled water. The attached bacteria were stained with 220 µL of 0.4% crystal violet solution (w/v) for 15 min. Excess stain was removed by washing thoroughly with water. The stained biofilms were solubilized with 225 µL of 30% acetic acid, incubated for 5 min and then read spectrophotometrically at 550 nm, using a microplate reader (Synergy H1 Multi-Mode Microplate Reader, Biotek Instruments, Winooski, USA). Each assay was performed in triplicate across three separate experiments to ensure reliable results. The biofilm formation was determined as a percentage of biofilm relative to negative control.

2.3.2.3. *Quorum sensing inhibition activity*

Quorum sensing inhibition capacity was assessed using the reporter bacteria *Chromobacterium violaceum* CV026 (DSM 30191; obtained from the DSMZ-German collection of Microorganisms and cell cultures GmbH) which produces a violet pigment on standard laboratory media. Bacteria were cultured in TSA at 30 °C, and samples tested by the disk diffusion method (1 mg/disk). DMSO and 5-fluorouracil were used as negative and positive control, respectively. The plates were incubated at 30 °C for 24 hours, and checked for any reduction in pigment production. This assay was performed in triplicate.

2.3.2.4. *Inhibition of microalgae growth*

Chaetoceros calcitrans (Paulsen) Takano, (1968), *Phaeodactylum tricornutum* (Bohlin, 1897), *Nitzschia* sp., and *Amphora* sp. were obtained from MARE-IPLeiria biobank and were grown in F2 medium (Nutribloom, Necton, Olhão, Portugal) with silicates, at 20 °C, under a 16/8 (light/dark) photoperiod.

The growth inhibitory potential was assessed using the disk diffusion method, following the protocol described by Pinteus et al. (2021). Initially,10 mL of a 8 days diatom culture was concentrated at 4000 rpm for 5 minutes, and 100 µL were used to inoculate F2 solid media (F2 media with silicates and 1.5% agar). Extracts (1 mg/disk) were applied onto 6 mm paper disks, and placed onto the inoculated agar surface. DMSO was used as a negative control, while $CuSO_4$ was used as a positive control (1 mg/disk). This assay was performed in triplicate to ensure reliable results. The plates were incubated at 20 °C under a constant photoperiod of 16/8 hours (light/dark) for 15 days. Finally, the inhibition halos around the disks were measured using a ruler.

2.3.2.5. *I*n vitro *enzymatic assays*

The enzymes acetylcholinesterase (AChE) and tyrosinase were associated with the adhesive processes in the settlement of different biofouling species (Gaudêncio & Pereira, 2022), studying the inhibition of these enzymes can provide valuable insights into disrupting the settlement of biofouling organisms, potentially leading to the development of effective antifouling strategies. DTNB (5,5'-Dithiobis 2-nitrobenzoic acid), ATCI (acetylthiocholine iodine), Donepezil, L-DOPA (3,4-dihydroxy-L-phenylalanine) and Kojic acid were obtained from Sigma.

2.3.2.5.1. *Acetylcholinesterase inhibitory activity*

The acetylcholinesterase inhibition assay followed the method previously described by Sharififar et al. (2012) and modified by Pinteus et al., (2021). A reaction mixture was prepared by adding 156 µL of 200 mM phosphate buffer at pH 7.7, 2 µL of extract, 20 µL of DTNB (prepared by dissolving 3.96 mg of DTNB and 1.5 mg of sodium bicarbonate in 10 mL of phosphate buffer, pH 7.7), and 2 µL of enzyme (2 U/mL). After incubating the mixture at 25 °C for 5 minutes, 20 µL of ATCI (10.85 mg dissolved in 5 mL of phosphate buffer) were added and incubated again for 10 minutes at 25 °C. Extracts were tested at concentrations of 1000 µg/mL, 500 µg/mL, and 250 µg/mL, using DMSO as the negative control and Donepezil (400 µg/mL) as the positive control. Blanks were run for each sample without adding the enzyme. The assay was conducted in triplicate within three different experiments to ensure consistency and accuracy of the results. The reaction absorbance was measured at 412 nm using a Synergy H1 Multi-Mode Microplate Reader (Biotek Instruments, Winooski, USA), and enzymatic activity was calculated relative to the control (the activity of enzyme without samples), as follows in equation 2.1:

$$\text{Enzymatic activity } (\%) = \left(\frac{(A_c - Ab_c) - (A_s - A_b)}{A_c - Ab_c}\right) * 100 \qquad \text{(Eq. 2.1)}$$

Ac – Absorbancy of control
Abc– Control blank absorbancy

As– Absorbancy of the extract to be tested
Ab– Absorbancy of the extract blank

2.3.2.5.2. *Anti-tyrosinase activity*

The tyrosinase inhibition assay followed the method described by Susano et al., 2022. It was added 68 µL of 0.5 mM potassium phosphate buffer at pH 6.8, 2 µL of extract, 100 µL of L-DOPA (1mM dissolved in potassium phosphate buffer). Control blanks were run for each sample without adding the enzyme. After incubating the mixture at 37 °C for 5 minutes in the dark, 30 µL of the enzyme (100 U/mL) (with the plate on ice) were added. Read at 475nm, every minute thereafter for 15 min in the Synergy H1 Multi-Mode Microplate Reader (Biotek Instruments, Winooski, USA). Extracts were tested at concentrations of 1000 µg/mL, 500 µg/mL, and 250 µg/mL, using DMSO as the negative control and Kojic acid as the positive control. The assay was conducted in triplicate across three separate experiments to verify the reliability and reproducibility of the results. The inhibition was calculated with the same formula of the anti-acetylcholinesterase assay (Equation 2.1).

2.3.2.6. *Antifouling field assay*

The *Undaria pinnatifida* extracts were incorporated into an inert paint (Titanlux ecológico,Titan), at a concentration of 2.5 mg/mL, based on laboratory findings and comparisons with similar antifouling studies. For each test plate, 2 mL of this paint-extract mixture was applied in two layers. Plates coated with only inert paint served as the negative control, while those with commercial antifouling paint were used as the positive control.

All plates were weighed prior to exposure and then randomly placed in a crate, which was submerged at the Marina de Peniche (39°21'19.3" N, 9°22'34.1" W) for a period of two months (Figure 2.2). After retrieval, the plates were washed gently for debris, dried overnight in a fume hood, and reweighed. The results were expressed as a percentage of biofouling relative to the controls, and each condition was tested in triplicate to ensure accuracy.

Figure 2.2. Acrylic plates painted with non-active paint incorporated with samples, fixed to the crate and lowered in the Marina of Peniche (Leiria, Portugal) in May of 2024.

2.4. Valorization of the post-extracted seaweed biomass

Another objective of this work was the valorization of the post-extracted biomass from *U. pinnatifida* through the production of biochar by using processes such as slow pyrolysis and hydrothermal carbonization, their characterization, and comparison with biochars

obtained from the intact seaweed biomass. The remediation potential of the obtained biochars was assessed by testing the adsorption of pharmaceutical compounds: diclofenac, ibuprofen and paracetamol (Figure 2.3).

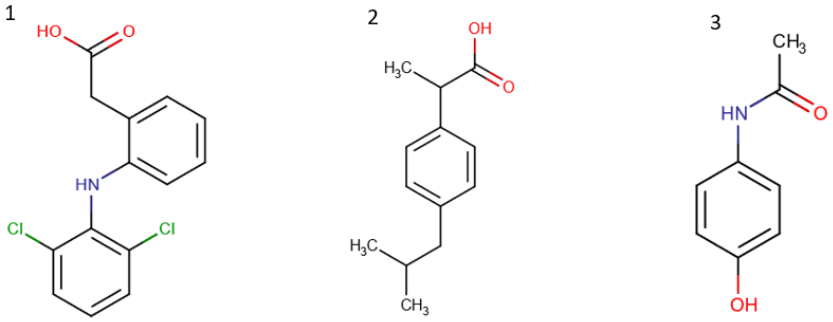

Figure 2.3. Chemical structures of (1) Diclofenac, (2) Ibuprofen, and (3) Paracetamol (Acetaminophen) (https://go.drugbank.com/drugs).

2.4.1. *Carbonization of seaweed biomass*

The biochars used in this study were produced from the intact and post-extracted biomass of the brown algae *Undaria pinnatifida*, harvested from Spain. Two thermochemical processes were employed for their production: slow pyrolysis and hydrothermal carbonization (HTC). Slow pyrolysis involved the thermal decomposition of the algae in an oxygen-limited environment. Conversely, HTC was performed under subcritical water conditions, producing hydrochar with distinct physicochemical properties. Additionally, an attempt was made to enhance the properties of the hydrochar through steam activation, aiming to increase its porosity and surface area.

2.4.1.1. *Slow pyrolysis*

For the conventional approach, slow pyrolysis was assayed using 6 g of sample, weighted in a small ceramic boat, placed in a horizontal oven (Thermolyne, model 21 100), equipped with a stainless-steel tube and closed with a lid with a small slit for gas exit or other substances, shown in Figure 2.4 (1). The carbonization occurred at 10 °C/min heating up to 400 °C followed by a plateau of 1 h and cooling down until room temperature, always under N_2 flow $(5\ cm^3/s)$. The process was repeated with a temperature of 800 °C, to evaluate the influence of the carbonization temperature in the biochar produced at different temperatures.

2.4.1.2. *Hydrothermal carbonization*

For the process of hydrochar production (from intact and post-extracted seaweed biomass) 3 g of sample was weighted (in duplicate) and placed in a Teflon line stainless steel autoclave with subsequent addition of 10 cm^3 of ultrapure water as presented in Figure 2.4 (2), heated at 170 °C for 24 h in the oven (Medline Scientific Limited, model ON-O2G). The autoclave was cooled down to room temperature, and the solid product was washed with distilled water and then filtered (VWR®, Qualitative filter papers, grade 415). Five filtrations were carried out with 1000 mL of distilled water each, three with cold water and two with heated water (200 °C) until the water no longer came out colored and the pH was close to

distilled water.

Then, the hydrochar would dry in the oven overnight (110 °C), weighed the next day and crushed in an agate mortar to obtain a powder with < 150 µm, for consistency in results once in the liquid phase assays.

One of the HTC was executed with the addition of 10 cm^3 of process water (1st PW and repetition - 2nd PW) obtained upon filtration process of a previous synthesis in the same conditions instead of the ultrapure water (Type I). The aim of this process was to reuse the process water and to check whether there was an increase in yield percentage and possible changes in the resultant biochar properties. The remaining water from the filtration process was stored at -20 °C until it was tested against biofilm-producing bacteria or was tested for its antimicrobial activity, in a way to create a biorefinery process and in the search of a possible application for this process water that would otherwise be discarded.

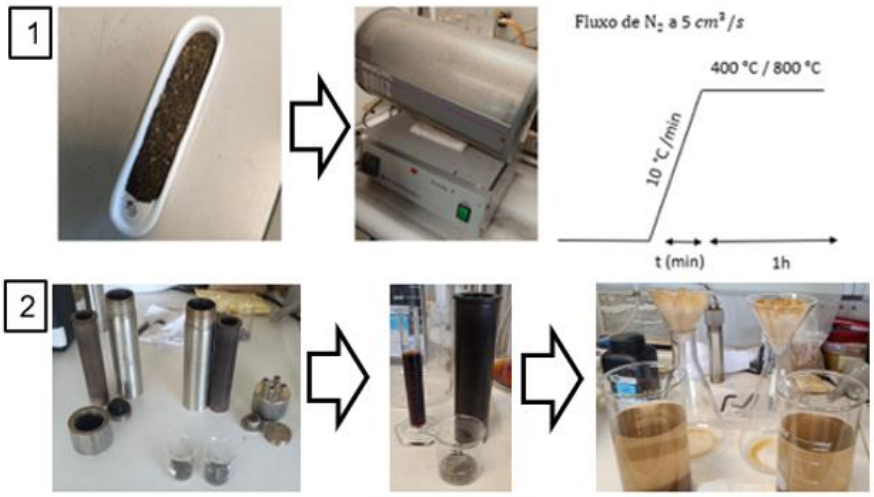

Figure 2.4. Process of Pyrolysis (1) and process of Hydrothermal carbonization (2).

2.4.1.3. *Steam activation*

The hydrochar prepared with post-extraction *U. pinnatifida* using the process water of a previous similar synthesis (peUP 1st PW) was submitted to physical activation with steam at 700 °C for 1 h in a vertical furnace (Thermolyne, model 21100) (Figure 2.5) under a nitrogen flow of 5 $cm^3\ S^{-1}$ and using a heating rate of 10 °C min^{-1}. After cooling down to room temperature under N_2 flow, the materials were crushed to a fine powder (particles with dimensions <150 µm). This procedure followed the conditions previously described in Mestre et al. (2007) and Mestre et al. (2019).

Figure 2.5. Vertical furnace (Thermolyne, model 21100).

2.4.1.4. *Nomenclature of the materials*

The nomenclature of the materials prepared in this study is summarized in the following:

- Pyrolysis precursor in- (intact) or pe- (post-extracted)/Pyro(temperature)/W (if washed with water)

  Examples: in/Pyro400 or pe/Pyro800/W

- HTC precursor in- (intact) or pe- (post-extracted)/Hydro/type of solution (type I water or 1st PW/2nd PW if reusing process water)/S700 (if steam treated)

  Examples: in/Hydro/TypeI or pe/Hydro/1st PW/S700

2.4.2. *Characterization of biochars from Undaria pinnatifida*

2.4.2.1. *Moisture and ash*

The moisture content was estimated by calculating the difference in the weight of the biochar before and after being placed in the oven (Medline Scientific Limited, model ON-O2G) at 110 °C, overnight, according with equation 2.2.

The ash content of the biochar was estimated by the mass residue left after the combustion of the samples in air, according to Mestre et al. (2007). Initially, 100 mg of biochar was placed in a small ceramic boat and dried overnight in the oven (Medline Scientific Limited, model ON-O2G) at 110 °C. After weighing the dried sample in a Mettler AE 240 analytical balance, it was introduced in a muffle (Nabertherm L3/12/P320) heated at 650 °C for 2 h. After cooling to a temperature near 150 °C, the sample was placed in a desiccator to reach the ambient temperature and then weighed. The ash content was calculated as shown in equation 2.3, and for some materials it was determined in duplicate.

$$\%\ Moisture = \frac{m\ (initial) - m\ (final)}{m\ (initial)} \text{ x } 100 \qquad \text{(Eq. 2.2)}$$

$$\%\ Ash = \frac{m\ (ash)}{m\ (dry\ sample)} \text{ x } 100 \qquad \text{(Eq. 2.3)}$$

2.4.2.2.*Surface chemistry (pH at the point of zero charge, pHpzc)*

The Point of Zero Charge (PZC) is a key property that describes the surface charge characteristics of materials like biochar. It represents the pH at which the material's surface has no net charge, meaning the positive and negative charges are balanced. This property is crucial for understanding how the material interacts with its environment, particularly in water-based systems, influencing processes like adsorption, catalysis, or ion exchange. The PZC is determined using a method called reverse mass titration, which examines how the pH of a mixture (or slurry) changes with varying amounts of the solid material, following the method described in Mestre et al., (2007).

Powdered biochar (100 mg) is mixed with ultra-pure water obtained from a Milli-Q: water purification system (Millipore, Bedford, MA, USA) and treated to remove carbon dioxide by adding nitrogen gas and sealing the container. Mixtures are prepared at different solid-to-liquid ratios, specifically 2%, 4%, 6%, 8%, and 10% (by weight, m/m) (Table 2.1 and Equation 2.4). Each slurry is stirred at 700 rpm for at least 24 hours to reach equilibrium. The pH of the slurry is measured three times to ensure accuracy, and the average pH value is recorded. The measured pH values are plotted against the solid weight fractions (concentration of biochar in the mixture). A plateau (a flat or stable section) on the curve indicates where the pH stops changing significantly. The pH value at this plateau corresponds to the PZC of the biochar.

Table 2.1. Slurries of 2%, 4%, 6%, 8%, and 10%, measured over 5 days for each biochar.

1º Day	2º Day	3º Day	4º Day	5º Day
10%	8%	6%	4%	2%
0.9 mL of water added	0.25 mL of water added	0.41 mL of water added	0.84 mL of water added	2.5 mL of water added

$$\% \text{ (m/m)} = \frac{\text{m (sample)}}{\text{m (sample)} + \text{total volume of water}} \text{ x } 100 \qquad \text{(Eq. 2.4)}$$

2.4.2.3. *Apparent density*

The biochar apparent density was calculated, according to equation 2.5 and as reported in Mestre et al. (2019). The samples was added with a micro spoon spatula in a graduated beaker of 5 mL and tapped in a rubber pad for several minutes until the surface was well compacted. The volume and mass was then recorded, and the process was repeated three times. The apparent density corresponds to the mean value of at least three assays and the final value was calculated with the % moisture previously determined in previous topic 2.4.2.2.

$$\text{Apparent density} = \frac{\text{weigh of sample in g}}{\text{volume of sample in } m^3} \text{ x } \frac{100 - \% \text{ Moisture}}{100} \qquad \text{(Eq. 2.5)}$$

2.4.2.4. *N_2 Adsorption isotherm at -196 ºC*

The textural characterization of biochar was made by analysis of N_2 adsorption isotherm at -196 °C, in a NOVA 2200e equipment from Quantachrome. Each sample (100 mg) was previously outgassed at 120 °C for about 16 h under vacuum (pressure < 10^{-2} Pa). The textural parameters reported in the results and discussion sections were obtained from the report generated by the equipment software.

2.4.2.5. *Scanning electron microscopy with Energy-Dispersive X-ray Spectroscopy (SEM-EDS)*

The morphology of the elements in the original biomass and biochars was evaluated by Scanning Electron Microscopy (SEM) performed at a Phenom ProX apparatus using 15kV as accelerating voltage. These analysis were carried out by specialized infrastructure technicians.

2.4.2.6. *X-ray diffraction (XRD)*

The crystallinity of selected samples was assessed by powder X-ray diffraction (XRD) data obtained in a Pan analytical PW3050/60X'Pert PRO apparatus equipped with a X'Celerator detector and with automatic data acquisition (X'Pert Data Collector (v2.0b) software). The diffractograms were collected at room temperature using monochromatized CuKa radiation as incident beam (40 kV-30 mA), the range of 10-80 was scanned with a step size of 0.017 and a time per step of 100s. These analysis were carried out by specialized infrastructure technicians

2.4.3. *Preliminary assays in liquid phase*

Biochars were tested for the removal of three pharmaceutical compounds (PhCs) – ibuprofen (Fluka Analytical), diclofenac (J62609 Alfa Aesar) and paracetamol (Merck Schuchardt, Germany) – from aqueous solution, following the protocol used by Mestre et al., (2019). These solutions were prepared with ultra-pure water (Millipore, Bedford, MA, USA) at the concentrations of 60 mg/L. Before the tests as adsorbents of PhCs in liquid phase each biochar was previously dried overnight at 110 ºC. The 12 mg of previously dried biochar was added to 9 mL of the PhC solution in glass vials maintained at 30 ºC (water bath, Grant GD100 controller) and stirred at 700 rpm (multipoint agitation plate Variomag Poly 15) for 24 h (Figure 2.6).

After removing the biochar by filtration with a syringe filter of 0.45 µm, the amount of PhC remaining in solution was determined by UV–vis spectrophotometry (Genesys 10S) at the wavelength of maximum absorbance (222 nm for ibuprofen, 276 nm for diclofenac, and 243 nm for paracetamol) using quartz cuvettes with a 5 mm optical path, and the amount adsorbed onto the biochar was calculated with equation 2.6 (Mestre et al., 2007).

$$q_e = \frac{C_0 - C_f}{m} \text{ x } V \qquad \text{(Eq. 2.6)}$$

q_e - adsorption capacity in mg of pharmaceutical per gram of biochar (mg/g).
C_0- initial pharmaceutical concentration in mg/L.
C_f - final pharmaceutical concentration in mg/L.
V - volume of the solution in L.
m - mass of biochar used in g.

Calibration curves for ibuprofen and diclofenac were constructed to quantify the compounds during the analysis. Standard solutions of ibuprofen were prepared at concentrations of 30, 60, 90, and 120 ppm using ultra-pure water and 30, 60 and 90 ppm for diclofenac. The absorbance of these solutions was measured at the characteristic wavelength of each compound and plotted against the corresponding concentrations to generate a linear calibration curve. The calibration equations and coefficients of determination (R^2) were determined and presented in the results section.

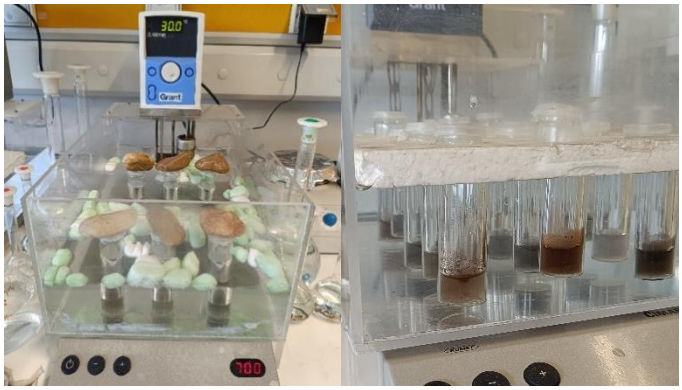

Figure 2.6. Preliminary assay to assess the adsorption capacity of the biochars to remove pharmaceutical compounds in liquid phase.

2.5. Process water

2.5.1. *Antimicrobial assays with process water*

The bacterial growth inhibitory potential of process water from the hydrothermal carbonization process with the remaining biomass of *U. pinnatifida* was conducted with the same bacteria and protocol as the antibacterial activity with the extracts from *U. pinnatifida*. The negative control was conducted with ultrapure water while oxytetracycline was used as a positive control. The inhibitory capacity was determined as the percentage of growth relative to control. The test was carried out with a series of dilutions, beginning with 10 µl of 10 mL of process water collected from the HTC synthesis which used 3 g of algae in 10 mL of ultrapure water. All experiments were performed in triplicate.

2.5.2. *Biofilm inhibition assays with process water*

The biofilm inhibition assay with process water had the same protocol described before with the extracts from the seaweed and the same biofilm producing bacteria were used in this assay. All experiments were performed in triplicate, and the volume used was 10 µl of 10 mL of process water collected from the HTC synthesis which used 3 g of algae in 10 mL of ultrapure water.

2.6. Data assessment and statistical analysis

All calculations were done with Graphpad Prism v.9.3.0 (San Diego, CA, USA). Data was checked for normality and homoscedasticity using the Shapiro-Wilk and Levene's test, respectively, and comparisons checked recurring to a one-way ANOVA, with Dunnett's multiple comparisons or Kruskal-Wallis tests, depending on the variance and distribution statistical assumptions (Zar, 1999). The IC_{50} was determined by nonlinear regression ($Y = 100/(1 + 10^{(X-Log(IC50)}$). For all tests the level of significance was set at *p-value* < 0.05, with results being expressed as mean ± standard error of the mean.

3. Results

This study explores the use of *U. pinnatifida* biomass from Portugal and Spain, focusing on solvent-based extraction to identify antifouling agents and valorizing the residual biomass via pyrolysis and hydrothermal carbonization. The workflow involves evaluating the antifouling potential of extracts, characterizing biochars derived from residual biomass collected in Spain, and testing their properties in preliminary assays in liquid phase (Figure 3.1).

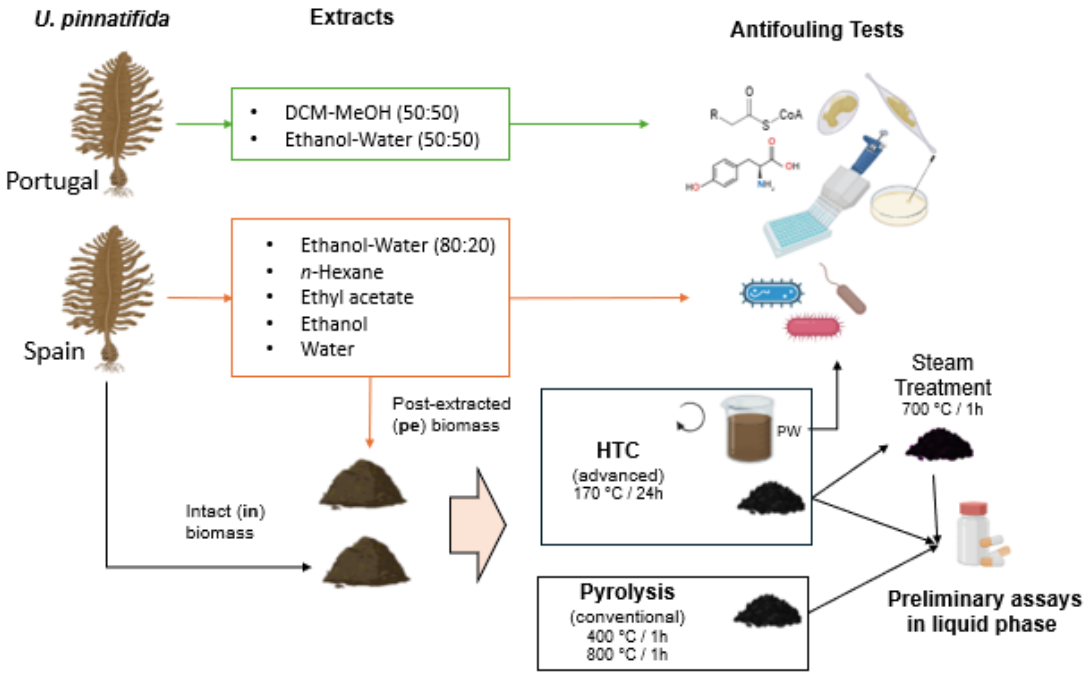

Figure 3.1. Overview of the experimental workflow for the extraction and evaluation of antifouling activity from *Undaria pinnatifida* (figure made in Biorender.com). Biomass of *Undaria pinnatifida* was collected from Portugal and Spain and subjected to extraction using various solvents. The extracts were tested for antifouling activity. Residual post-extracted (pe) biomass and intact (in) biomass were processed using conventional pyrolysis and advanced hydrothermal carbonization (HTC) at varying conditions. Preliminary assays in liquid phase were conducted with the biochars that presented the higher BET area values.

3.1. Extractions

3.1.1. *Extraction yields*

The extraction yield (g dried extract/100 g dried seaweed) was calculated for each extract obtained with different polarity grade solvents (Table 3.1).

Table 3.1. Yield of extraction (w/w, %) of *Undaria pinnatifida* biomass with different solvents. DCM-MeOH – dichloromethane-methanol.

Solvents	**Yield (%)**
Ethanol-Water (80:20)	8.2
n-Hexane	0.4
Ethyl acetate	0.3
Ethanol	1.6
Water	3.4
DCM-MeOH (50:50)	7.8
Ethanol-Water (50:50)	10.3

Among the performed extractions, the ethanol-water extracts (50:50 and 80:20) had the best yields (10.3% and 8.2%, respectively) followed by the DCM-MeOH (50:50) and aqueous extracts (7.8% and 3.4%, respectively). Conversely, the *n*-hexane and ethyl acetate extracts exhibited lower yields (0.4% and 0.3%, respectively).

3.1.2. *Chemical profile of extracts*

A preliminary chemical screening of extracts by thin layer chromatography (TLC) evidenced a complex composition of the extracts obtained with ethanol-water (80:20) and DCM-MeOH (50:50), since both mixtures can extract a broad range of less polar and more polar compounds. On the contrary, an enrichment of apolar and mid-polar molecules was found in the *n*-hexane and ethyl acetate extracts, respectively, while the most polar components were found in the ethanol, ethanol-water (50:50) and water (100%) extracts.

3.2. Biological assays

3.2.1. *Ecotoxicity studies*

The ecotoxicity of *U. pinnatifida* extracts was tested against the brine shrimp *Artemia*

salina and the results are presented in Figure 3.2 as % survival relative to control.

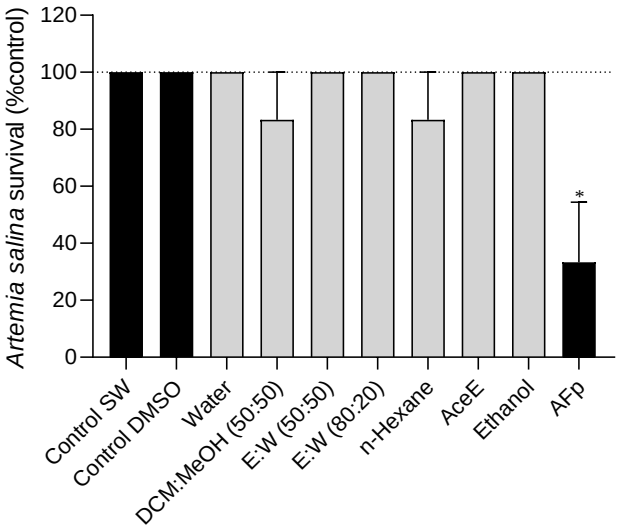

Figure 3.2. *Artemia salina* survival after 24 h of exposure to *Undaria pinnatifida* extracts from (water; DCM:MEOH – dichloromethane-methanol; E:W – ethanol-water; *n*-hexane; AceE – ethyl acetate; ethanol). The negative controls were SW (salt water only) and another with DMSO added. The positive control was commercial antifouling paint (AFp). Each bar represents the mean of 6 replicas in the experiment and vertical lines represent SEM. The symbol * represent significant differences with DMSO - dimethyl sulfoxide (One-Way ANOVA, Dunnett's test; $p < 0.05$).

Both negative controls demonstrated a survival rate of 100%. The positive control (antifouling paint) showed the lowest survival rate (33%), reflecting its toxicity. The dichloromethane-methanol and *n*-hexane extracts had a survival rate of 83%, however, these extracts did not show statistically significant differences with the control. The remaining extracts exhibited a survival rate of 100%.

3.2.2. *Antifouling activity*

3.2.2.1. *Antimicrobial activity against marine bacteria*

The initial colonization of submerged structures by bacteria is a key stage in biofouling. This study assessed the growth inhibition of various bacterial species, including *Serratia* sp., *Vibrio* sp., *Citricoccus* sp., *Pseudomonas* sp., and *Bacillus subtilis* to evaluate the potential of *U. pinnatifida* extracts as antifouling agents – at five different concentrations, from 62,5 to 1000 µg/mL (Figure 3.3). DMSO was used as negative control and oxytetracycline was used as positive control.

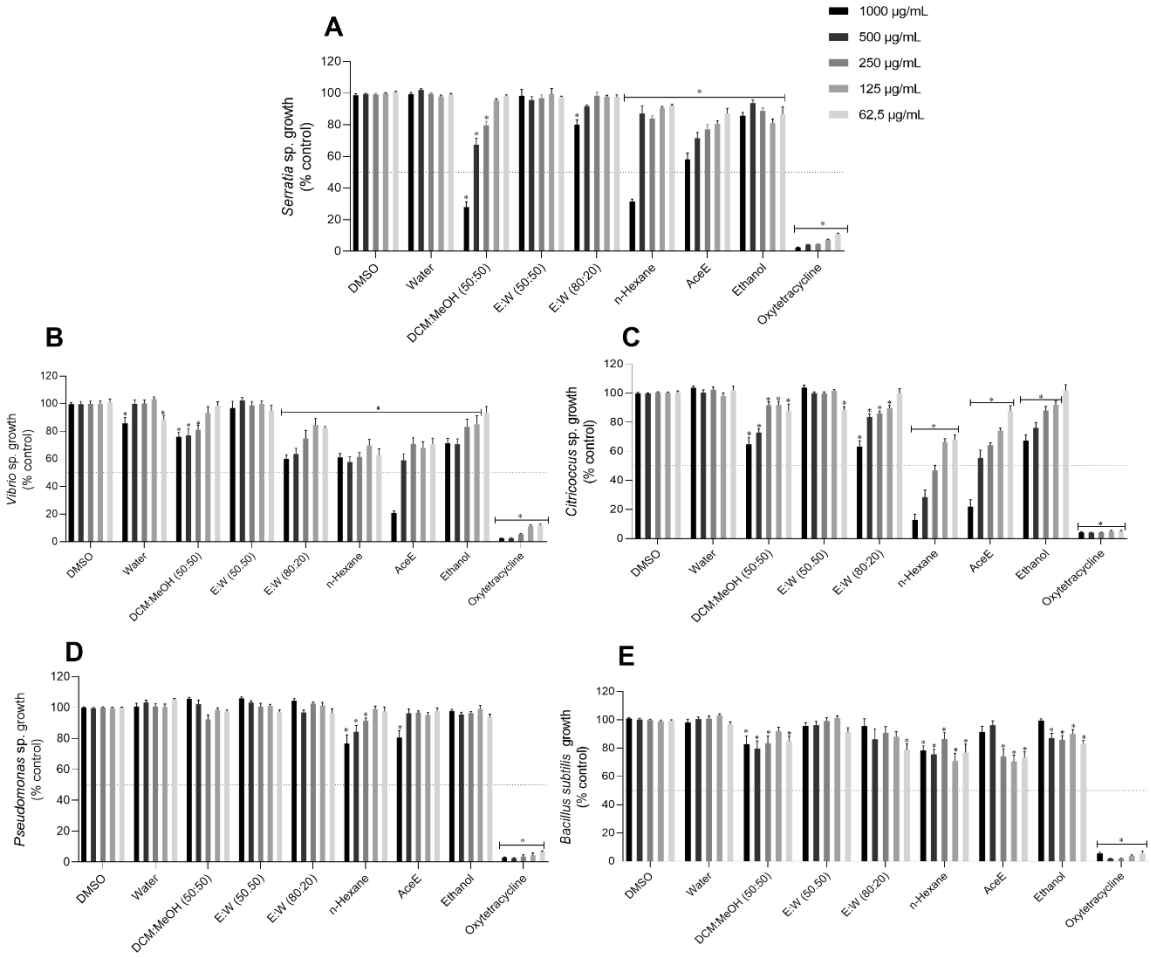

Figure 3.3. Capacity of *Undaria pinnatifida* extracts (1000 µg/mL to 62.5 µg/mL) to inhibit the growth of (A) *Serratia* sp., (B) *Vibrio* sp., (C) *Citricoccus* sp., (D*) Pseudomonas* sp., and (E) *Bacillus subtilis*. The values in each column represent the mean ± standard error of the mean (SEM) from three independent experiments carried out in triplicate. The symbol * represent significant differences with DMSO - dimethyl sulfoxide (One-Way ANOVA, Dunnett's test; $p < 0.05$); DCM:MeOH – dichloromethane-methanol; E:W – ethanol-water; AceE – ethyl acetate.

The extracts that induced a growth reduction in more than 50% at 1 mg/mL were further studied for their dose-response profile and IC_{50} (concentration that inhibits 50% growth) was determined. The results are presented in Figure 3.4.

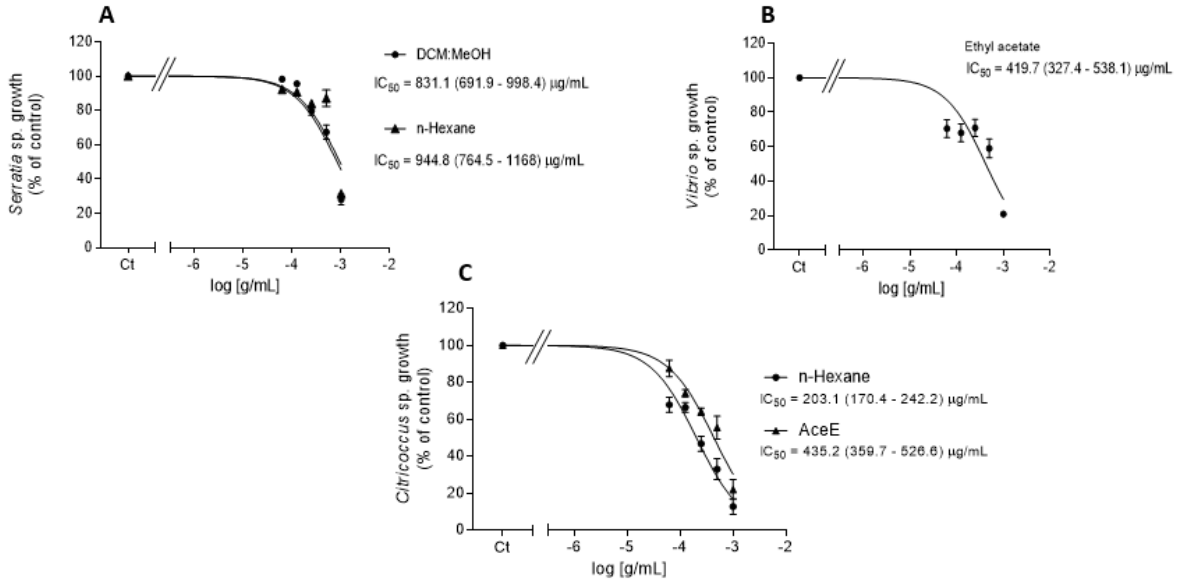

Figure 3.4. Dose-response analysis and IC_{50} determination of the most potent extracts. A- *Serratia* sp. growth exposed to DCM:MeOH, and *n*-Hexane extracts; B- *Vibrio* sp. growth exposed to AceE extract; C- *Citricoccus* sp. growth exposed to *n*-Hexane and AceE extracts. Data are shown as means ± SEM, n = 3. IC_{50} values were determined for a 95% confidence interval.

The extracts obtained with *n*-hexane and AceE were the ones showing the broadest spectrum of activity, showing capacity to inhibit all microorganism's growth. Nevertheless, their potency was the highest against *Citricoccus* sp., exhibiting an IC_{50} of 203.1 and 435.2 µg/mL, respectively. The AceE also revealed a great inhibitory activity against *Vibrio* sp., exhibiting an IC_{50} of 419.7 µg/mL.

The DCM:MeOH extract revealed a high inhibitory potential, particularly against *Serratia* sp. growth, exhibiting an IC_{50} of 831.1 µg/mL. This microorganism growth was also markedly inhibited by the *n*-hexane extract, which presented an IC_{50} of 944.8 µg/mL.

The hydroethanolic extract (80:20) revealed capacity to inhibit *Vibrio* sp. growth ranging from ≈20% (at 62.5 µg/mL) to ≈40% (at 1 mg/mL), and against *Citricoccus* sp. ranging from ≈20% (at 125 µg/mL) to ≈40% (at 1 mg/mL).

Inhibition values of *Undaria pinnatifida* extracts against *B. subtilis and Pseudomonas* sp. remained below ≈30.0%.

3.2.2.2. *Biofilm inhibition activity*

The extracts of *U. pinnatifida* were tested against five biofilm producing bacteria - *Serratia* sp., *Vibrio* sp., *Citricoccus* sp., *Pseudomonas* sp. and *Bacillus subtilis* (Figure 3.5) – at five different concentrations – from 62.5 to 1000 µg/mL. The negative control was conducted with DMSO.

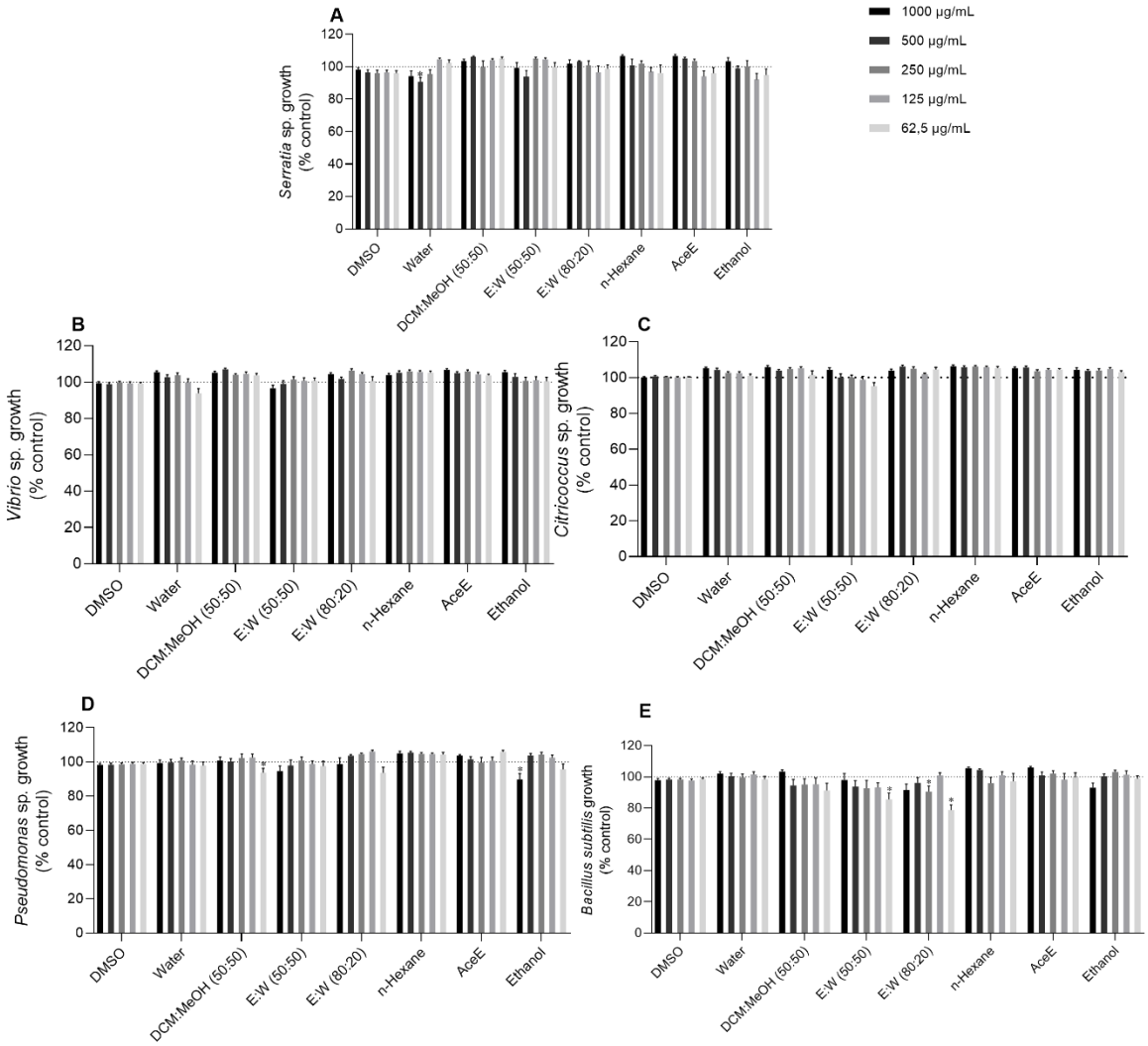

Figure 3.5. *Undaria pinnatifida* extracts (1000 µg/mL - 62.5 µg/mL) capacity to inhibit the biofilm production of (A) *Serratia* sp., (B) *Vibrio* sp., (C) *Citricoccus* sp., (D) *Pseudomonas* sp., and (E) *Bacillus subtilis.* The values in each column represent the mean ± standard error of the mean (SEM) from three independent experiments carried out in triplicate. The symbol * represents significant differences with DMSO - dimethyl sulfoxide) (One-Way ANOVA, Dunnett's test; $p < 0.05$). DMSO – dimethyl sulfoxide; DCM:MeOH – dichloromethane-methanol; E:W – ethanol-water; AceE – ethyl acetate.

In a general way, the *U. pinnatifida* extracts were not able to reduce bacterial biofilm formation, however, the hydroethanolic extracts inhibited around 20% *Bacillus subtilis* biofilm, at the lowest tested concentration. The DCM-MeOH was also able to reduce *Pseudomonas* biofilm formation in about 10%, at 62.5 µg/mL and the ethanolic extract reduced about 15% at 1 mg/mL.

This suggests that the compounds present in the extracts may not possess antimicrobial properties effective against the biofilm of these bacteria. It is possible that the biofilm structure of this bacteria provides a protective environment that the extracts could not penetrate or disrupt. Further investigation may be necessary to explore different concentrations, extraction methods, or other types of extracts to determine their potential effects on the biofilms of this species.

3.2.2.3. *Quorum sensing inhibition activity*

The bacteria *Chromobacterium violaceum* was used to assess the impact of extracts from the brown seaweed *U. pinnatifida* on QS mechanism (Figure 3.6). This bacteria is commonly used in *quorum sensing* assays due to its ability to produce violacein, a purple pigment, in response to QS signals. By inhibiting or disrupting this signaling pathway, it is possible to evaluate interferences with bacterial communication, essential for biofilm formation.

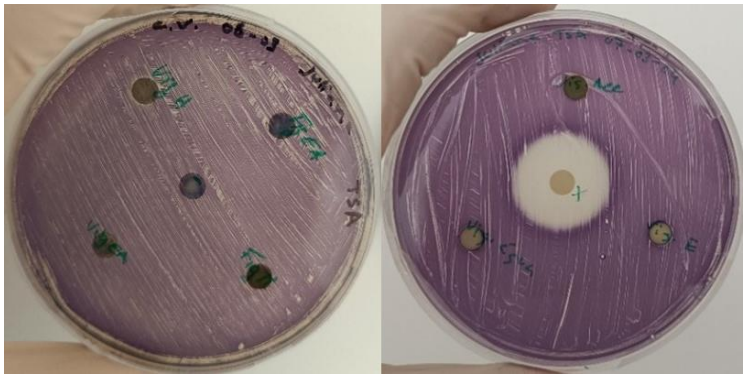

Figure 3.6. Effects of *Undaria pinnatifida* extracts on *Chromobacterium violaceum* growth and QS mechanism. Violet represents areas with functioning QS mechanism. White halos represent an inhibition of the QS mechanism and transparent halos represent growth inhibition.

The data presented indicate that the tested extracts did not inhibit either the QS activity or the growth of the bacteria *C. violaceum*. The positive control exhibited an inhibition zone of 10 mm.

3.2.2.4. *Inhibition of microalgae growth*

For the inhibition of microalgae growth, the extracts were tested against four diatoms: *Chaetoceros calcitrans*, *Phaeodactylum tricornutum*, *Nitzschia* sp. and *Amphora* sp. and the results are presented in Table 3.2 and Figure 3.7. DMSO was used as negative control and $CuSO_4$ as positive control.

Table 3.2. Effect of *Undaria pinnatifida* extracts on the growth (mm) of diatoms *Chaetoceros calcitrans*, *Phaeodactylum tricornutum*, *Nitzschia* sp. and *Amphora* sp.

Samples (1 mg/disk)	**Growth Inhibition (mm)**			
	Chaetoceros calcitrans	***Phaeodactylum tricornutum***	***Nitzschia* sp.**	***Amphora* sp.**
E-W (80:20)	1.0 ± 0.0	0.0 ± 0.0	1.0 ± 0.0	2.0 ± 0.0
n-Hexane	10.0 ± 0.0	1.7 ± 0.3	3.0 ± 0.0	8.0 ± 0.0
AceE	4.3 ± 0.3	1.7 ± 0.3	5.0 ± 0.0	8.0 ± 0.0
Ethanol	0.0 ± 0.0	0.0 ± 0.0	1.0 ± 0.0	0.0 ± 0.0
Water	0.0 ± 0.0	0.0 ± 0.0	0.0 ± 0.0	1.0 ± 0.0
DCM-MeOH (50:50)	4.7 ± 0.3	0.0 ± 0.0	3.0 ± 0.0	4.0 ± 0.0
E-W (50:50)	0.0 ± 0.0	0.0 ± 0.0	0.0 ± 0.0	0.0 ± 0.0
$CuSO_4$	25.0 ± 1.6	2.3 ± 0.3	7.0± 0.0	4.0 ± 0.0
DMSO (10 µL)	0.0 ± 0.0	0.0 ± 0.0	0.0 ± 0.0	0.0 ± 0.0

Table 3.2 and Figure 3.7 shows the growth inhibition effects of different extracts and controls on four microalgae species: *Chaetoceros calcitrans*, *Phaeodactylum tricornutum*, *Nitzschia* sp., and *Amphora* sp. Each sample was applied at a concentration of 1 mg per disk.

For *Chaetoceros calcitrans*, the *n*-hexane extract was the most effective with a 10 mm inhibition halo. Moderate activity was observed with the dichloromethane-methanol extract (4.7 mm) and the ethyl acetate extract (4.3 mm). The ethanol-water extract (80:20) had minor activity (1 mm), while other extracts and DMSO showed no inhibition. Copper sulfate ($CuSO_4$) positive control exhibited 25 mm of inhibition.

Against *Phaeodactylum tricornutum*, only the *n*-hexane and ethyl acetate extracts showed activity, with a 1.7 mm inhibition halo. The copper sulfate ($CuSO_4$) positive control, had a inhibition halo of 2.3 mm.

Regarding *Nitzschia* sp., the positive control had the highest inhibition (7 mm), followed by the ethyl acetate extract (5 mm). The *n*-hexane and dichloromethane-methanol extracts each showed 3 mm of inhibition. The ethanol-water extract (80:20) and ethanol extract showed minimal inhibition (1 mm each), while the other samples showed no activity.

Against *Amphora sp.*, the *n*-hexane and ethyl acetate extracts were the most effective, each with an 8 mm inhibition halo. The dichloromethane-methanol extract and the $CuSO_4$ control showed 4 mm inhibition, followed by the ethanol-water extract (80:20) (2 mm), and the water extract (1 mm). Other extracts and controls showed no inhibition.

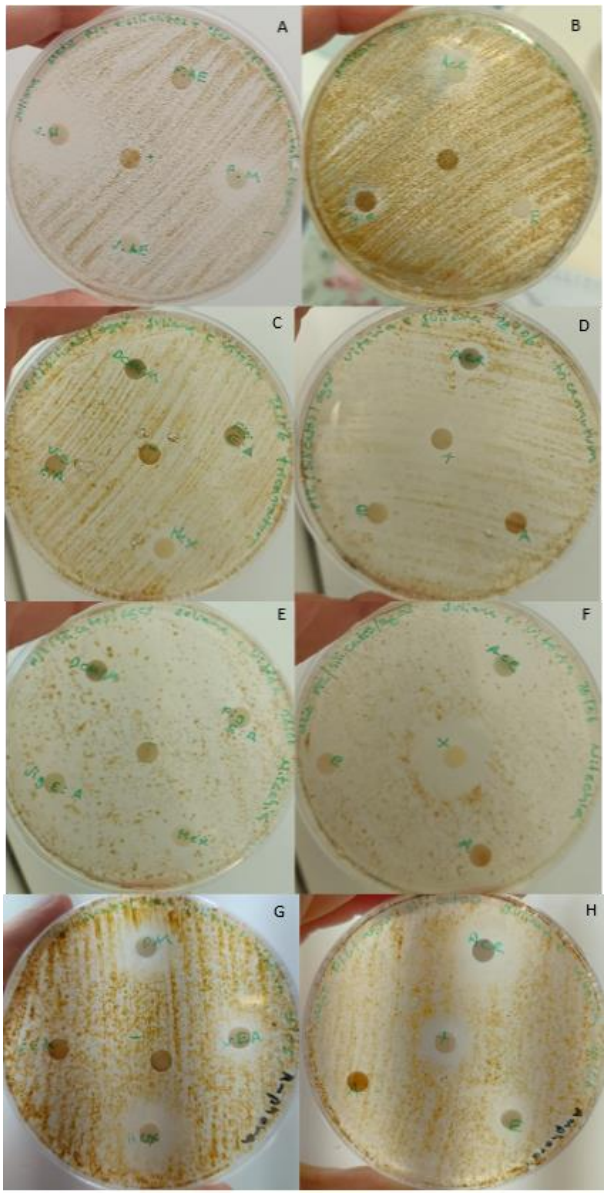

Figure 3.7. Disk diffusion assays for growth inhibition of diatoms by the extracts from *Undaria pinnatifida.* *Chaetoceros calcitrans* – A and B; *Phaeodactylum tricornutum* – C and D; *Nitzschia* sp. – E and F; *Amphora* sp. – G and H. Inhibition halos are characterized by their transparency in the plates. DMSO and $CuSO_4$ were used as negative and positive controls, respectively.

3.2.2.5. *Anti-enzymatic activity of extracts*

The inhibitory effects of *U. pinnatifida* extracts on acetylcholinesterase and tyrosinase are depicted in Figure 3.8, and the results were compared with the control (DMSO) (100 % enzyme activity).

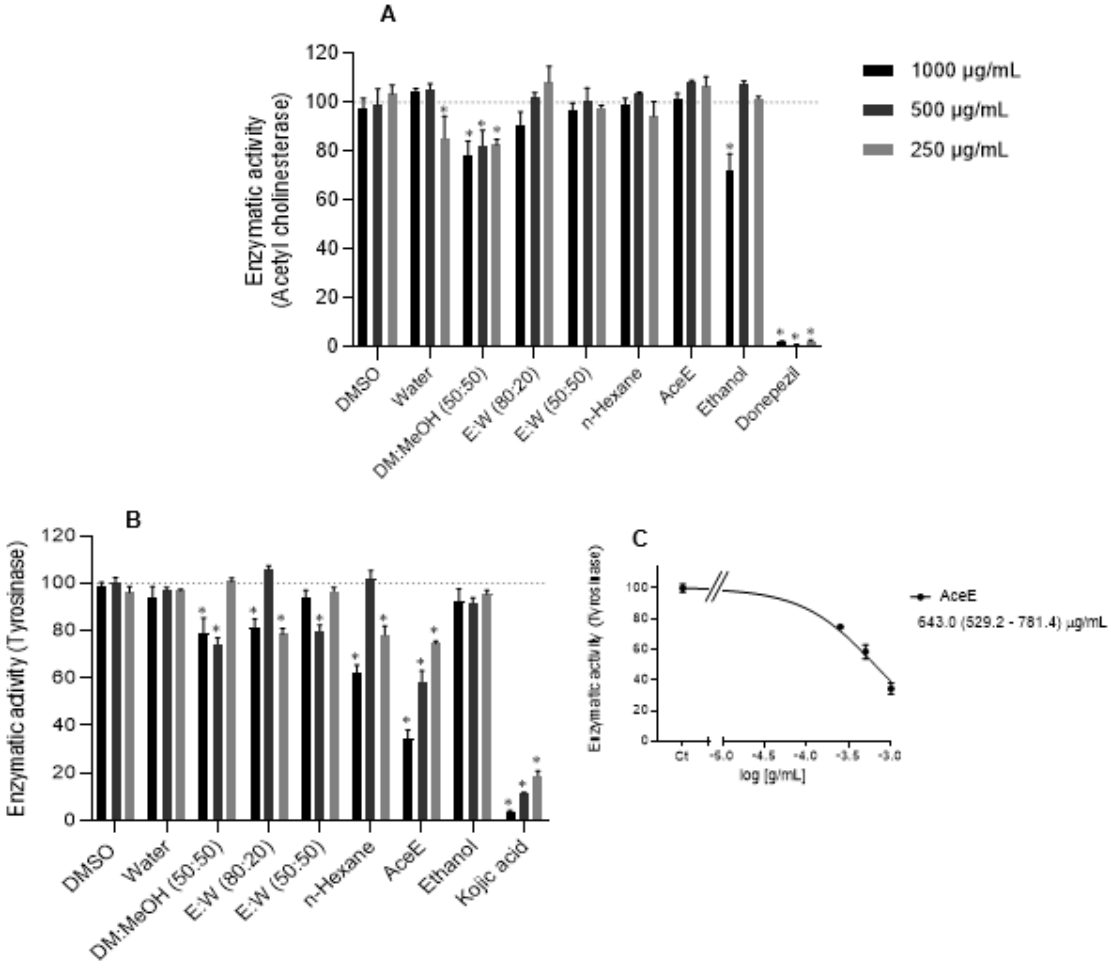

Figure 3.8. Enzymatic inhibitory activity of *Undaria pinnatifida* extracts: Water, DM:MeOH (dichloromethane-methanol extract), E:W (ethanol-water), *n*-hexane, AceE (ethyl acetate) and ethanol on A) Acetylcholinesterase and B-C) Tyrosinase. The DMSO and Donepezil were used as negative and positive controls, respectively, for the acetylcholinesterase activity and Kojic acid as positive for the tyrosinase enzyme. The extracts were tested in three different concentrations 1000, 500 and 250 µg/mL. Bars correspond to the mean ± standard error of the mean (SEM) from three independent experiments carried out in triplicate. The symbol * represents significant differences with DMSO (One-Way ANOVA, Dunnett's test; $p < 0.05$). IC_{50} values were determined for a 95% confidence interval.

The ethanol extract and the dichloromethane-methanol extract (50:50) presented the best results in the inhibition of the enzyme acetylcholinesterase with 28.2% and 21.8%, respectively, at the concentration of 1000 µg/mL. Donepezil totally inhibited this enzyme activity in all tested concentrations.

As concerns to tyrosinase, the ethyl acetate extract exhibited the highest inhibitory potential, exhibiting an IC_{50} of 643 (529.2 – 791.4) µg/mL. This was followed by the *n*-hexane extract with 37% inhibition at 1000 µg/mL. Among other extracts, the DCM-MeOH extract inhibited 26% of activity at 500 µg/mL. The ethanol-water (80:20) and ethanol-water (50:50) extracts showed moderate inhibition, with 21% at 250 µg/mL and 20% at 500 µg/mL, respectively. The aqueous extract and ethanol extract had lower activity, inhibiting 13% and 19% at 1000 µg/mL, respectively. In comparison, the positive control, Kojic acid, exhibited the highest inhibition with an IC_{50} <250 µg/mL. The negative control showed no inhibitory activity.

3.2.2.6. *Antifouling field assay*

The antifouling effects of *U. pinnatifida* extracts on plates collected after two months underwater were tested. The results are depicted in Figure 3.9 and compared with the negative control (DMSO) and positive control with antifouling paint. The weight of the acrylic plates was also measured before and after recollection and compared with control (Figure 3.10).

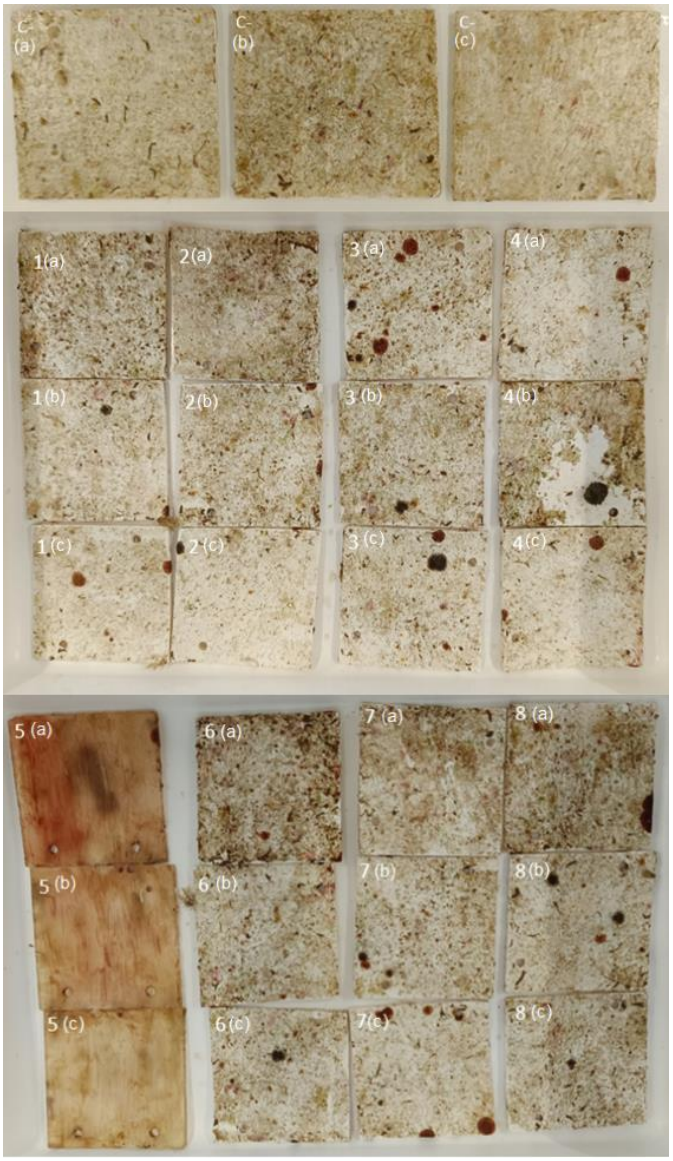

Figure 3.9. Acrylic plates containing paint incorporated with extracts of *Undaria pinnatifida* collected after two months underwater, in triplicate. Negative control (C-) with DMSO; Ethanol-water extract (50:50) (1); *n*-Hexane (2); Ethyl acetate (3); Ethanol (4); Antifouling paint (5); Water (6); Dichloromethane-methanol (50:50) (7); Ethanol-water (80:20) (8). The replicas are labeled alphabetically (a,b,c).

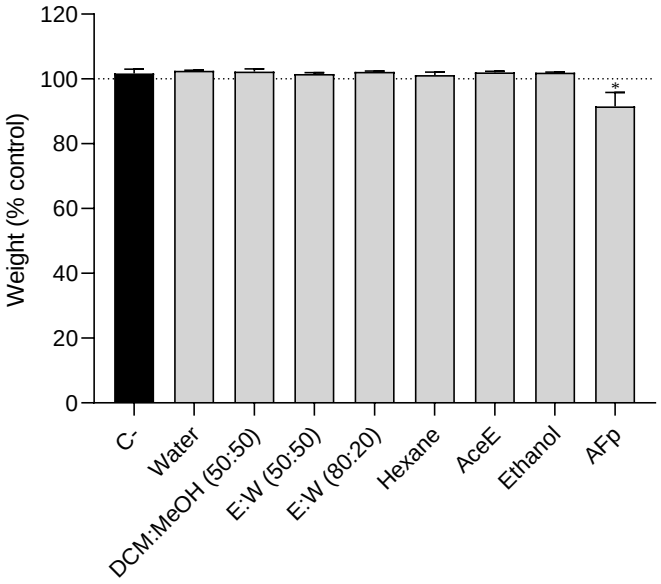

Figure 3.10. Weight, in percentage of control, for each acrylic plate containing paint incorporated with *Undaria pinnatifida* extracts. C- refers to the negative control (DMSO). The AFp is commercial antifouling paint and represents the positive control. Bars correspond to the mean ± standard error of the mean (SEM) of three independent replicas. The symbol * represents significant differences with DMSO (One-Way ANOVA, Dunnett's test; $p < 0.05$).

The plates coated with the antifouling paint demonstrated reduced biofouling on their surface (Figure 2.9 (5)) and exhibited a lower weight percentage compared to the control and the other samples (Figure 3.10).

The extracts had a similar weight to the control plates. It's important to highlight that the weight on the plates is significantly influenced by the types of organisms present. For example, in Figure 3.9 (4b) one of the ethanol extract plates contained a sea snail, which contributed to more weight compared to plates with smaller organisms. Additionally, the presence of the snail resulted in a noticeable halo on the plate.

For the identification of the organisms, the plates were observed in a Zoom Stereoscopic Microscope (Figure 3.11). The findings were compared to other species observed in other studies done in Portugal(Azevedo et al., 2020,Vinagre et al., 2020 and Vinagre & Fonseca, 2022).

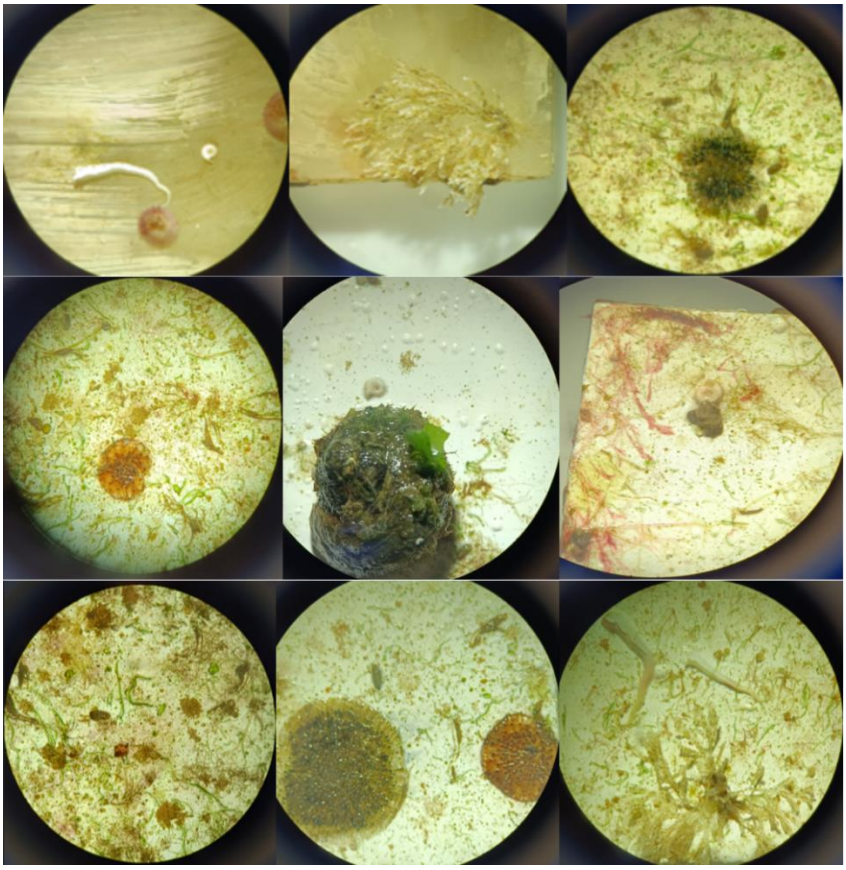

Figure 3.11. Observations of some biofouling organisms in the acrylic plates under a Zoom Stereoscopic Microscope.

Some organisms identified in the acrylic plates were: Calcareous tube worms (Small marine worms of the *Serpulidae* family like *Spirorbis* spp.); *Ciona intestinalis* (Sea vase, Vase tunicate); *Watersipora* spp. (Invasive fouling bryozoan); *Membranipora membranacea* (kelp lace bryozoan); *Mytilus* spp. mussel larvae; Green seaweed (species such as *Ulva intestinalis, Bryopsis* spp., *Spirogyra* spp. or *Cladophora* spp.); gastropods (such as *Littorina littorea*); *Amphibalanus amphitrite (*striped barnacle*)*; red seaweed (such as *Polysiphonia* spp., *Asparagopsis* spp. *or Ceramium ciliatum*); brown seaweed (such as *Hincksia* spp. or *Ectocarpus* spp., a genus of filamentous brown seaweed); Protozoan Cysts or Spores. The brownish clusters and some of the small, round or oval shapes might be diatoms. Thin green filaments could also include cyanobacteria, like *Oscillatoria*.

3.3. Valorization of residual biomass

2.3.1. Characterization of biomass and biochars

The non-extracted and post-extracted biomass of *U. pinnatifida* and the carbon materials produced by hydrothermal carbonization and slow pyrolysis were characterized by yield (%), moisture content (%), ash content (%), surface chemistry (pH at the point of zero charge, pHpzc), apparent density, N_2 adsorption isotherm at -196 ºC, SEM and powder XRD analysis.

The characterization of the non-extracted (inUP) and post-extracted biomass (peUP) summarized in Table 3.3, show similar results between both biomasses with the non-extracted biomass presenting slightly higher percentage of ash and moisture. The post-extracted

biomass had higher apparent density.

Table 3.3. Ash content, moisture and apparent density of the initial biomass (inUP) and post-extracted biomass (peUP) from *Undaria pinnatifida*.

Sample	peUP	inUP
% Ash	21.7	23.7
% Moisture	11.7	14.3
Apparent Density (kg/m^3)	802	719

The characterization of the hydrochars produced from non-extracted and post-extracted biomass through HTC are presented in Table 3.4. The use of process water instead of ultrapure water increases the yield of the hydrothermal carbonization process by 3 to 6 percentual points. Also, the use of process water (1stPW or 2ndPW) during HTC resulted in hydrochars with higher ash content than that obtained in the hydrochar synthetized with ultrapure water. The peUP hydrochar had higher ash content than the inUP hydrochar. The BET area value (A_{BET} in m²/g) was similar for all samples, below 5 m²/g. The pHpzc was also similar for all samples (7 or 8). As expected, the hydrochars present lower density than the original biomass (Tables 3.3 and 3.4).

Table 3.4. Yield of the hydrothermal carbonization process, ash content, moisture, apparent density and textural and surface characterization of hydrochar materials obtained from original biomass and post-extracted biomass of *Undaria pinnatifida*.

Sample	peUP/Hydro/ TypeI	peUP/Hydro/ 1 st PW	peUP/Hydro/ 2 nd PW	inUP/Hydro/TypeI
% Yield	26.4	32.8	29.2	26.7
% Ash	19.2	29.6	22.6	15.3
% Moisture	5.1	2.9	2.7	1.4
pHpzc	7.3	7.1	8.2	7.5
Apparent Density (kg/m^3)	426	532	504	531
A_{BET} (m²/g)	3.6	2.6	4.2	5.0

The hydrochar prepared from the post-extracted biomass with 1st process water (peUP/Hydro/1stPW) went through an activation process (steam treatment) aiming to develop the nanoporous network and obtain activated carbon materials with high BET area and better adsorption capacities than the hydrochars. Table 3.5 shows the characteristics of material obtained after the steam treatment.

Table 3.5. Yield, ash content, moisture and textural and surface characterization of the steam treatment material after the process of hydrothermal carbonization with post-extracted biomass of *Undaria pinnatifida* (peUP/Hydro/1stPW/S700). The same material was also analyzed after being washed with distilled water (peUP/ Hydro/1stPW/S700/W). n.a – not analyzed.

Sample	% Yield	% Ash	% Moisture	pHpzc	A_{BET} (m²/g)
peUP/Hydro/1stPW/S700	27.5	67.1	3.3	11.6	130
peUP/Hydro/1stPW/S700/W	n.a.	n.a.	n.a.	8.4	n.a.

This sample's content in ash was high and the pHpzc was highly basic. After the steam activation, the material presented a BET area of 130 m²/g, much superior to the ones obtained only by HTC. But still, this carbon material cannot be considered an activated carbon since, besides the high ash content, the BET area value is below the values commonly presented by

activated carbons that often attain 1000 m²/g or even higher values. After being washed with distilled water (peUP/Hydro/1stPW/S700/W) the pHpzc decreased.

The characterization of the pyrochars obtained through slow pyrolysis at two different temperatures (400 °C and 800 °C) is summarized in Table 3.6. The pyrochars prepared at 400 °C had higher yields, but the ash content was superior at 800 °C, which was already expected. The pryochars synthetized at 800 °C were also the more basic ones with a pHpzc of 13 and showed a higher apparent density. The BET area was higher in the materials prepared at 800 °C. Regardless of the pyrolysis temperature, pyrochar from post-extracted biomass had double the area of the pyrochar from the initial biomass. After being washed with distilled water the pHpzc value of the pyrochars decreased 3 pH units and, in general, the BET area values doubled, with peUP/Pyro/W reaching 138 m²/g.

Table 3.6. Yield of the pyrolysis process at different temperatures (400 °C and 800 °C), ash content and moisture, textural and surface characterization of pyrochars derived from non-extracted biomass (in-) and post-extraction biomass (pe-) of *Undaria pinnatifida*. The same material was also analyzed after being washed with distilled water (W). n.a – not analysed.

Sample	% Yield		% Ash		% Moisture		pHpzc		Apparent Density (kg/m^3)		A_{BET} (m²/g)	
	400 °C	800 °C	400 °C	800 °C	400 °C	800 °C	400 °C	800 °C	400 °C	800 °C	400 °C	800 °C
peUP/ Pyro	41	33	59	80	0.7	1.8	10.8	12.5	641	876	<1	64
peUP/ Pyro/W	n.a	n.a	30	80	2.7	2.5	7.4	9.2	n.a	n.a.	7.9	138
inUP/ Pyro	40	28	53	70	1.2	1.8	10.7	13.1	658	816	3.6	37
inUP/ Pyro/W	n.a	n.a	26	61	2.9	3.0	7.6	8.6	n.a	n.a	5.7	54

The N_2 adsorption isotherms at -196 ºC of the different biochars are represented in Figure 3.12. The post-extracted pyrochar obtained at 800 ºC and further washed (peUP/Pyro800/W) and the post-extracted hydrochar further steam activated at 700 ºC (peUP/Hydro/1stPW/S700) were the biochars with the highest BET areas, attaining 138 m²/g and 130 m²/g, respectively, and with the most developed micro-mesoporous network (Table 3.7). In contrast, the hydrochars showed incipient porous networks, with BET area values below 5 m²/g. Overall, biochars from pyrolysis at 800 °C outperformed hydrochars and pyrochars produced at 400 °C in terms of surface area (A_{BET}). Additionally, the post-extracted biomass was more effective than the non-extracted biomass in yielding a biochar with a higher BET area.The washing with distilled water doubled the BET areas of the pyrochars.

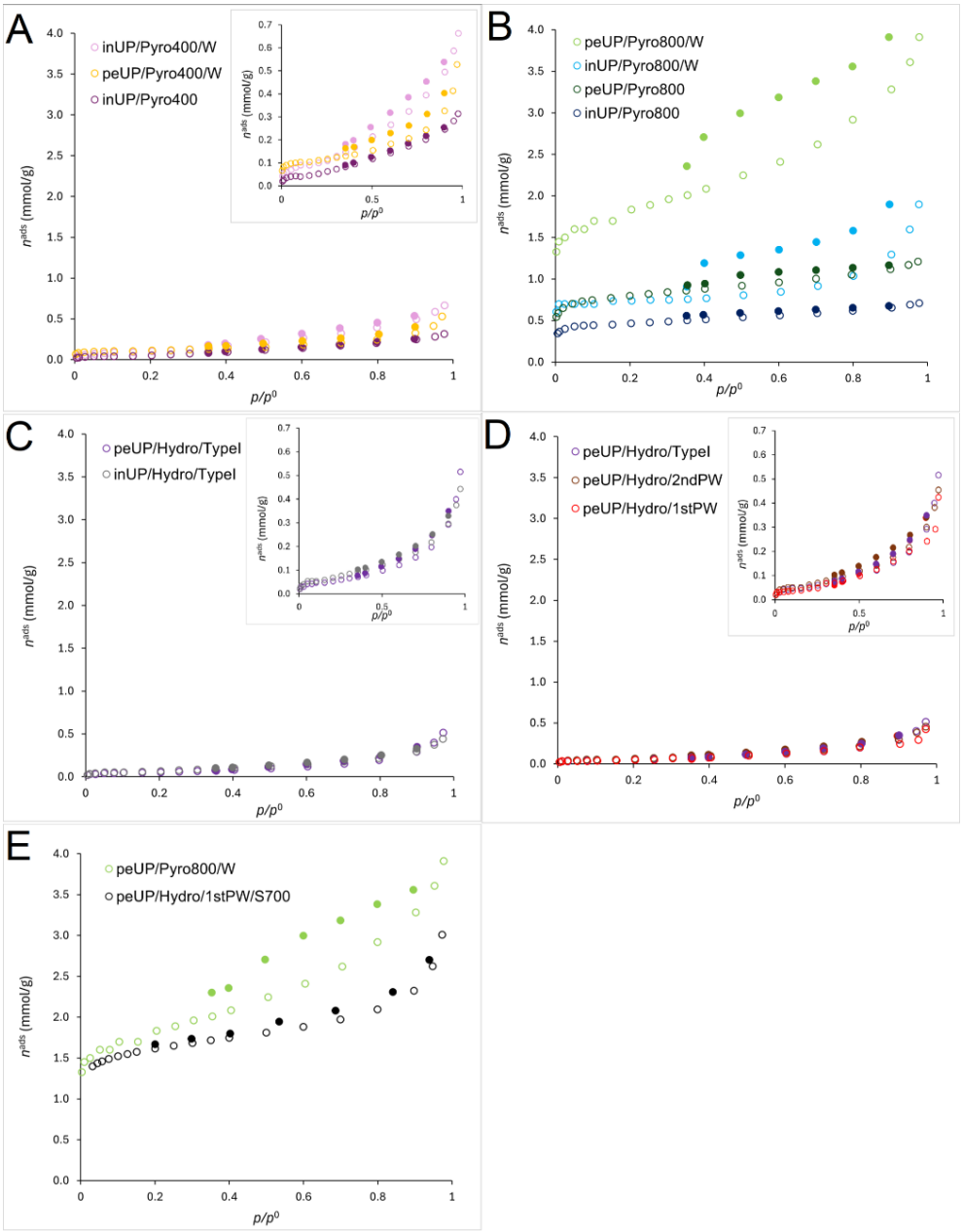

Figure 3.12. N_2 adsorption isotherms at -196 ºC for the hydrochars (Hydro) and pyrochars (Pyro) at different temperatures - 400 ºC (A) or 800 ºC (B) - obtained from *Undaria pinnatifida* intact (in-) and post-extracted (pe-) biomass. The W means that the biochar was washed with distilled water after being produced. Type I refers to a hydrochar prepared with ultrapure water (C) and the PW to a hydrochar prepared with 1st or 2nd processed water (D). The graph E shows the best BET areas of all the materials. Insets in A, C and D allow discriminating adsorption isotherm profiles for the less adsorbing materials . Empty symbols correspond to adsorption data and full symbols represent desorption data. The textural parameters reported were obtained from the report generated by the equipment (NOVA 2200e from Quantachrome) software.

The Isotherms in Figure 3.12 qualify as Type IV with H3 or H4 hysteresis loops (see Figures A1 and A2 in the Annex section). As described by Thommes et al. (2015), the type IV isotherms are typical of mesoporous adsorbents and the H4 loops are often found with aggregated crystals of zeolites and micro-mesoporous carbons. Loops of type H3 are given by non-rigid aggregates of plate-like particles (e.g., certain clays) but also if the pore network consists of macropores which are not completely filled with pore condensate (Thommes et al., 2015). Materials obtained by pyrolysis at 800 ºC and the hydrochar further steam activated (Figure 3.12 B and E) present some adsorption capacity at low relative pressure pointing for

the presence of some microporosity.As shown in Table 3.7, the pyrochars, particularly those prepared at higher temperatures (800 °C), demonstrate significantly enhanced porosity and surface area compared to those produced at 400 °C. For example, inUP/Pyro800 achieves a BET area of 37 m^2/g, while inUP/Pyro400 only reaches 4 m^2/g. Higher temperatures result in higher consumption of the matrix with the release of more lose volatile compounds, promoting the development of micropores and increasing the overall porosity.

Washing post-pyrolysis further enhances the material's adsorption properties by cleaning occluding substances (e.g. soluble salts). For instance, inUP/Pyro800/W exhibits higher BET area (53 m^2/g), and total pore volume (0.07 cm^3/g) compared to the unwashed inUP/Pyro800 (BET area: 37 m^2/g; total pore volume: 0.02 cm^3/g). Similarly, for post-extracted samples, peUP/Pyro800/W achieves a higher BET area of 138 m^2/g, highlighting the significant effect of washing on improving pore accessibility and external surface area.

Post-extracted samples (peUP) consistently outperform intact materials (inUP) in porosity and surface area. The removal of certain components during extraction results in biochars with higher pore development. For instance, inUP/Pyro800/W achieved a BET area of 53 m^2/g and the post-extracted counterpart, peUP/Pyro800/W, more than doubled this value.

Among the pyrolysis samples, peUP/Pyro800/W emerges as the most promising material, with the highest total pore volume (0.14 cm^3/g), micropore volume of 0.03 cm^3/g, and specific surface area. The large external surface area (66.5 m^2/g) indicates the presence of mesopores and macropores.

In comparison, hydrothermal carbonization (Hydro) materials showed lower porosity and surface area, limiting their direct applicability for adsorption. There were not significant differences between those prepared with process water (PW) or ultrapure water (Type I). However, steam activation significantly enhances the properties of hydrochars. For instance, peUP/Hydro/1stPW/S700 displays a high micropore area (97.9 m^2/g) and specific surface area (ABET: 130 m^2/g), making it a material with some micropore possibly effective for adsorbing small molecules. It is important to mention that the high ash content and limited percentage of carbon of the pyrochars does not allow to envisage their further steam activation to obtain materials with higher porosity development.

Table 3.7. Total pore volume, micropore volume, micropore area and external surface area of the biochar samples from *Undaria pinnatifida.*

Samples	Total pore volume (cm^3/g)	Micropore volume (cm^3/g)	Micropore area (m^2/g)	External surface area (m^2/g)	A_{BET} (m^2/g)
inUP/Pyro400	0.01	-	-	3.6	3.6
inUP/Pyro400/W	0.02	-	-	5.7	5.7
peUP/Pyro400/W	0.02	-	-	7.9	7.9
inUP/Pyro800	0.02	0.01	25.6	10.9	36.5
inUP/Pyro800/W	0.07	0.02	41.2	12.3	53.5
peUP/Pyro800	0.04	0.02	45.2	18.4	63.6
peUP/Pyro800/W	0.14	0.03	71.9	66.5	138.4
inUP/Hydro/Type I	0.02	-	-	4.6	4.6
peUP/Hydro/Type I	0.02	-	-	3.6	3.6
peUP/Hydro/1stPW	0.01	-	-	2.6	2.6
peUP/Hydro/2ndPW	0.02	-	-	4.2	4.2
peUP/Hydro/1stPW/S700	0.11	0.04	97.9	31.6	129.5

3.3.2. *Morphological and mineral characterization*

3.3.2.1. *SEM analysis*

The SEM analysis provided detailed images of the materials' morphology at a micrometric scale, while SEM-EDS allowed for elemental mapping of the starting biomass (intact and post-extracted) and ash of the materials. The SEM images of the starting biomass and some of the derived materials, all captured at x750 magnification, and the ash images, all in x155 magnification, are presented in Figure 3.13. Table 3.8 presents the atomic percentage of the elements identified in the biomass and respective ash.

The SEM images reveal significant differences in the morphology of *Undaria pinnatifida* biomass across various treatments. The intact biomass (inUP) exhibits a more homogeneous structure, reflecting its original cellular morphology, while the post-extracted biomass (peUP) shows visible structural alterations, likely due to the removal of components by solvents. The original cellular morphology is observed after pyrolysis (Pyro), but Hydrothermal carbonization (Hydro) reflects in morphology changes. HTC processes influence the morphology, with ultrapure water (Type I) producing smoother and more uniform structures, while process water treatments (1^{st}PW and 2^{nd}PW) result in greater morphological variation, potentially due to impurities or cumulative effects. Overall, pyrolysis preserves more of the original structure, whereas HTC increases morphological heterogeneity influenced by water chemistry.

The observed changes in elemental composition (Table 3.8) between intact and post-extracted biomass can be attributed to the solubility of specific elements or compounds in the solvents used for extraction. For example, Na, C, and N are significantly reduced, indicating these elements or their associated compounds are likely dissolved in the solvent. In contrast, O, S, and Si increased, suggesting they were less soluble possibly resulting in their relative concentration increase. Overall, the elemental analysis indicates that the extraction process alters the elements´ distribution, often concentrating minerals in the ash while removing or reducing organic components. Nitrogen, primarily from proteins and amino acids, is reduced after extraction and is completely volatilized during ashing, leaving no detectable nitrogen in the ash. While oxygen in the ash reflects the presence of oxygen-rich inorganic compounds like oxides or carbonates originally present in the biomass or formed during combustion. Trace amounts of strontium were quantified in both inUP and peUP ashes, in line with other literature studies such as Marzocchi et al.(2016) that report the ability of brown macroalgae, including *U. pinnatifida*, for concentrating this and other heavy metals from the environment.

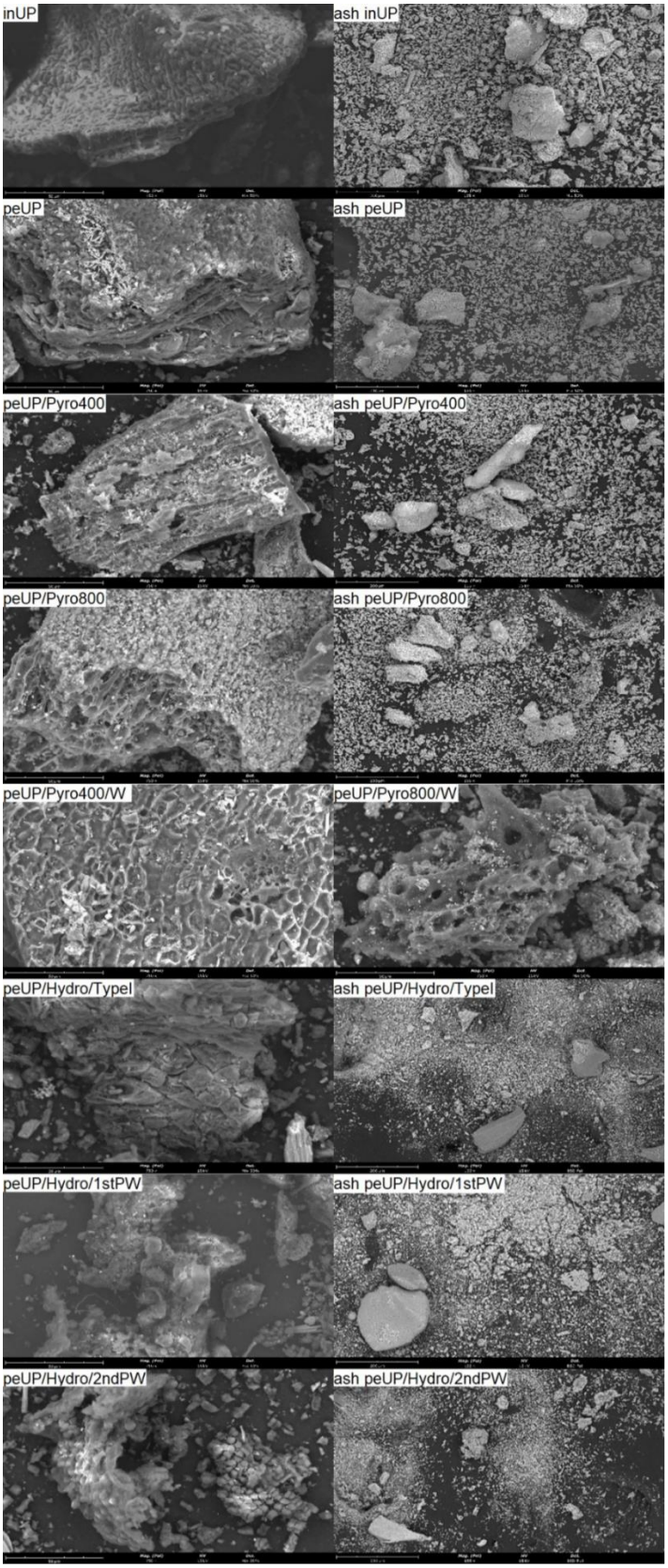

Figure 3.13. SEM images for the intact (in-) and post-extracted (pe-) biomass of *Undaria pinnatifida* and some of the derived materials (amplification – x750) on the left column and the corresponding ash (amplification x155) on the right column Hydro – Hydrothermal carbonization; Pyro – Pyrolysis, followed by the temperature used (400ºC or 800ºC); 1st and 2nd PW – process water; Type I – ultrapure water; W- post-washed.

Table 3.8. Atomic percentage of the elements identified in *Undaria pinnatifida* biomass (intact and post-extracted) and respective ash.

Element	Intact biomass		Post-extracted biomass	
	Biomass	Ash	Biomass	Ash
C	37.7	6.6	31.6	5.9
N	2.4	n.i.	1.9	n.i.
O	38.1	52.9	41.2	47.9
F	n.i.	n.i.	1.0	n.i.
Na	4.4	3.2	1.8	13.7
Mg	0.5	2.4	0.9	0.8
P	0.2	1.6	0.5	1.8
S	1.6	0.7	3.1	5.0
Cl	6.2	2.4	1.5	3.4
K	2.7	3.4	4.0	4.9
Ca	5.9	13.2	5.2	12.4
Si	0.1	7.0	6.6	3.6
Al	0.1	6.4	0.5	0.5
Sr	n.i.	0.2	n.i.	0.1

n.i. – Not identified

3.3.2.2. *XRD analysis*

The crystalline structures of the materials were obtained through powder XRD (X-ray diffraction) analysis. In the present study, the XRD patterns revealed peaks within the range of characteristic values of metals salts of the cations identified by SEM-EDS analysis, as for example NaCl, $CaCO_3$, KCl or SiO_2. The diffractograms in Figure 3.14 point for differences in the crystalline phases of the ash resultant from inUP and peUP, reflecting the influence of the extraction solvents in the inorganic composition of the post-extracted biomass compared to the non-extracted one. However, the presence of numerous crystallin peaks indicates the need for future detailed identification to fully characterize the material.

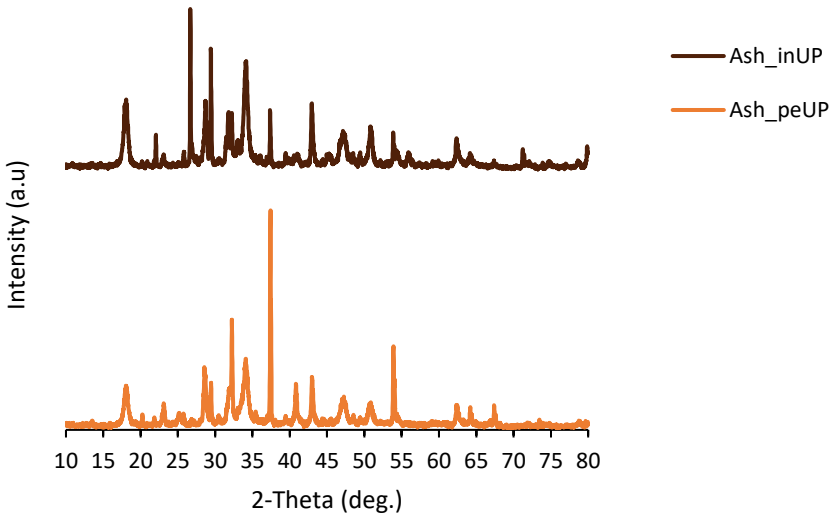

Figure 3.14. XRD pattern of the ashes obtained from intact (in-) and post-extracted (pe-) biomass from *Undaria pinnatifida.*

The XRD patterns of the ashes of the pyrochars (Figure 3.15) and hydrochars (Figure 3.16) produced from the non-extracted and post-extracted biomass and compared with Figure 3.14. Materials obtained by pyrolysis or HTC present only some of the crystalline phases observed in the ashes of the biomass. The washing process after pyrolysis tends to reduce the intensity of certain peaks which is expected to be related with the removal of soluble salts.

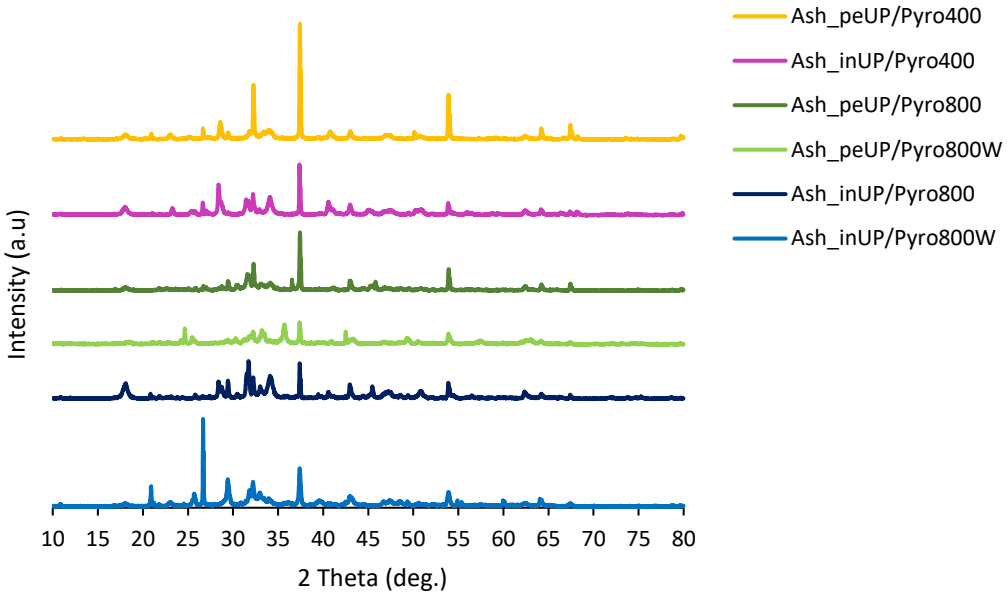

Figure 3.15. XRD pattern of the ashes from pyrochars (pyro) processed at 400 °C or 800 °C derived from intact (in-) or post-extracted (pe-) biomass from *Undaria pinnatifida.* W- washed with distilled water.

.

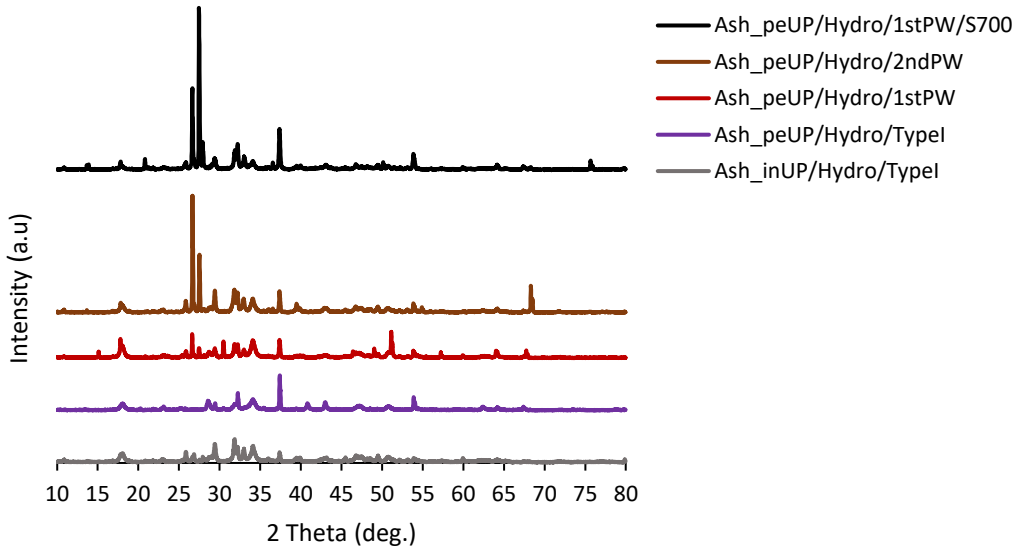

Figure 3.16. XRD pattern of the ashes obtained from hydrochars (Hydro) derived from intact (in-) and post-extracted (pe-) biomass from *Undaria pinnatifida.* AP – Process water. Type I – Ultrapure water. The S700 refers to the steam treatment sample at 700 ºC.

3.3.3. *Preliminary assays in liquid phase*

In the preliminary assays in liquid phase the samples were selected in terms of their more promising characteristics such as BET areas and micro-mesoporous network, for testing in adsorption of selected PhCs (ibuprofen, diclofenac and paracetamol) at 60 mg/L of concentration.

3.3.3.1. Adsorption of ibuprofen

Standard solutions of ibuprofen were prepared at concentrations of 30, 60, 90, and 120 ppm using ultra-pure water. The absorbance values at 222 nm were plotted against the corresponding concentrations to generate a linear calibration curve (Figure 3.17).

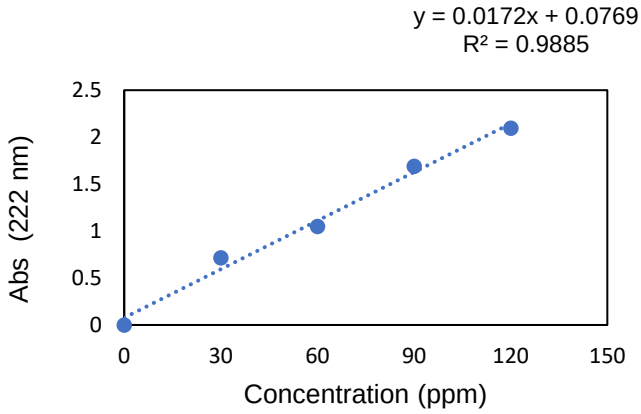

Figure 3.17. Calibration plot of ibuprofen solution obtained using a quartz cuvette with 5 mm of optical path.

The adsorption of ibuprofen was assessed after 24 h of contact time with the selected biochars and the adsorption of ibuprofen was minimal (Figure 3.18) with values lower than 1 mg/g (Table 3.9).

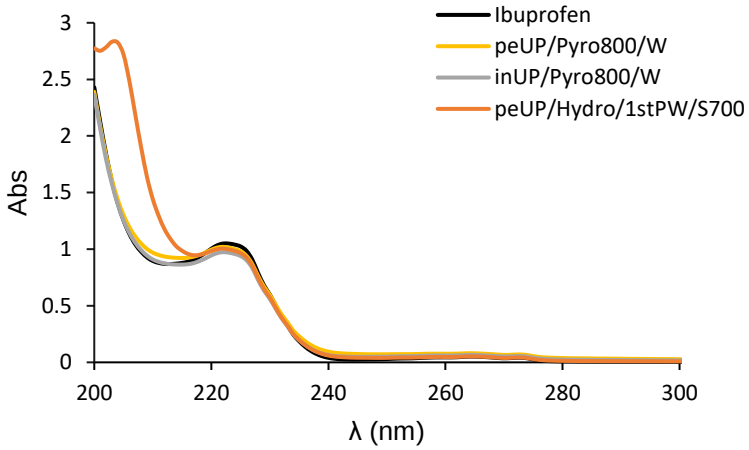

Figure 3.18. UV absorption spectra of ibuprofen solution (60 mg/L) before and after adsorption by the selected pyrochars (Pyro) at 800 ºC and hydrochar (Hydro) with steam treatment (700 ºC) from intact (in-) and post-extracted (pe-) biomass of *Undaria pinnatifida* (PW – Process water, W – washed).

Table 3.9. Ibuprofen adsorption capacity for the presented biochars.

Sample	**peUP/Pyro800/W**	**inUP/Pyro800/W**	**peUP/Hydro/1stPW/S700**
q_e (mg/g)	0.105	0.731	0.257

3.3.3.2. Adsorption of diclofenac

Standard solutions of diclofenac were prepared at concentrations of 30, 60 and 90 ppm using ultra-pure water. The absorbance values at 276 nm were plotted against the corresponding concentrations to generate a linear calibration curve (Figure 3.19).

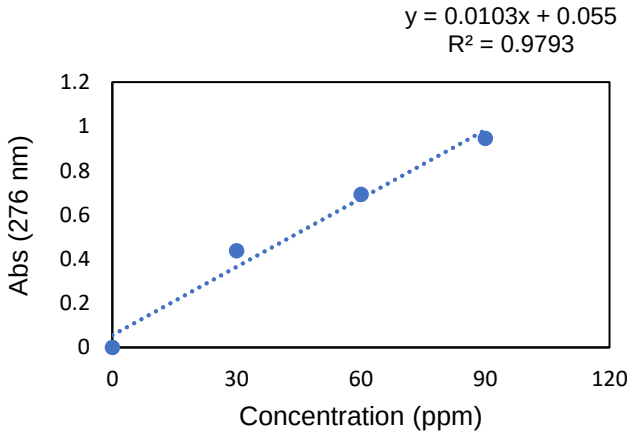

Figure 3.19. Calibration plot of diclofenac solution obtained using a quartz cuvette with 5 mm of optical path.

The adsorption of diclofenac was assessed, after 24 h of contact time with the selected biochars, and the adsorption of diclofenac was superior to the adsorption of ibuprofen (Figure 3.20), but the values were only approximately 2 mg/g (Table 3.10).

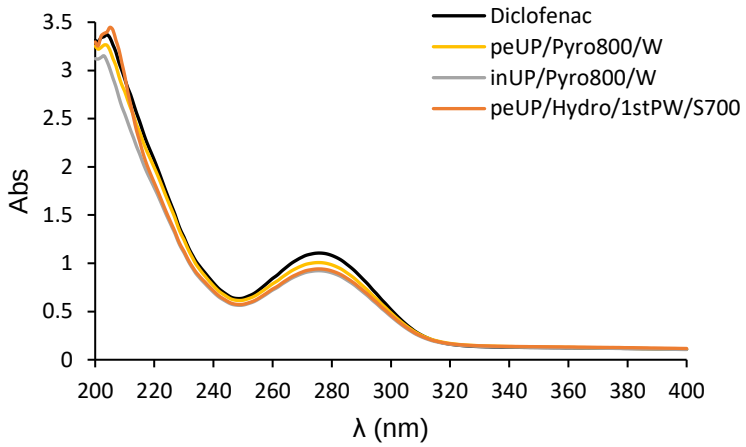

Figure 3.20. UV absorption spectra of diclofenac solution (60 mg/L) before and after adsorption by the selected pyrochars (Pyro) at 800 ºC and hydrochar (Hydro) with steam treatment (700 ºC) from intact (in-) and post-extracted (pe-) biomass of *Undaria pinnatifida* (PW – Process water, W – washed).

Table 3.10. Diclofenac adsorption capacity for the presented biochars.

Sample	**peUP/Pyro800/W**	**inUP/Pyro800/W**	**peUP/Hydro/1stPW/S700**
q_e (mg/g)	1.233	2.290	2.293

3.3.3.3. *Adsorption of paracetamol*

Through observation of Figure 3.21, it seems to have occurred degradation of paracetamol with the post-extracted and intact pyrochars at 800 ºC and washed (peUP/Pyro800/W and inUP/Pyro800/W, respectively) and modification of the paracetamol compound structure with the post-extracted hydrochar with steam treatment at 700 ºC (sample peUP/Hydro/1stPW/S700). The replica (*) presents the same results. These results are quite interesting and need further investigation.

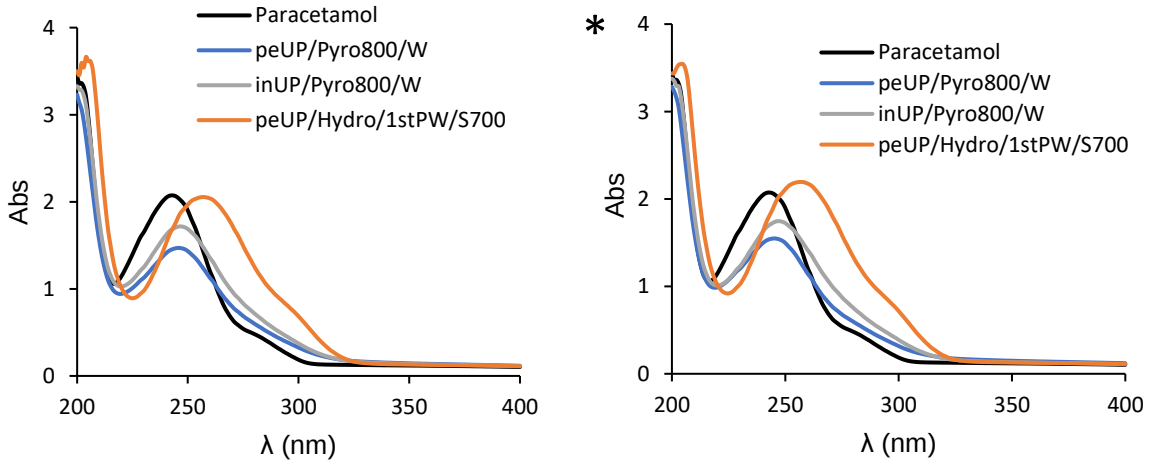

Figure 3.21. UV absorption spectra of paracetamol solution (60 mg/L) before and after adsorption by the selected pyrochars (Pyro) at 800 ºC and hydrochar (Hydro) with steam treatment (700 ºC) from intact (in-) and post-extracted (pe-) biomass of *Undaria pinnatifida* (PW – Process water, W – washed).

3.4. Process water assay

The hydrothermal carbonization process is a sustainable way to convert wet biomass into biochar, requiring less energy than traditional methods like pyrolysis. However, it generates large volumes of process water that usually requires filtration and is often discarded. To repurpose this byproduct, the HTC water was tested against biofilm-forming bacteria, previously studied with *U. pinnatifida* extracts. This testing aims to evaluate possible antimicrobial properties in the process water, potentially adding value to the HTC process by turning waste into a useful bioactive product.

3.4.1. *Antimicrobial activity assay*

The results of the antibacterial assay with process water from HTC against *Serratia* sp., *Vibrio* sp., *Citricoccus* sp., *Pseudomonas* sp. and *Bacillus subtilis* are depicted in Figure 3.22.

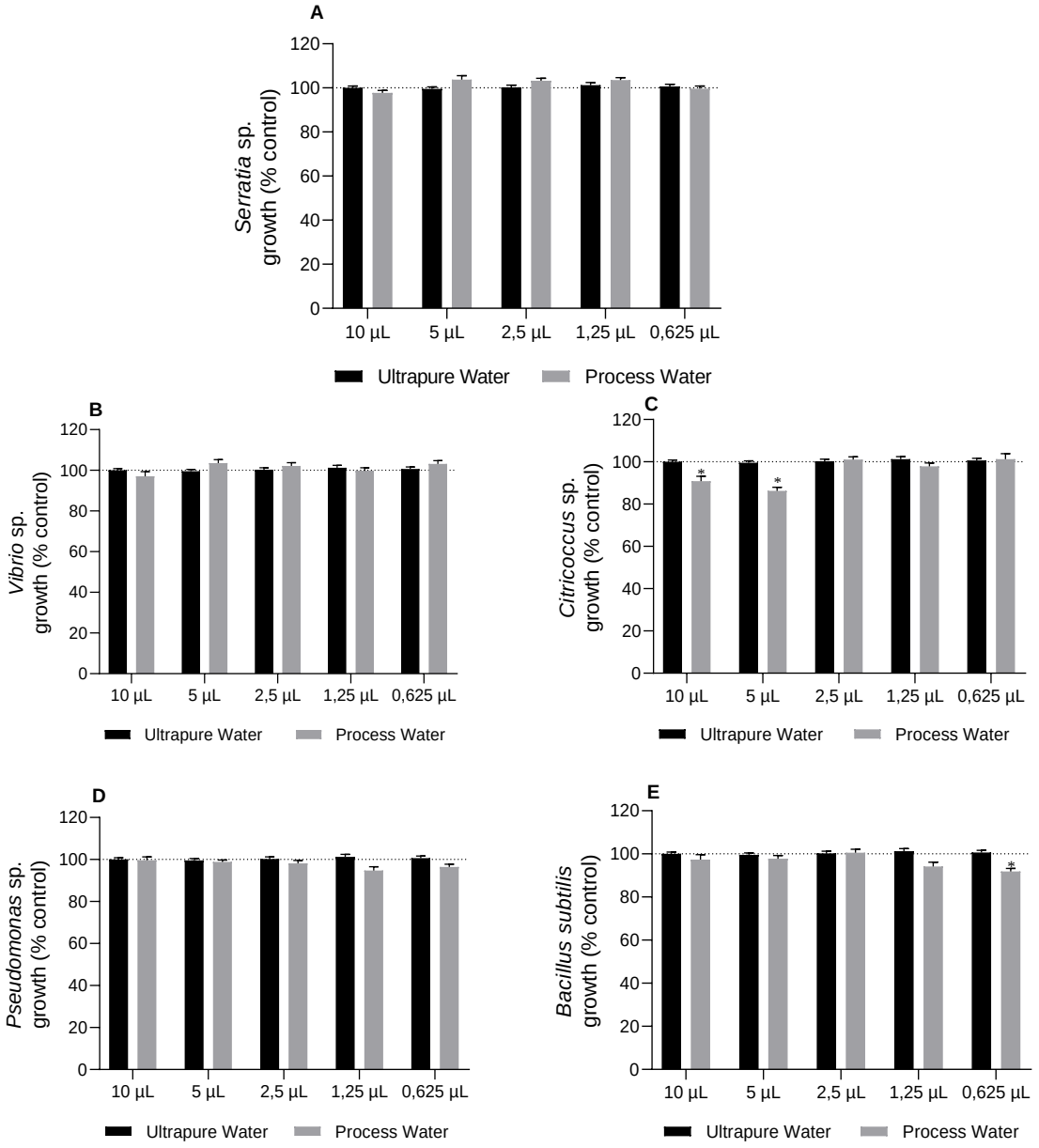

Figure 3.22. Process water (residual from HTC at 170 °C) capacity to inhibit the growth of (A) *Serratia* sp., (B) *Vibrio* sp., (C) *Citricoccus* sp., (D) *Pseudomonas* sp., and (E) *Bacillus subtilis*. The values in each column represent the mean ± standard error of the mean (SEM) from three independent experiments carried out in triplicate. Negative control (C-) was conducted with the addiction of ultrapure water. The symbol * represents significant differences with negative control (One-Way ANOVA, Dunnett's test; $p < 0.05$).

The process water from hydrothermal carbonization showed minimal antibacterial effects in this assay. Only against *Citricoccus* sp. it exhibited some inhibition (14%) at higher concentrations, while with *Bacillus subtilis* the process water showed less than 10% inhibition at the lowest concentration. These results suggest that the process water has limited effectiveness in inhibiting the growth of these biofilm-forming bacteria.

3.4.2. *Biofilm inhibition activity*

The results of the biofilm inhibition assay with process water from HTC against five biofilm-producing bacteria: *Serratia* sp., *Vibrio* sp., *Citricoccus* sp., *Pseudomonas* sp. and *Bacillus*

subtilis are presented in Figure 3.23.

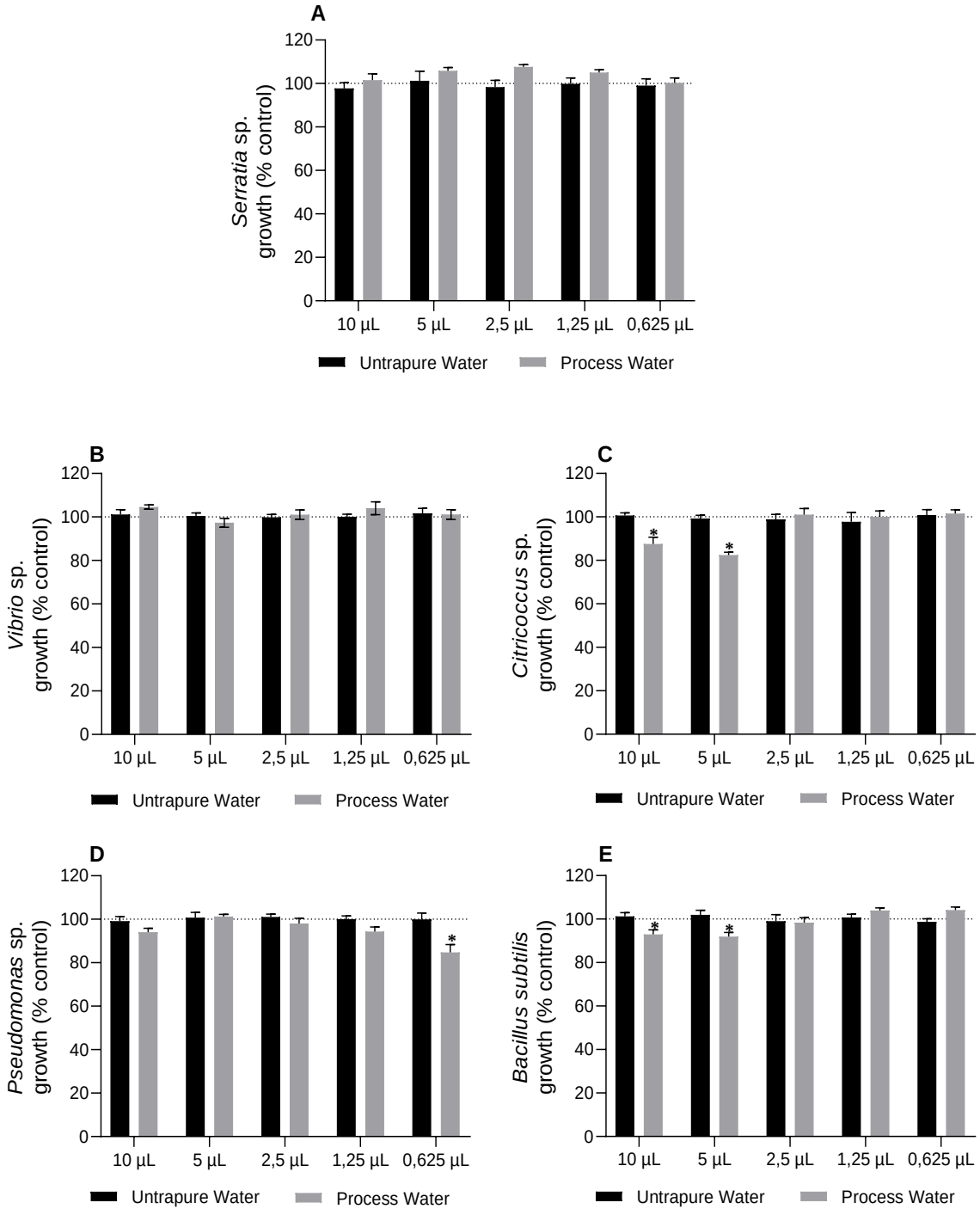

Figure 3.23. Process water (residual from HTC at 170 °C) capacity to inhibit the biofilm of (A) *Serratia* sp., (B) *Vibrio* sp., (C) *Citricoccus* sp., (D) *Pseudomonas* sp., and (E) *Bacillus subtilis*. The values in each column represent the mean ± standard error of the mean (SEM) from three independent experiments carried out in triplicate. Negative control was conducted with the addiction of ultrapure water. The symbol * represent significant differences with negative control (One-Way ANOVA, Dunnett's test; $p < 0.05$).

The process water showed an inhibition of 15% of *Pseudomonas* sp. biofilm growth at the lowest concentration, and against the biofilm of bacteria *Citricoccus* sp. there was a 18%, and 13% inhibition with 5 µL and 10 µL, respectively. Both, 10 µL and 5 µL inhibited 10% *B. subtilis* biofilm formation.

4. Discussion

In response to the growing demand for more sustainable solutions to combat biofouling, there has been increasing interest in exploring natural compounds with antifouling properties. Seaweed, as highly adaptive sessile organisms, have developed various strategies to survive in their environment, including the production of secondary metabolites to deter biofouling species. This study investigated the antifouling potential of crude extracts from the invasive brown seaweed *U. pinnatifida*, obtained using different solvents: water and/or ethanol, *n*-hexane, ethyl acetate, dichloromethane and methanol. While there is abundant research on the antimicrobial properties of marine seaweed, and *U. pinnatifida* has been shown to possess bioactive compounds like fucoidan and fucoxanthin with potential antimicrobial effects, there is a lack of studies focusing on *U. pinnatifida* in the biofouling context.

U. pinnatifida is widely harvested as a food source, yet much of the seaweed is still discarded. Additionally, it is a global invasive species, ranking among the top 10 invasive species in Europe. Finding applications for this biomass could address two issues: it would reduce waste from unused portions and offer sustainable solutions for antifouling or antimicrobial applications. Repurposing *U. pinnatifida* could thus help mitigate its invasive impact while unlocking new uses for this abundant resource.

Extraction techniques significantly influence not only the yield, purity, and efficacy, but also the production cost and biofunctional activity (Park et al., 2024). Chemical extraction with organic solvents is widely used to extract bioactive compounds from seaweed (Park et al., 2024). In this work, one of the main objectives was to incorporate green solvents to support sustainable practices with minimal environmental impact. Water, ethanol, and ethyl acetate were selected due to their renewable sources, biodegradability, and lower toxicity compared to other conventional solvents. However, *n*-hexane, dichloromethane and methanol were also included in this study. This approach allowed us to compare the extraction efficiency of green solvents against more conventional ones. Also, the sequential extraction with solvents of increasing polarity allows for a broader extraction of different polarity compounds from the seaweed.

The yield of a chemical extraction depends on distinct factors, like the extraction technique, time, temperature, as well as the class of solvents (Silva et al., 2021). Park et al. (2024) also referenced that differences in extraction efficiencies among different parts of seaweed (such as the blade or root) were statistically significant.

From the extraction with different solvents, the best yield (10.3%) was obtained from ethanol-water (50:50) followed by the ethanol-water (80:20) extract (8.2%), while the hexane and ethyl acetate extracts had lower yields (0.4% and 0.3%, respectively). Silva et al. (2021) reported smaller yield percentages of *U. pinnatifida* extraction with hexane and ethyl acetate, and the higher yield was obtained with ethanol. Ethanol:water (80:20) mixture is a relatively polar solvent, which likely helps to extract lipophilic and hydrophilic compounds. Ethyl acetate is a medium-polarity solvent and hexane is a non-polar solvent, and the low yield suggests that non-polar compounds are present in lower quantities in *U. pinnatifida*, or the compounds may not be easily extracted in the conditions used.

Some ways to obtain higher yields could be the optimization of temperature and extraction time, which could help balance yield with compound integrity, or adopting green extraction techniques like ultrasound-assisted extraction, microwave-assisted extraction or CO_2 supercritical fluid extraction, which is considered environmentally friendly and efficient for extracting non-polar and semi-polar compounds (Park et al., 2024).

Ecotoxicology examines how chemicals affect organisms in various environments, including marine, freshwater, terrestrial, and air. It considers the risks to a wide range of species, from plants and fungi to mammals (Martins et al., 2024). With nearly 6.5 million terrestrial and 2.2 million marine species, complete knowledge of chemical effects is unattainable (Martins et al., 2024). Instead, ecotoxicologists focus on a few indicator organisms and the physicochemical properties of compounds to understand their

environmental impact (Martins et al., 2024). In the ecotoxicity studies with *Artemia salina* the dichloromethane-methanol and *n*-hexane extracts both had a survival of 83%, and the other extracts presented similar to the negative controls a survival of 100%. This data is useful in determining the relative safety of various extracts. The lower survival rate could be a result of specific compounds that *Artemia salina* may have some sensitivity to that was better extracted with those solvents.

The extracts were tested against various organisms responsible for biofouling, including bacteria and microalgae, and on their ability to inhibit biofilm formation, *quorum sensing* mechanism, and anti-enzymatic activity (acetylcholinesterase and tyrosinase).

Citricoccus are Gram-positive, non-motile bacteria within the phylum Actinobacteria, commonly found in environments adhered to marine seaweed (Chandrasekaran et al., 2019). Both the hexane and ethyl acetate extracts have shown strong inhibition of this bacteria at 1000 µg/mL, 87.2% (IC_{50} of 203.1) and 78.0% (IC_{50} of 435.2 µg/mL), respectively. This suggests that *Citricoccus* sp. might be particularly susceptible to the active compounds in both extracts. The fact that both extracts still show significant inhibition at low concentrations highlights the potential of these extracts for targeting this organism.

For *Vibrio* sp., the ethyl acetate extract proved to be notably effective, with 79.1% inhibition at 1000 µg/mL and a decrease to 41.0% inhibition at 500 µg/mL (IC_{50} of 419.7 µg/mL). This suggests that the active compounds in the ethyl acetate extract exhibit strong antibacterial activity against *Vibrio* sp. at higher concentrations and moderate activity at lower concentrations. The hexane and hydroethanolic (80:20) extracts showed some antimicrobial activity, with inhibition rates of 42.3% and 40.0%, respectively, indicating the presence of antimicrobial compounds, though with lesser efficacy as compared to the ethyl acetate extract. *Vibrio* sp*.* are Gram-negative, rod-shaped bacteria prevalent in aquatic environments, known for their association with diseases in aquatic life and human seafood consumption (Baker-Austin et al., 2018).The differences in activity suggest that ethyl acetate might extract more specific bioactive compounds that are effective against *Vibrio*. A study by Stabili et al. (2023) demonstrated the effectiveness of lipidic extracts from *U. pinnatifida* against a broad range of *Vibrio* species, including pathogenic strains affecting farmed fish. The inhibition zones for these extracts were comparable to traditional antimicrobial agents, measuring around 12 mm, depending on the concentration (Stabili et al., 2023).

The results of the antibacterial assay using *U. pinnatifida* extracts show that both the dichloromethane-methanol and hexane extracts exhibited significant antibacterial activity, with inhibition rates of 72.9% (IC_{50} of 831.1 µg/mL) and 68.4% (IC_{50} of 944.8 µg/mL) at 1000 µg/mL, respectively, against *Serratia* sp., a gram-negative, rod-shaped bacteria that is facultatively anaerobic and commonly found in various environments, including soil and water (Friedrich et al., 2021).

The inhibition of *Pseudomonas* sp. and *Bacillus subtilis* was relatively low (below ≈30.0%), with hexane and ethyl acetate being the best-performing extracts. *Pseudomonas* sp. are Gram-negative bacteria notorious for their pathogenicity, robust biofilm formation, and resistance to treatment in clinical and marine settings (Wu et al., 2016) and *Bacillus subtilis* is a motile, Gram-positive bacteria known for biofilm formation and spore production under nutrient scarcity, often serving as a model for biofilm studies (Mohsin et al., 2021). The results could indicate that these bacteria are less susceptible to the compounds in the extracts, or that higher concentrations would be needed for a more significant effect.

Ferreira et al. (2021) reported significant antimicrobial effects, including against common wound pathogens such as *Staphylococcus aureus* and *Pseudomonas aeruginosa* with *U. pinnatifida* extracts, specifically focusing on phlorotannin-enriched fractions.

It is important to note that the limited effectiveness of the extracts on some of the Gram-negative bacteria could stem from their unique structure, which includes an outer membrane and a periplasmic space absent in Gram-positive bacteria. This outer membrane serves as a

barrier against many antibiotics, and the periplasmic space contains enzymes that can degrade foreign substances entering the cell (Pinteus et al., 2015).

The extracts showed less inhibitory effectiveness compared to the positive control, Oxytetracycline. Oxytetracycline is a purified compound, with great antimicrobial activity, being used in human and animal medicine, on the other hand, the extracts here analyzed are a complex mixture of compounds that can camouflage the effect of the bioactive ones (Pinteus et al., 2015).

The ability of bacteria to form and maintain biofilms is crucial for their persistence and resistance to antibacterial treatments. Biofilms are complex three-dimensional aggregates of bacteria that adhere to surfaces and materials such as metals, glass, plastics, tissues, and medical devices. The biofilm matrix provides protection against environmental factors such as pH changes, nutrient deficiencies, and mechanical stress (Srinivasan et al., 2021). Bacterial cells within biofilms communicate and coordinate their behavior through signaling molecules in a process known as *quorum sensing*. QS plays a crucial role in biofilm formation among various Gram-negative and Gram-positive bacterial pathogens. It regulates the physiological state of the microbial community and controls biofilm development through specific signal molecules: *N*-acyl-homoserine lactones in Gram-negative bacteria and auto-inducing peptides in Gram-positive bacteria (Srinivasan et al., 2021).

None of the extracts significantly inhibited biofilm formation or affected QS activity in the tested bacteria, nor did they impact the growth of *C. violaceum.* This could suggest that the concentrations of the extracts used may have been too low to exert any significant effect or the chemical composition of the extracts might lack the specific active compounds necessary to inhibit biofilm formation, and the QS mechanism on this specific bacteria. Also the interaction between the compounds in the mixture of crude extracts could interfere with the activity of certain active compounds present in the *U. pinnatifida* extract.

There is limited research directly focusing on the effect of *U. pinnatifida* extracts on the growth of diatoms. Diatoms are single-celled seaweed that belong to the group of eukaryotic phytoplankton and have been around for over 180 million years. They are found in various regions around the globe, thriving particularly in nutrient-rich coastal ecosystems and at high latitudes. Diatoms exhibit either radial symmetry or bilateral symmetry. Ranging in size from 1 µm to 200 µm, these unicellular photosynthetic organisms play crucial roles in major biogeochemical cycles, including carbon sequestration, oxygen production, and nutrient recycling. In fact, diatoms contribute to about 20% of global carbon fixation (Celi et al., 2022). They are effective indicators for environmental monitoring due to their year-round presence, quick response to environmental changes, and strong adherence to various substrates (Akcaalan et al., 2022).

The diatoms used in this study were: *Chaetoceros calcitrans* (Paulsen) Takano, (1968), *Phaeodactylum tricornutum* (Bohlin, 1897)*, Nitzschia* sp. and *Amphora* sp. These diatoms are widespread in marine environments and were chosen due to their ability to colonize submerged structures, playing a critical role in biofilm formation, making them highly relevant targets in anti-biofouling studies (Abed, R. et al., 2019, Beekrum et al., 2023, Celi et al., 2022, Li et al., 2017, S.-D. Lee & Lee, 2011, Suriyanti & Usup, 2017).

The results from the diatom growth inhibition assay with those four types of microalgae indicate that both hexane and ethyl acetate extracts from *U. pinnatifida* exhibit promising potential as inhibitors of diatom growth, particularly in the case of *C. calcitrans* and *Amphora* sp*.* The hexane extract demonstrated the strongest inhibition, with a 10 mm inhibition zone. This is a significant result, as it suggests that this extract contains potent bioactive compounds that can effectively inhibit the growth of *C. calcitrans.* Against *Amphora* sp., the *n*-hexane and ethyl acetate extracts were the most effective, each with an 8 mm inhibition halo.

Now focusing on the enzyme study, the inhibition of tyrosinase and acetylcholinesterase was investigated, as these enzymes are associated with the adhesive processes involved in the settlement of various biofouling species. Acetylcholinesterase is an essential enzyme found in many living organisms, mainly within the nervous system and muscles, where it controls acetylcholine levels during nerve signal transmission in both the central and peripheral nervous systems (Wiesner et al., 2007).

The tyrosinase enzyme is an important part of the settlement of mussels and tubeworms in rocks or other surfaces. Marine invertebrates rely on proteinaceous underwater adhesives for both permanent and temporary attachment to rocks in the intertidal zone. The presence of DOPA is a distinctive feature common to proteins identified in the adhesive systems of both mussels and tubeworms. DOPA is produced by the post-translational hydroxylation of tyrosine residues of the adhesive proteins by tyrosinase enzymes (Duthoo et al., 2024). The inhibition of this enzyme can prevent their attachment to anthropogenic surfaces.

Ethyl acetate extract was the most effective in inhibiting tyrosinase activity, exhibiting an IC_{50} of 643 (529.2 – 791.4) µg/mL, followed by the hexane extract with 37% inhibition. Kim et al., (2024) investigated the effects of *U. pinnatifida* sporophyll extracts on tyrosinase activity (which also acts in human melanin biosynthesis) and found that a polysaccharide-rich fraction significantly reduced tyrosinase activity.

In the field assay, the weight of the plates obtained was similar to the negative control. Several factors may affect this antifouling study. The plates were positioned randomly, and the crate was placed at a mid-depth in the marine environment where sunlight could penetrate, mimicking conditions similar to those experienced by a ship's hull. Additionally, the immersion time, the drying process of the plates, different weights and colonization rates of different organisms must be carefully considered when interpreting the results. These factors can lead to inconsistencies in biofouling assessment across the plates. One way to reduce the impact of these variables would be to increase the time of the test. In fact, the industry demands a 2 years trial in the ocean to attest the efficiency of new compounds (*personal communication of Biomimetex company*).

Observations were conducted using a binocular stereoscopic microscope to identify some of the organisms present on the plates, and similar organisms were identified in other studies on Portuguese waters. In the future, further analysis might be required to accurately identify the species present. Identifying exact species from a microscope image requires higher magnification, specific staining, or molecular techniques, especially for distinguishing similar microorganisms. To gain a more comprehensive understanding of biofouling dynamics, it would be advantageous to employ advanced techniques, such as computational image analysis. This method could enable more accurate measurements of the percentage of surface coverage by biofouling organisms.

In recent years, biochar derived from seaweed has attracted considerable attention due to its adsorption efficiency, high regeneration rate and low price since seaweed can grow in natural freshwater, seawater and wastewater without additional land and fertilizer. Also, seaweeds grow quickly and exhibit higher biomass yield and shorter harvesting cycles compared to terrestrial plants (Martins et al., 2024; Yao et al., 2020).

This work also explored the potential of synthesizing biochar from the residual biomass of *U. pinnatifida* collected in Spain, which would otherwise be discarded, aiming to establish a circular economy approach. The intact and post-extracted biomass as well as the resulting biochar materials were thoroughly analyzed and characterized. The adsorption of PhCs in water - ibuprofen, diclofenac and paracetamol - was evaluated.

The physicochemical properties of the biochar can be improved by a further activation process enhancing their application as adsorbents or catalysts. Generally, the activation improves the specific surface area and pore volumes and will also influence surface charge, composition, and functional groups. The activation process is mainly divided into physical and chemical activations. Physical activation mainly refers to the processing of biochar to increase its surface porosity by reaction with CO_2 or high steam temperatures usually between 700–900 °C. Physical activation is safer and more environment-friendly than chemical activation (Tan et al., 2023). This treatment enhances the surface area and creates a network of pores that are crucial for applications like adsorption, catalysis, and energy storage (Mestre & Carvalho, 2018b).

The intact and post-extracted biomass of *U. pinnatifida* had 24% and 22% ash content, respectively. Park et al. (2024) reported between 20% to 42% ash content for this seaweed, and different parts of the seaweed were tested, the root had the most ash and the sporophyll had the less percentage of ash. Jung et al. (2016) reported 24.5% ash content for the raw

biomass of the root of this seaweed. The results in the present study are in accordance with the literature values. Jung et al., (2016) also reported 6.98 pH for the raw biomass of *U. pinnatifida.*

According to the literature the biochar yields in pyrolysis process increase with a decrease in pyrolysis temperature (750 to 300 ºC) and a preferable low heating rate. In addition, feedstock properties, such as moisture content and particle size, also significantly affect the yield of biochar produced via pyrolysis (Yu et al., 2017). The pyrochars here produced from *U. pinnatifida* had 28-40% yield, being higher at 400 ºC. Jung et al. (2016) reported 67.7% and 39.3% yields at 400 ºC and 800 º C, respectively, for *U. pinnatifida* root derived pyrochars. Roberts et al. (2015) reported that six species of red and brown seaweed (including *U. pinnatifida*) yielded between 45-62% after slow pyrolysis for 1 h at 450 ºC, and biochar yield did not differ significantly between biochar produced from red and brown species, while Mondal et al., (2024) reported a 42-47% yield from pyrochars of two brown seaweeds, produced at 600 °C. In the present work the pyrolysis yields were lower than those reported by other literature studies with *Undaria* species, these may be related with the heating protocol and/or the fact that Jung et al. (2016) used the root while in this work the whole seaweed was used.

The ash content obtained by pyrolysis was between 53-59% at 400 ºC and 70-80% at 800 ºC. Jung et al., (2016) study showed 41.9% and 50.4% of ash content for pyrochars of 400 ºC and 800 ºC, respectively, with the root of *U. pinnatifida*, also Mondal et al. (2024) reported 42-52% ash content in two pyrochars (600 ºC) derived from two brown seaweed, more than the red and green seaweed also studied. The pyrochars values in this study were higher in ash content than the ones reported in literature, but the values were reduced to half, especially with pyrochars of 400 º C (26-30%), after the post-synthesis washing. The persistent high ash content (80%) in the post-extracted pyrochar at 800 ºC, even after washing, could be attributed to high temperature leading to higher carbon matrix consumption that results in higher quantity of inorganic compounds less soluble in water, meaning the washing process may not effectively remove them or the post-extracted biomass might already have a high concentration of mineral content or inorganic compounds that resist dissolution.

Seaweed-based biochar primarily consists of carbon (C), hydrogen (H), and oxygen(O), with additional inorganic elements like potassium (K), calcium (Ca), sodium (Na), and magnesium (Mg). High-temperature pyrolysis leads to the formation of inorganic salts, resulting in higher pH (pH > 7) and influencing biochar properties, particularly surface charge (Tan et al., 2023). The pH_{pzc} noted from the *U. pinnatifida* was highly basic, between 11-13 for pyrochars. Roberts et al. (2015) also noted basic pH values of 10-11 for biochar from *U. pinnatifida* while Jung et al., (2016) reported 8.1 and 10.1 for pyrochars of 400 ºC and 800 ºC, respectively. This study had slightly higher pH than the literature values, but after washed the values lowered to 7-9, indicating the effective removal of soluble basic salts during post-synthesis washing.

The pH of biochar is found to be affected by the pyrolysis temperature and the seaweed samples. The increase in the relative ash content in the biochar causes a rise in the pH of the biochar especially under severe pyrolysis conditions (Yu et al., 2017).But in this study the post-synthesis washing allowed to decrease the ash content and the basic surface chemistry pH_{pzc}.

The hydrochars prepared during 24 h at 170 ºC had a yield range of 27-31%. Yu et al., 2017 reported yields of 18.4 to 52.3% for hydrochars from brown macroalgae with the highest being reported after reaction times of up to 16 h and temperature between 180 ºC and 250 ºC.

The HTC process water contains organic acids that, when recirculated in later synthesis steps, can help increase mass yields (Martins et al., 2024). Incorporating process water into the hydrochar resulted in a higher yield, more 5 percentual points, with slightly higher ash content (9 percentual points). However, a substantial amount of process water still remains unused and is typically discarded. This study attempted to repurpose this excess process water as an antifouling agent against bacteria and biofilm formation.

Unfortunately, the results showed limited effectiveness, with inhibition rates mostly below 30% or comparable to the control. Other studies have explored adding value to HTC process

water by using it to produce bio-methane through anaerobic digestion, along with recovering nutrients and salts suitable for use as soil fertilizers. Additionally,HTC process water shows potential as a nutrient source for cultivating microalgae and as an effective additive for seed priming and enhancing germination (Martins et al., 2024).

The biochars synthesized by HTC presented similar ash content to the intact and post-extracted biomass (15-27%) and lower ash content than those obtained by pyrolysis. The pHpzc noted from the *U. pinnatifida* was between 7-8 for hydrochars. The hydrochar with steam treatment had similar results to the pyrochars. The steam treatment of hydrochar (700 ºC) creates a material with ash content of 67%, like those of pyrochars synthesized at 800 ºC, which was already expected. Also had a similar basic pH of 12 lowered to 8 after washed with distilled water.

Specific surface area, pore volume, and pore size are the relevant parameters to predict the adsorption performance of biochars. The surface area of seaweed biochar is generally low, but some studies reported that an increase in the pyrolysis temperature could result in a higher surface area (Tan et al., 2023, Yu et al., 2017). The biochars with the most developed micro-mesoporous network and the highest BET areas were from the pyrochar produced at 800 ºC from the post-extracted biomass after washing, and the hydrochar after steam treatment with 138 m²/g and 130 m²/g, respectively. Even so, the steam treatment of the hydrochar did not allow to produce an activated carbon most probably due to the high ash content of this seaweed, regardless using the intact or post-extracted biomass. All BET areas of pyrochars increased after washing. Jung et al. (2016) reported 70.3 m²/g BET area and a total pore volume of 0.11 cm³/g for pyrolysis at 400 ºC and a BET area of 44.5 m²/g and a total pore volume of 0.06 cm³/g at 800 ºC with *U. pinnatifida* roots. Jung et al. (2016) also reports that at higher pyrolysis temperatures (600–800 °C), biochar properties deteriorated due to pore blockage caused by material softening, melting, and carbonization. In this study the results observed for both temperature were the opposite, using the whole seaweed rather than just the root introduces more diverse organic compounds, which might influence pore formation and thermal decomposition behavior during pyrolysis. Higher pyrolysis temperatures (800 °C) often enhance BET areas due to increased devolatilization and pore development, though melting or sintering can sometimes reduce these effects. Washing likely removed residual salts, further exposing active surfaces in this study. Roberts et al., (2015) reported BET areas between 1.3 and 8.9 m²/g for *U. pinnatifida* pyrochars produced at 450 ºC for 60 min, values similar to the ones reported in this work for the pyrochars at 400 ºC.

These biochars exhibit Type IV isotherms with H3 and H4 hysteresis loops, typical of mesoporous materials with micropore-mesopore combinations in line with finding by Yao et al. (2020) study also on, biochar from *U. pinnatifida* were type IV isotherms were obtained.

Post-extracted materials (peUP) outperformed intact ones (inUP) in porosity and surface area, with peUP/Pyro800/W reaching the highest BET area. It also exhibits the greatest total pore volume (0.14 cm³/g) and significant meso- and macropore presence, evidenced by a large external surface area (66.5 m²/g). Yao et al. (2020) reported that the specific surface area of a pyrochar prepared at 800 ºC (2 h) from *U. pinn*atifida was 69.70 m²/g, with a total pore volume of 0.04 cm³/g. In the present study, the peUP/Pyro800 without washing also had the same total pore volume (0.04 cm³/g) and BET area of 64 m²/g.

The steam activation significantly enhanced the properties of the hydrochars. For instance, peUP/Hydro/1stPW/S700 displays a high micropore area (97.9 m²/g) and specific surface area, making it a more micropore material and possibly effective for adsorbing small organic molecules.

In general, the present work obtained biochars with properties within the range reported in the literature. The results allow us to understand the influence of the extraction process on the final properties of these materials, a novel aspect not previously addressed in studies that predominantly use intact biomass. By utilizing post-extraction biomass, this study

aligns with the principles of circular economy and biorefinery, providing a sustainable and value-added application for residual biomass that might otherwise remain underutilized.

In terms of the morphology and element composition, Yao et al., 2020 described the preparation of a pyrochar from *U. pinn*atifida (China) prepared in similar conditions of inUP/pyro800 from the present study. SEM images of the prepared samples showed a dense, rigid, and substantial morphology with sporadic pores and a compact structure (Yao et al., 2020), similarly to the present work. The Marzocchi et al., (2016) study on metals in *Undaria pinnatifida* and *Sargassum muticum* around Venice, Italy, reported the presence of various elements, including calcium (Ca), magnesium (Mg), iron (Fe), zinc (Zn), copper (Cu), manganese (Mn), strontium (Sr), lead (Pb), chromium (Cr), aluminum (Al), cobalt (Co), cadmium (Cd), nickel (Ni), arsenic (As), mercury (Hg), and barium (Ba). These elements were quantified using Inductively Coupled Plasma Mass Spectrometry, revealing variations linked to environmental factors and sampling locations (Marzocchi et al., 2016) . The present study identified same similar elements in the biomass of *U. pinnatifida* (Ca, Mg, Sr and Al). Calcium and magnesium are consistently high in both *U. pinnatifida* from the Venice Lagoon and the one from the present study. These comparisons suggest that while there are some regional variations, *Undaria pinnatifida* overall elemental profile remains relatively stable across studies. Adams et al., (2011) study on brown seaweed *Laminaria digitata* highlights the seasonal variability in its chemical composition, and when compared to *Undaria* from this present study, *Laminaria* shares similarities in its elemental profile. *U. pinnatifida* intact biomass contains 31.6% carbon and 6.6% ash. These values align closely with *Laminaria* summer composition, where ash content is minimized, and carbon is elevated (Adams et al., 2011). Martins et al., (2024) reported, for the hydroethanolic post-extracted green seaweed *Codium* sp., a lower amount of calcium and sulfur levels compared to *U. pinn*atifida. For example, calcium in the biomass of *Undaria* (5.2%) in this study is much higher than in *Codium* sp. (0.5%) from Martins et al., (2024) study, with a similar trend in ash content (12.4% vs. 3.1% respectively).

Water plays a crucial role in spreading contaminants of emerging concern such as pharmaceuticals, pesticides, and hormones. The European Union has highlighted this issue, recognizing the potential risks posed by biologically active pharmaceuticals even at low concentrations. Wastewater treatment plants currently struggle to filter out these compounds effectively, posing a challenge for future regulations that may require stronger barriers against these contaminants to protect ecosystems and human health (Viegas et al., 2022).

Among the most-consumed drugs, ibuprofen stands out, particularly in the UK, where production reaches several kilotons per year. Its solubility in water and organic solvents enables significant mobility through aquatic systems, challenging traditional water treatments. This has prompted interest in advanced methods, such as activated carbon filtration, which can better adsorb benzene ring structures like those in ibuprofen (Mestre et al., 2007). Similarly, diclofenac, another widely used anti-inflammatory drug, is often detected in wastewater due to its prevalent use in both urban and rural settings. These residues easily enter the environment, raising concerns and their effects on aquatic ecosystems (Johnson et al., 2007). Paracetamol, known for its pain-relieving and fever-reducing effects, is also commonly found in water systems, particularly where it lingers following excretion or improper disposal (Bursztyn Fuentes et al., 2020). Wastewater treatment plants currently face difficulties in fully removing paracetamol,which contributes to potential bioaccumulation in aquatic life and environmental degradation (Bursztyn Fuentes et al., 2020).

The adsorption of these PhCs onto the biochars with the more developed porous networks were minimal, with adsorption of ibuprofen and diclofenac incapable of surpassing 2 mg/g. The assays aiming the removal of paracetamol with the pyrolysis samples

(peUP/Pyro800/W and inUP/Pyro800/W) and the HTC sample further steam treated (peUP/Hydro/1stPW/S700) revealed that during the contact time of the biochars with the paracetamol solution under natural light there was a modification of the UV-vis absorption spectra of the solution thus pointing for the modification of the species in solution. Advanced oxidation processes are commonly employed in wastewater treatment, relying on free radicals to degrade organic pollutants (Tan et al., 2023). Algae-based biochar is particularly effective in this process due to its abundant surface functional groups and specific surface area, enhanced by endogenous nitrogen impurities (Tan et al., 2023). These characteristics provide the biochar with flexible electronic properties and a strong capacity for electron transfer, leading to an efficient degradation of organic pollutants (Tan et al., 2023). Jung et al. (2016) reported the adsorption of phosphate with pyrochars from roots of *U. pinnatifida* of 18 mg/g (400ºC) and 13 mg/g (800 ºC), the roots' biochar surface functional groups, including oxygen-containing groups like carboxyl and hydroxyl, contribute to cationic exchange capabilities. This enables interactions with phosphate ions in solution (Jung et al. 2016). This could be a possible application for the biomass of this study, or the adsorption of heavy metals which are adsorbed through similar mechanisms or, alternatively, it could be used as a fertilizer for soil amendment considering the high ash and pH values obtained.

6. Conclusions and Future Perspectives

Managing biofouling is likely to become increasingly difficult due to climate change. As ocean temperatures rise and acidity increases, the composition and quantity of biofouling organisms may change. For instance, calcifying species like barnacles, mussels, and tubeworms, which typically dominate biofouling, could decline, potentially being replaced by softer species such as ascidians. Additionally, marine growth tends to be more abundant and develops faster in warmer areas, suggesting that biofouling issues could worsen in temperate and polar regions as ocean temperatures continue to rise. Targeted extraction of specific antifouling compounds, using advanced solvent combinations, could enhance efficacy in bacterial *quorum sensing* disruption and biofilm inhibition.

U. pinnatifida extracts showed limited potential as a source of antifouling agents, but more research is needed to attest the presence of bioactive molecules. Based on the analysis of the different assays and ecotoxicity results, the ethyl acetate extract stands out as the most suitable solvent to concentrate antifouling compounds, exhibiting activity against different microfouling bacteria and enzymes essential for macrofouling organisms' settlement. Therefore, future works should be carried out to concentrate the bioactive compounds, which can encompass several chromatographic techniques such as column chromatography (CC), high performance liquid chromatography (HPLC), thin layer chromatography (TLC), etc. However, the main drawback is the relatively low extraction yield, which could be improved with optimized extraction conditions or by exploring alternative extraction methods, together with an exhaustive chemical characterization of the most bioactive extract.

Pursuing the framework of a circular economy approach, seaweed biomass was converted into a new material through carbonization methods aiming its application for bioremediation purposes.

Biochar derived from *U. pinnatifida* at 800 °C, especially the post-extracted and washed, had the most developed micro-mesoporous network with BET surface area reaching 138 m^2/g. Pyrochars outperformed hydrochars, aligning with Type IV isotherms with H4 hysteresis loops characteristic of materials with some micro and mesopores. This structure positions them as candidates for adsorption applications, though they showed limited adsorption of the chosen contaminants, but their high pH and rich ash content, offer valuable applications for both soil amendment and other water treatments. The alkaline nature of these biochars helps to neutralize acidic soils, improving fertility and water retention, while their mineral-rich ash content enhances plant growth by providing essential nutrients. In water treatment, these biochars could adsorb anionic species like phosphates and cationic heavy metals, such as lead and copper, improving water quality. The high surface charge and functional groups on the biochar enable these interactions, while the ash content supports metal precipitation.

The UV-vis absorption spectra of the paracetamol solution after contact with the biochars was modified pointing for the modification of the species in solution rather than the expected removal by adsorption. Further studies are needed to better understand paracetamol's interaction since these materials may have potential to be applied in advanced oxidation processes to degrade paracetamol or in other industrially relevant oxidation processes.

Characterization is important for the understanding of biomass and biochar chemical and physical properties which are useful for determining their potential applications (adsorbent for water treatment or for soil amendment purposes). Given the amount of ash content the biomass may be valuable for agricultural means. If aiming to obtain higher porosity development a potential future solution to remove most of the soluble ash would be to wash the biomass prior to carbonization, either with hot water (multiple washings) and higher stirring times or with an acid, such as hydrochloric acid, though the latter is less environmentally friendly. It would also be interesting to study the different parts of *Undaria* separated, like the sporophyll which has been reported to have less ash content. Conditions could also be

optimized (such as high temperature of 800 ºC with reduced residence time) to a more ash-free pyrochar. Aligned with the circular economy principles the process water was successfully recycled in the synthesis of hydrochar allowing to increase the yield of approximately 4.6 percentual points, but its possible application as anti-biofouling coating didn't work as intended. Other applications like bio-methane production, nutrient recovery for fertilizers, microalgae cultivation, and improving seed germination could be considered.

7. References

Adams, J. M. M., Ross, A. B., Anastasakis, K., Hodgson, E. M., Gallagher, J. A., Jones, J. M., & Donnison, I. S. (2011). Seasonal variation in the chemical composition of the bioenergy feedstock *Laminaria digitata* for thermochemical conversion. *Bioresource Technology*, *102*(1), 226–234. https://doi.org/10.1016/j.biortech.2010.06.152

Akcaalan, R., Kaleli, A., & Köker, L. (2022). Distribution of marine benthic diatoms on the coasts of the sea of Marmara and their responses to environmental variables. *Journal of Marine Systems*, *234*. https://doi.org/10.1016/j.jmarsys.2022.103780

Athanasiadou, V., Klontza, E. E., Dimitriou-Christidis, P., Fountoulakis, M., & Lekkas, D. F. (2023). Evaluation of *Arthrospira* (Spirulina) *platensis* growth on cheese whey in the context of circular economy. *Sustainable Chemistry and Pharmacy*, *34*. https://doi.org/10.1016/j.scp.2023.101173

Azevedo, J., Antunes, J. T., Machado, A. M., Vasconcelos, V., Leão, P. N., & Froufe, E. (2020). Monitoring of biofouling communities in a Portuguese port using a combined morphological and metabarcoding approach. *Scientific Reports*, *10*(1). https://doi.org/10.1038/s41598-020-70307-4

Baker-Austin, C., Oliver, J. D., Alam, M., Ali, A., Waldor, M. K., Qadri, F., & Martinez-Urtaza, J. (2018). *Vibrio* spp. infections. *Nature Reviews Disease Primers*, *4*(1). https://doi.org/10.1038/s41572-018-0005-8

Bursztyn Fuentes, A. L., Canevesi, R. L. S., Gadonneix, P., Mathieu, S., Celzard, A., & Fierro, V. (2020). Paracetamol removal by Kon-Tiki kiln-derived biochar and activated carbons. *Industrial Crops and Products*, *155*. https://doi.org/10.1016/j.indcrop.2020.112740

Celi, C., Fino, D., & Savorani, F. (2022). Phaeodactylum tricornutum as a source of value-added products: A review on recent developments in cultivation and extraction technologies. In *Bioresource Technology Reports* (Vol. 19). Elsevier Ltd. https://doi.org/10.1016/j.biteb.2022.101122

Chandrasekaran, L., Drautz-Moses, D. I., Uchida, A., Purbojati, R. W., Wong, A., Kushwaha, K. K., Putra, A., Gaultier, N. E., Premkrishnan, B. N. V., Heinle, C. E., Vettath, V. K., Junqueira, A. C. M., & Schuster, S. C. (2019). Complete Genome Sequence of *Citricoccus* sp. Strain SGAir0253, Isolated from Indoor Air in Singapore. *Microbiology Resource Announcements*, *8*(37). https://doi.org/10.1128/mra.00606-19

Cunningham, S., South, P., & Cahill, P. L. (2020). *Biosecurity Considerations for Farming Non-Native Seaweeds: A Case Study of Undaria pinnatifida in New Zealand*. https://doi.org/10.13140/RG.2.2.35410.79043

Dafforn, K. A., Lewis, J. A., & Johnston, E. L. (2011). Antifouling strategies: History and regulation, ecological impacts and mitigation. *Marine Pollution Bulletin*, *62*(3), 453–465. https://doi.org/10.1016/j.marpolbul.2011.01.012

Dimitrova, P. D., Damyanova, T., & Paunova-Krasteva, T. (2023). Chromobacterium Violaceum: A Model for Evaluating the Anti-Quorum Sensing Activities of Plant Substances. In *Scientia*

Pharmaceutica (Vol. 91, Issue 3). Multidisciplinary Digital Publishing Institute (MDPI). https://doi.org/10.3390/scipharm91030033

Duthoo, E., Delroisse, J., Maldonado, B., Sinot, F., Mascolo, C., Wattiez, R., Lopez, P. J., Van De Weerdt, C., Harrington, M. J., & Flammang, P. (2024). *Abundance, diversity and evolution of tyrosinase enzymes 3 involved in the adhesive systems of mussels and tubeworms 4 5 6*. https://doi.org/10.1101/2024.07.05.602216

Epstein, G., & Smale, D. A. (2017). *Undaria pinnatifida: a case study to highlight challenges in marine invasion ecology and management Ecol Evol. 2017; 7: 8624-8642* https://doi.org/10.1002/ece3.3430

Ferreira, C. A. M., Félix, R., Félix, C., Januário, A. P., Alves, N., Novais, S. C., Dias, J. R., & Lemos, M. F. L. (2021). A biorefinery approach to the biomass of the seaweed *Undaria pinnatifida* (Harvey suringar, 1873): Obtaining phlorotannins-enriched extracts for wound healing. *Biomolecules*, *11*(3), 1–20. https://doi.org/10.3390/biom11030461

Friedrich, I., Bodenberger, B., Neubauer, H., Hertel, R., & Daniel, R. (2021). Down in the pond: Isolation and characterization of a new Serratia marcescens strain (LVF3) from the surface water near frog's lettuce (Groenlandia densa). *PLoS ONE*, *16*(11 November). https://doi.org/10.1371/journal.pone.0259673

Gaudêncio, S. P., & Pereira, F. (2022). Predicting Antifouling Activity and Acetylcholinesterase Inhibition of Marine-Derived Compounds Using a Computer-Aided Drug Design Approach. *Marine Drugs*, *20*(2). https://doi.org/10.3390/md20020129

Gizer, G., Önal, U., Ram, M., & Sahiner, N. (2023). Biofouling and Mitigation Methods: A Review. In *Biointerface Research in Applied Chemistry* (Vol. 13, Issue 2). AMG Transcend Association. https://doi.org/10.33263/BRIAC132.185

Gomez-Banderas, J. (2022). Marine Natural Products: A Promising Source of Environmentally Friendly Antifouling Agents for the Maritime Industries. In *Frontiers in Marine Science* (Vol. 9). Frontiers Media S.A. https://doi.org/10.3389/fmars.2022.858757

González-Ballesteros, N., Fernandes, M., Machado, R., Sampaio, P., Gomes, A. C., Cavazza, A., Bigi, F., & Rodríguez-Argüelles, M. C. (2023). Valorisation of the Invasive Macroalgae *Undaria pinnatifida* (Harvey) Suringar for the Green Synthesis of Gold and Silver Nanoparticles with Antimicrobial and Antioxidant Potential. *Marine Drugs*, *21*(7). https://doi.org/10.3390/md21070397

Herget, K., Hubach, P., Pusch, S., Deglmann, P., Götz, H., Gorelik, T. E., Gural'skiy, I. A., Pfitzner, F., Link, T., Schenk, S., Panthöfer, M., Ksenofontov, V., Kolb, U., Opatz, T., André, R., & Tremel, W. (2017). Haloperoxidase Mimicry by CeO2−x Nanorods Combats Biofouling. *Advanced Materials*, *29*(4). https://doi.org/10.1002/adma.201603823

Horta, A., Pinteus, S., Alves, C., Fino, N., Silva, J., Fernandez, S., Rodrigues, A., & Pedrosa, R. (2014). Antioxidant and antimicrobial potential of the *Bifurcaria bifurcata* epiphytic bacteria. *Marine Drugs*, *12*(3), 1676–1689. https://doi.org/10.3390/md12031676

Jin, H., Tian, L., Bing, W., Zhao, J., & Ren, L. (2022). Bioinspired marine antifouling coatings: Status, prospects, and future. In *Progress in Materials Science* (Vol. 124). Elsevier Ltd. https://doi.org/10.1016/j.pmatsci.2021.100889

Johnson, A. C., Keller, V., Williams, R. J., & Young, A. (2007). A practical demonstration in modelling diclofenac and propranolol river water concentrations using a GIS hydrology model in a rural UK catchment. *Environmental Pollution*, *146*(1), 155–165. https://doi.org/10.1016/j.envpol.2006.05.037

Jung, K. W., Kim, K., Jeong, T. U., & Ahn, K. H. (2016). Influence of pyrolysis temperature on characteristics and phosphate adsorption capability of biochar derived from waste-marine macroalgae (*Undaria pinnatifida* roots). *Bioresource Technology*, *200*, 1024–1028. https://doi.org/10.1016/j.biortech.2015.10.016

Kim, J. H., Kim, J. H., Lee, J. H., Eom, S. J., Lee, N. H., Lee, S., Lim, T. G., Song, K. M., & Kang, M. C. (2024). Anti-Melanogenic Effects of a Polysaccharide Isolated from *Undaria pinnatifida* Sporophyll Extracts. *International Journal of Molecular Sciences*, *25*(19). https://doi.org/10.3390/ijms251910624

Lee, H. H., Kim, J. S., Jeong, J. H., Park, S. M., Sathasivam, R., Lee, S. Y., & Kim, C. S. (2022). Effect of Different Solvents on the Extraction of Compounds from Different Parts of *Undaria pinnatifida* (Harvey) Suringar. *Journal of Marine Science and Engineering*, *10*(9). https://doi.org/10.3390/jmse10091193

Lehmann, J., Rillig, M. C., Thies, J., Masiello, C. A., Hockaday, W. C., & Crowley, D. (2011). Biochar effects on soil biota - A review. In *Soil Biology and Biochemistry* (Vol. 43, Issue 9, pp. 1812–1836). https://doi.org/10.1016/j.soilbio.2011.04.022

Mack, R. N., Simberloff, D., Lonsdale, W. M., Evans, H., Clout, M., & Bazzaz, F. A. (2000). Biotic Invasions: Causes, Epidemiology, Global Consequences, and Control. *Ecological Applications*, *10*(3), 689. https://doi.org/10.2307/2641039

Martins, A., Silva, J., Alves, C., Pinteus, S., Félix, C., Augusto, A., Pedrosa, R., Mestre, A. S., Santos, R. M. M., Carvalho, A. P., Goettert, M., Laufer, S., & Lemos, M. F. L. (2024). Towards a zero-waste sustainable biorefinery of *Codium* sp. seaweed: From bioactives application to soil enhancement materials. *Journal of Cleaner Production*, *453*. https://doi.org/10.1016/j.jclepro.2024.142191

Marzocchi, M., Badocco, D., Piovan, A., Pastore, P., Di Marco, V., Filippini, R., & Caniato, R. (2016). Metals in *Undaria pinnatifida* (Harvey) Suringar and Sargassum muticum (Yendo) Fensholt edible seaweeds growing around Venice (Italy). *Journal of Applied Phycology*, *28*(4), 2605–2613. https://doi.org/10.1007/s10811-016-0793-8

Mestre, A. S., & Carvalho, A. P. (2018). Nanoporous Carbon Synthesis: An Old Story with Exciting New Chapters. In *Porosity - Process, Technologies and Applications*. InTech. https://doi.org/10.5772/intechopen.72476

Mestre, A. S., Hesse, F., Freire, C., Ania, C. O., & Carvalho, A. P. (2019). Chemically activated high grade nanoporous carbons from low density renewable biomass (Agave sisalana) for the removal of pharmaceuticals. *Journal of Colloid and Interface Science*, *536*, 681–693. https://doi.org/10.1016/j.jcis.2018.10.081

Mestre, A. S., Pires, J., Nogueira, J. M. F., & Carvalho, A. P. (2007). Activated carbons for the adsorption of ibuprofen. *Carbon*, *45*(10), 1979–1988. https://doi.org/10.1016/j.carbon.2007.06.005

Minchin, D., & Nunn, J. (2014). The invasive brown alga *Undaria pinnatifida* (Harvey) suringar, 1873 (laminariales: Alariaceae), spreads northwards in europe. *BioInvasions Records*, *3*(2), 57–63. https://doi.org/10.3391/bir.2014.3.2.01

Mohsin, M. Z., Omer, R., Huang, J., Mohsin, A., Guo, M., Qian, J., & Zhuang, Y. (2021). Advances in engineered *Bacillus subtilis* biofilms and spores, and their applications in bioremediation, biocatalysis, and biomaterials. In *Synthetic and Systems Biotechnology* (Vol. 6, Issue 3, pp. 180–191). KeAi Communications Co. https://doi.org/10.1016/j.synbio.2021.07.002

Mondal, A. K., Hinkley, C., Krishnan, L., Ravi, N., Akter, F., Ralph, P., & Kuzhiumparambil, U. (2024). Macroalgae-based biochar: preparation and characterization of physicochemical properties for potential applications. *RSC Sustainability*, *2*(6), 1828–1836. https://doi.org/10.1039/d4su00008k

Nunes, B. S., Carvalho, F. D., Guilhermino, L. M., & Van Stappen, G. (2006). Use of the genus *Artemia* in ecotoxicity testing. In *Environmental Pollution* (Vol. 144, Issue 2, pp. 453–462). https://doi.org/10.1016/j.envpol.2005.12.037

Park, J. S., Han, J. M., Park, S. W., Kim, J. W., Choi, M. S., Lee, S. M., Haq, M., Zhang, W., & Chun, B. S. (2024). Subcritical Water Extraction of *Undaria pinnatifida*: Comparative Study of the Chemical Properties and Biological Activities across Different Parts. *Marine Drugs*, *22*(8). https://doi.org/10.3390/md22080344

Pinteus, S., Alves, C., Monteiro, H., Araújo, E., Horta, A., & Pedrosa, R. (2015). *Asparagopsis armata* and *Sphaerococcus coronopifolius* as a natural source of antimicrobial compounds. *World Journal of Microbiology and Biotechnology*, *31*(3), 445–451. https://doi.org/10.1007/s11274-015-1797-2

Pinteus, S., Lemos, M. F. L., Alves, C., Neugebauer, A., Silva, J., Thomas, O. P., Botana, L. M., Gaspar, H., & Pedrosa, R. (2018). Marine invasive macroalgae: Turning a real threat into a major opportunity - the biotechnological potential of *Sargassum muticum* and *Asparagopsis armata*. In *Algal Research* (Vol. 34, pp. 217–234). Elsevier B.V. https://doi.org/10.1016/j.algal.2018.06.018

Pinteus, S., Lemos, M. F. L., Alves, C., Silva, J., & Pedrosa, R. (2021). The marine invasive seaweeds *Asparagopsis armata* and *Sargassum muticum* as targets for greener antifouling solutions. *Science of the Total Environment*, *750*. https://doi.org/10.1016/j.scitotenv.2020.141372

Pinteus, S., Susano, P., Alves, C., Silva, J., Martins, A., & Pedrosa, R. (2022). Seaweed's Role in Energetic Transition from Environmental Pollution Challenges to Enhanced Electrochemical Devices. In *Biology* (Vol. 11, Issue 3). MDPI. https://doi.org/10.3390/biology11030458

Roberts, D. A., Paul, N. A., Dworjanyn, S. A., Bird, M. I., & De Nys, R. (2015). Biochar from commercially cultivated seaweed for soil amelioration. *Scientific Reports*, *5*. https://doi.org/10.1038/srep09665

Romeu, M. J., & Mergulhão, F. (2023). Development of Antifouling Strategies for Marine Applications. In *Microorganisms* (Vol. 11, Issue 6). MDPI. https://doi.org/10.3390/microorganisms11061568

Saha, M., Goecke, F., & Bhadury, P. (2018). Minireview: algal natural compounds and extracts as antifoulants. In *Journal of Applied Phycology* (Vol. 30, Issue 3, pp. 1859–1874). Springer Netherlands. https://doi.org/10.1007/s10811-017-1322-0

Sharififar, F., Moshafi, M. H., Shafazand, E., & Koohpayeh, A. (2012). Acetyl cholinesterase inhibitory, antioxidant and cytotoxic activity of three dietary medicinal plants. *Food Chemistry*, *130*(1), 20–23. https://doi.org/10.1016/j.foodchem.2011.06.034

Silva, A., Rodrigues, C., Garcia-Oliveira, P., Lourenço-Lopes, C., Silva, S. A., Garcia-Perez, P., Carvalho, A. P., Domingues, V. F., Barroso, M. F., Delerue-Matos, C., Simal-Gandara, J., & Prieto, M. A. (2021). Screening of bioactive properties in brown algae from the northwest iberian peninsula. *Foods*, *10*(8). https://doi.org/10.3390/foods10081915

Srinivasan, R., Santhakumari, S., Poonguzhali, P., Geetha, M., Dyavaiah, M., & Xiangmin, L. (2021). Bacterial Biofilm Inhibition: A Focused Review on Recent Therapeutic Strategies for Combating the Biofilm Mediated Infections. In *Frontiers in Microbiology* (Vol. 12). Frontiers Media S.A. https://doi.org/10.3389/fmicb.2021.676458

Stabili, L., Acquaviva, M. I., Cecere, E., Gerardi, C., Petrocelli, A., Fanizzi, F. P., Angilè, F., & Rizzo, L. (2023). Screening of *Undaria pinnatifida* (Laminariales, Phaeophyceae) Lipidic Extract as a New Potential Source of Antibacterial and Antioxidant Compounds. *Journal of Marine Science and Engineering*, *11*(11). https://doi.org/10.3390/jmse11112072

Susano, P., Silva, J., Alves, C., Martins, A., Pinteus, S., Gaspar, H., Goettert, M. I., & Pedrosa, R. (2022). Mitigating the negative impacts of marine invasive species – *Sargassum muticum* - a key seaweed for skincare products development. *Algal Research*, *62*. https://doi.org/10.1016/j.algal.2022.102634

Tan, X., Zhang, F., Wang, H., & Ho, S. H. (2023). The magic of algae-based biochar: advantages, preparation, and applications. *Bioengineered*, *14*(1), 2252157. https://doi.org/10.1080/21655979.2023.2252157

Thommes, M., Kaneko, K., Neimark, A. V., Olivier, J. P., Rodriguez-Reinoso, F., Rouquerol, J., & Sing, K. S. W. (2015). Physisorption of gases, with special reference to the evaluation of surface area and pore size distribution (IUPAC Technical Report). *Pure and Applied Chemistry*, *87*(9–10), 1051–1069. https://doi.org/10.1515/pac-2014-1117

Veiga, P., Torres, A. C., Rubal, M., Troncoso, J., & Sousa-Pinto, I. (2014). The invasive kelp *Undaria pinnatifida* (Laminariales, Ochrophyta) along the north coast of Portugal: Distribution model versus field observations. *Marine Pollution Bulletin*, *84*(1–2), 363–365. https://doi.org/10.1016/j.marpolbul.2014.05.038

Viegas, R. M. C., Mestre, A. S., Mesquita, E., Machuqueiro, M., Andrade, M. A., Carvalho, A. P., & Rosa, M. J. (2022). Key Factors for Activated Carbon Adsorption of Pharmaceutical Compounds from Wastewaters: A Multivariate Modelling Approach. *Water (Switzerland)*, *14*(2). https://doi.org/10.3390/w14020166

Vinagre, P. A., & Fonseca, G. (2022). Early biofouling colonization stages: Implications for operation and maintenance planning in marine renewable energy projects. *Open Research Europe*, *2*, 108. https://doi.org/10.12688/openreseurope.14854.1

Vinagre, P. A., Simas, T., Cruz, E., Pinori, E., & Svenson, J. (2020). Marine biofouling: A European database for the marine renewable energy sector. In *Journal of Marine Science and Engineering* (Vol. 8, Issue 8). MDPI AG. https://doi.org/10.3390/JMSE8070495

Wiesner, J., Kříz, Z., Kuca, K., Jun, D., & Koca, J. (2007). Acetylcholinesterases - The structural similarities and differences. *Journal of Enzyme Inhibition and Medicinal Chemistry*, *22*(4), 417–424. https://doi.org/10.1080/14756360701421294

Wu, S., Liu, G., Jin, W., Xiu, P., & Sun, C. (2016). Antibiofilm and anti-infection of a marine bacterial exopolysaccharide against *Pseudomonas aeruginosa*. *Frontiers in Microbiology*, *7*(FEB). https://doi.org/10.3389/fmicb.2016.00102

Yao, X., Ji, L., Guo, J., Ge, S., Lu, W., Chen, Y., Cai, L., Wang, Y., & Song, W. (2020). An abundant porous biochar material derived from wakame (*Undaria pinnatifida*) with high adsorption performance for three organic dyes. *Bioresource Technology*, *318*. https://doi.org/10.1016/j.biortech.2020.124082

Yin, S., Shibata, M., & Hagiwara, T. (2019). Extraction of bioactive compounds from stems of *Undaria pinnatifida*. *Food Science and Technology Research*, *25*(6), 765–773. https://doi.org/10.3136/fstr.25.765

Yu, K. L., Lau, B. F., Show, P. L., Ong, H. C., Ling, T. C., Chen, W. H., Ng, E. P., & Chang, J. S. (2017). Recent developments on algal biochar production and characterization. In *Bioresource Technology* (Vol. 246, pp. 2–11). Elsevier Ltd. https://doi.org/10.1016/j.biortech.2017.08.009

Zeng, J., Luan, F., Hu, J., Liu, Y., Zhang, X., Qin, T., Zhang, X., Liu, R., & Zeng, N. (2022). Recent research advances in polysaccharides from *Undaria pinnatifida*: Isolation, structures, bioactivities, and applications. In *International Journal of Biological Macromolecules* (Vol. 206, pp. 325–354). Elsevier B.V. https://doi.org/10.1016/j.ijbiomac.2022.02.138

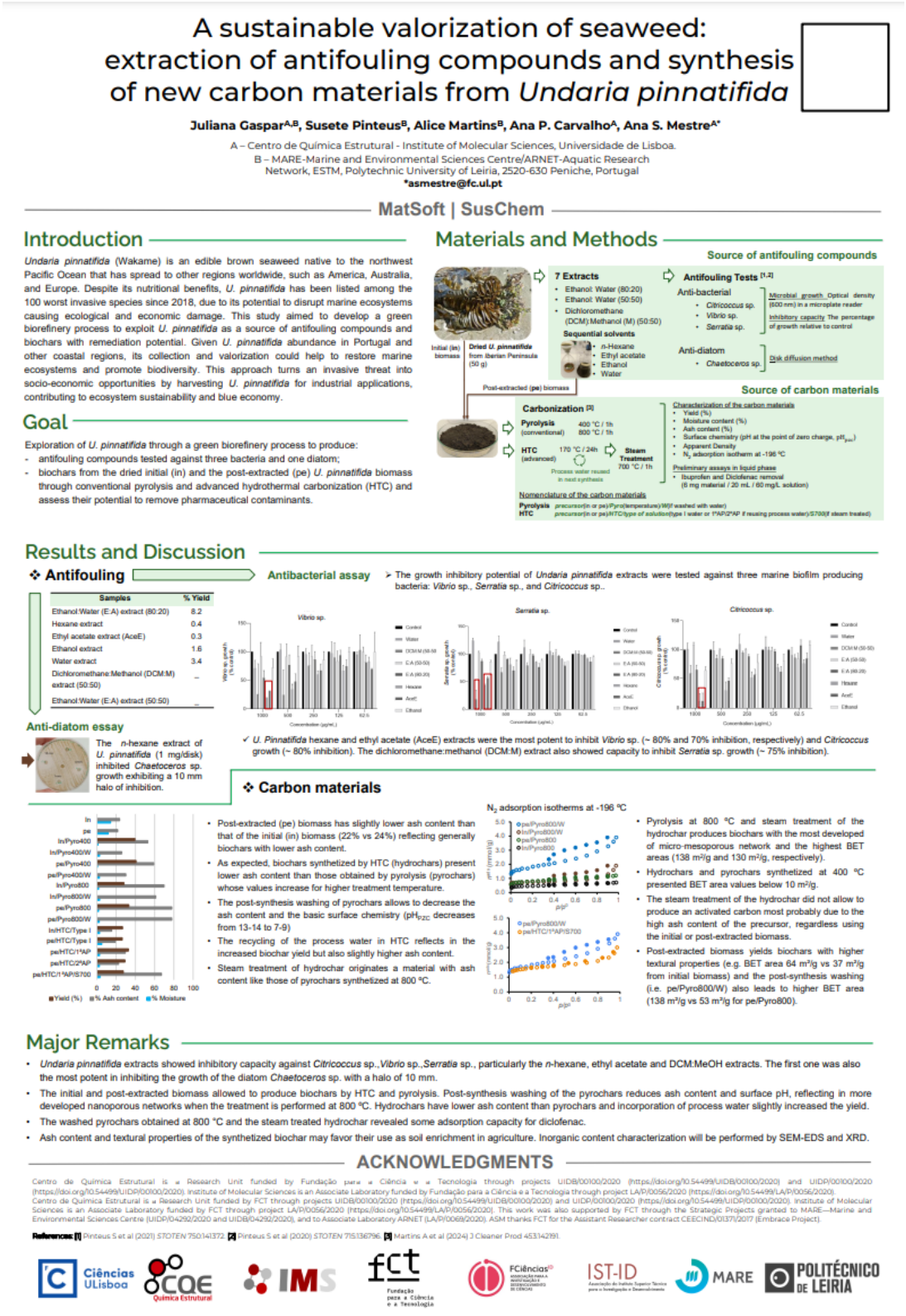

Figure A 1. Poster presented at CQE Days 2024.